UNIVERSITEIT
GENT

# The development of mesoporous phenolic resins as support for heterogeneous catalysis

## Ilke Muylaert

**Members of the dissertation jury**

Prof. dr. Annemie Adriaens, Ghent University (Chairman)
Prof. dr. Pegie Cool, University of Antwerp
Prof. dr. Christophe Detavernier, Ghent University
Prof. dr. ir. Bert Sels, Catholic University of Leuven
Prof. dr. Pascal Van Der Voort, Ghent University (Promotor)
Prof. dr. ir. Joris Thybaut, Ghent University
dr. ir. An Verberckmoes, University College Ghent

## Scientific publications

**A1 publications – articles indexed by the Thomson Reuters citation index**

- *Ultra stable ordered mesoporous phenol/formaldehyde polymers as a heterogeneous support for vanadium oxide.*
Muylaert Ilke, Borgers Marijke, Bruneel Els, Schaubroeck Joseph, Verpoort Francis, Van Der Voort Pascal, Chemical Communications, **2008**, 37, 4475-4477.

- *Supported vanadium oxide in heterogeneous catalysis: elucidating the structure-activity relationship with spectroscopy.*
Muylaert Ilke, Van Der Voort Pascal, Physical Chemistry Chemical Physics, **2009**, 11, 16, 2826-2832.

- *The remarkable catalytic activity of the saturated metal organic framework V-MIL-47 in the cyclohexene oxidation.*
Leus Karen, Muylaert Ilke, Vandichel Matthias, Marin Guy B, Waroquier Michel, Van Speybroeck Veronique, Van Der Voort Pascal, Chemical Communications, **2010**, 46, 28, 5085-5087.

- *The coordinatively saturated vanadium MIL-47 as a low leaching heterogeneous catalyst in the oxidation of cyclohexene.*
Leus Karen, Vandichel Matthias, Liu Ying-Ya, Muylaert Ilke, Musschoot Jan, Pyl Steven, Vrielinck Henk, Callens Freddy, Marin Guy B, Detavernier Christophe, Wiper Paul V, Khimyak Yaroslav Z, Waroquier Michel, Van Speybroeck Veronique, Van Der Voort Pascal, Journal of Catalysis, **2011**, 285, 196-207.

- *Atomic layer deposition of titanium and vanadium oxide on mesoporous silica and phenol/formaldehyde resins: the effect of the support in the liquid phase epoxidation of cyclohexene.*
Muylaert Ilke, Jan Musschoot, Karen Leus, Jolien Dendooven, Christophe Detavernier, Pascal Van Der Voort, European Journal of Inorganic Chemistry, **2012**, 251-260.

- *Ordered mesoporous phenolic resins: highly versatile and ultra-stable support materials*
  Muylaert Ilke, Verberckmoes An, De Decker Jeroen, Van Der Voort Pascal, Advances in Colloid and Interface Science, **2012**, accepted.

- *Non-covalent Immobilization of a Chiral Diamine Catalyst on Sulphonated Mesoporous Phenolic Resins as Novel Catalyst for Asymmetric Aldol Reactions.*
  Muylaert Ilke, Demuynck Anneleen, Li Peng, Sels Bert, Van Der Voort Pascal, ChemCatChem, **2012**, submitted.

- *Covalent immobilization of Jacobsen catalyst on mesoporous phenolic resins as high active catalyst for asymmetric olefin epoxidations.*
  Muylaert Ilke, De Decker Jeroen, Verberckmoes An, Van Der Voort Pascal, ChemCatChem, **2012**, in preparation.

## National and international oral presentations

- *Geordende mesoporeuze fenol/formaldehyde polymeren als 'low leaching' dragermateriaal voor vanadiumoxide.*
  Muylaert Ilke, 9de Vlaams Jongeren Congres van de Chemie, 4 April **2008**, Antwerp, Belgium.

- *Mesoporous phenol/formaldehyde resins as a new support material for vanadium oxide.*
  Muylaert Ilke, 6th International Mesostructured Materials Synposium, 8-11 September **2008**, Namen, Belgium.

- *Towards an ultra-stable and zero leaching supported metal oxide catalyst for liquid oxidation reactions: Mesoporous phenol/formaldehyde resins as an alternative support.*
  Muylaert Ilke, The Netherlands' Catalysis and Chemistry Conference NCCC-X, 3-5 March **2009**, Noordwijkerhout, The Netherlands.

- *Atomic layer deposition of titanium and vanadium oxide layers in the pores of SBA-15 and FDU-15.*
  Muylaert Ilke, 10th International Synposium of Preparation of Catalysts PREPA-X, 11-15 July **2010**, Louvain-La-Neuve, Belgium.

- *Sulphonated mesoporous phenolic resins as solid acid catalyst.*
  Muylaert Ilke, 6th International Conference of Nanoporous Materials NANO-VI, 20-24 August **2011**, Banff, Canada

## National and international poster presentations

- *Highly ordered mesoporous resol resins synthesized by a soft amphiphilic surfactant templating approach.*
  Muylaert Ilke, Roelandt Elke, Schaubroeck David, Vanhee Paul, Verpoort Francis, Van Der Voort Pascal, International Synposium "Baekeland 2007: Thermosets – 100 years after Bakelite", 23-26 September **2007**, Ghent, Belgium.

- *A comparative study of the leaching phenomenon of vanadium oxide supported on silica and mesoporous phenol/formaldehyde resins.*
  Muylaert Ilke, Borgers Marijke, Schaubroeck Joseph, Verpoort Francis, Van Der Voort Pascal, The Netherlands' Catalysis and Chemistry Conference NCCC-IX, 3-5 March **2008**, Noordwijkerhout, The Netherlands.

- *Towards an ultra-stable and zero leaching supported metal oxide catalyst for liquid oxidation reactions.*
  Muylaert Ilke, Van Der Voort Pascal, 9th Dutch Zeolite Association DZA9, 31 Oktober **2008**, Brussels, Belgium.

- *A hydrothermal synthesis way to synthesize mesoporous phenolic resins.*
  Muylaert Ilke, Van Der Stricht Andreas, Van Der Voort Pascal, Doctoraatssymposium UGent Faculteit Wetenschappen, **2009**, Ghent, Belgium.

- *Synthesis and catalytic activity of titanium oxide supported on mesoporous phenolic resins.*
  Muylaert Ilke, Wallaert Elien, Van Der Voort Pascal, The Netherlands' Catalysis and Chemistry Conference NCCC-XI, 1-3 March **2010**, Noordwijkerhout, The Netherlands.

- *The development of hierarchical titanium oxide monoliths as ideal heterogeneous catalysts.*
  Wallaert Elien, Muylaert Ilke, Van Der Voort Pascal, The Netherlands' Catalysis and Chemistry Conference NCCC-XI, 1-3 March **2010**, Noordwijkerhout, The Netherlands.

- *Development of metal organic frameworks as heterogeneous catalysts.*
  Leus Karen, Muylaert Ilke, Vandichel Matthias, Van Speybroeck Veronique, Marin Guy, Van Der Voort Pascal, The Netherlands' Catalysis and Chemistry Conference NCCC-XI, 1-3 March **2010**, Noordwijkerhout, The Netherlands.

- *The development of mesoporous phenolic resins as new solid acid catalysts.*
  Muylaert Ilke, De Canck Els, Spileers Jeremy, Verberckmoes An, Van Der Voort Pascal, The Netherlands' Catalysis and Chemistry Conference NCCC-XII, 28 February – 2 March **2011**, Noordwijkerhout, The Netherlands.

- *A study of the effect of electron donating and electron withdrawing groups on the catalytic performance of V-MIL-47.*
  Leus Karen, Liu Ying-Ya, Vandichel Matthias, Muylaert Ilke, Marin Guy, Waroquier Michel, Van Speybroeck Veronique, Van Der Voort Pascal, The Netherlands' Catalysis and Chemistry Conference NCCC-XII, 28 February – 2 March **2011**, Noordwijkerhout, The Netherlands.

- *How does alkene epoxidation with TBHP occur in MIL-47?*
  Vandichel Matthias, Leus Karen, Muylaert Ilke, Van Der Voort Pascal, Waroquier Michel, Van Speybroeck Veronique, Metal Organic Framework Conference 2011, 5-8 September **2011**, Marseille, France.

- *The catalytic performance of MIL-47 in the liquid phase oxidation of cyclohexene.*
  Leus Karen, Muylaert Ilke, Vandichel Matthias, Marin Guy, Waroquier Michel, Van Speybroeck Veronique, Van Der Voort Pascal, Metal Organic Framework Conference 2011, 5-8 September **2011**, Marseille, France.

## Acknowledgements

Bij het neerpennen van mijn 'Dagboek', had ik graag ook een aantal mensen bedankt.

In de eerste plaats dank aan mijn promotor Prof. Dr. Pascal Van Der Voort om me de kans te geven dit doctoraat te starten. Vol enthousiasme en ambitie, heeft u me ondergedompeld in de wondere wereld van het wetenschappelijk onderzoek. Pascal, dank voor uw vertrouwen en voor alle kansen die ik als één van de pioniers van de onderzoeksgroep gekregen heb. Ik ben er van overtuigd dat COMOC een mooie toekomst tegemoet gaat!

Dank ook aan de juryleden van de beoordelingscommissie van het IWT (Agentschap voor Innovatie door Wetenschap en Technologie) voor hun vertrouwen in mij en het project. Bedankt aan alle leden van de examencommissie voor hun tijd om het proefwerk door te nemen en voor hun kritische vragen en suggesties. Bedankt aan de Universiteit Gent en in het bijzonder aan de vakgroep Anorganische en Fysische Chemie voor het onderdak en de logistieke ondersteuning.

Het was soms eenzaam ploeteren, maar gelukkig kon ik rekenen op veel lieve mensen die zorgden voor een hele fijne tijd. In de eerste plaats denk ik aan alle huidige COMOC'ers: Els, Dolores, Frederik, Karen, Matthias, Shyam, Thomas en Ying-Ya. Bedankt voor jullie hulp en alle leuke, bijwijlen hilarische en onvergetelijke momenten! Ik wens jullie veel succes bij jullie onderzoek! Een speciale dank ook aan mijn thesisstudenten: Andreas, Elke, Jeremy, Jeroen, Jill en Marijke.

Dank ook aan alle huidige S3-collega's en aan hen die S3 ondertussen reeds verlaten hebben. Bedankt voor de broodnodige grapjes aan de koffietafel en ontspanning tussendoor. Ik wens jullie allen het beste! Bedankt ook aan de 'externen', Anneleen, Els en Jan, het was heel fijn samenwerken met jullie.

Tenslotte wil ik de mensen achter de schermen heel graag bedanken. Papa en mama, bedankt om steeds voor me klaar te staan en voor het warme nest waar ik altijd mag thuiskomen. Koen en Wouter, mijn lieve kleine broertjes, hoewel niet meer zo klein, zijn jullie wel nog altijd heel lief. Bert, lieve schat, bedankt voor al jouw lieve zorgen. Samen startten we een wonderlijke reis. Laten we deze hand in hand verder zetten en nog heel veel moois ontdekken...

## Preface

In recent years, the growing demand for new energy sources - and principally the process to become aware of the limitation of its available stock - has created new challenges for the chemical industry and for the scientific research in particular. In addition, the processing and reduction of waste originating from traffic, households, industries, etc. have become a crucial point of interest for scientists. Consequently, the up-coming years will be critical in the search for more sustainable solutions, essentially inspired by a green(er) chemistry.

From this perspective, catalysts are very straightforward materials which offer a variety of possibilities. A catalyst is a chemical substance which can participate actively in a chemical reaction and can be (theoretically) unlimitedly reused. Moreover, catalysts accelerate chemical reaction rates, lower the required reaction energies and are very selective in certain processes. For these reasons, catalysts are considered as the new generation of accelerators (rate) and driving-wheels (selectivity) in chemical processes. These unique properties make catalysts excellent candidates for participating in the concept of 'the ideal synthesis' (see Figure 0.1).
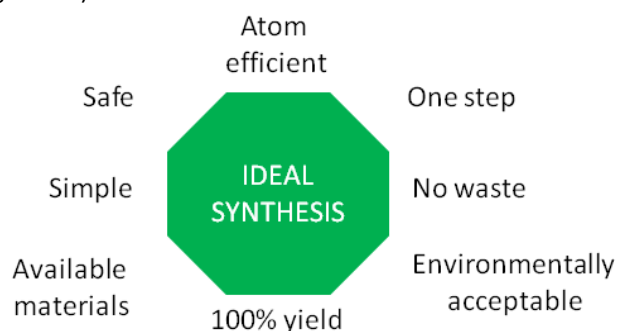


**Figure 0.1 – The concept of the ideal synthesis.**[1]

Heterogeneous solid catalysts in particular have the advantage over their homogeneous counterparts of simple regeneration due to easy separation from the reaction mixture after a catalytic run. Mostly, the catalyst exists of the catalytically active species supported on a solid. Here, the catalyst has to be stable: it may not decompose, poisoning has to be avoided and leaching has to be minimized under given reaction conditions. Mostly, the solid support is porous, creating additional surface for catalyst anchoring. Additionally, the

---

[1] J. Clark, *Green Chemistry*, **1999**, 1, 1, 1-8.

pore sizes can play a crucial role in the diffusion limitations of substrate molecules in the pores and consequently on the final catalytic performance of the catalyst (also called shape selectivity). The pores of porous solids are classified by the IUPAC according to their pore size: pore sizes below 2 nm are called micropores, between 2 and 50 nm are classified as mesopores and pores larger than 50 nm are referred as to macropores.

The research field of heterogeneous catalysis is mostly based on porous silica supports. A wide range of silica based micro- and mesoporous materials (zeolites, MCM-x, SBA-x, ...) are extensively reported in literature. Although these inorganic based catalysts have already proven their benefits as support candidate for numerous categories of catalytic species and for several catalytic purposes, the stability is rather low due to sensitivity to hydrolysis of the siloxane bridges in the porous framework. For this reason, the search for new stable support materials is still in progress…

At the start of this PhD research, the research group of Zhao et. al. published the synthesis of a new generation of mesoporous materials: mesoporous phenolic resins.[2] These materials combine the porosity characteristics of mesoporous materials with the organic nature of phenolic resins. Zhao et. al. referred to this novel type materials as FDU-x, with FDU referring to the Fudan University where these materials were developed and x corresponding to a specific morphology type (see further). In comparison with silica based materials, these porous phenolic resins show interesting properties like aromatic network, hydrophobicity, abundance of phenolic hydroxyl groups, etc.

The main goal of this research work is to evaluate these new mesoporous phenolic resin materials as support candidate for the immobilization of catalytic species. In essence, the influence of the phenolic nature of the support in different catalytic reactions will be evaluated. More in particular, the reproducibility of the support synthesis, the stability of the resins under certain stress conditions, the immobilization of catalytic species and finally the catalytic performance of the novel catalytic systems in different catalytic reactions is studied. Finally, these materials are compared to the standard silica materials. Here, a screening of the potential possibilities of mesoporous phenolic resins as support is presented as potential alternative for the standard silica supports. This research work may hopefully be a starting point and a source of inspiration for chemists and researchers to develop novel catalytic systems...

<div align="right">
Ilke Muylaert
Ghent, February 2012
</div>

---

[2] Y. Meng, D. Gu, F.Q. Zhang, Y.F. Shi, H.F. Yang, Z. Li, C.Z. Yu, B. Tu, D.Y. Zhao, *Angew Chem Int Edit*, **2005**, 44, 7053-7059.

## Outline

This research work consists of seven chapters. The first chapter is an extensive introduction into the field of ordered mesoporous phenolic resins. The second discusses the different analysis techniques used to characterize ordered functionalized mesoporous materials. The three following sections, chapter 3 to 5, comprise the heart of this research work and illustrate the versatility of mesoporous phenolic resins as potential support for heterogeneous catalyst. Finally, a general conclusion and a Dutch summary are provided in chapter 6 and 7 respectively. Figure 0.2 gives a schematic general overview of the topics who will be discussed in this research work.

**Chapter 1** provides an extensive literature overview of the main principles and the recent progress made in the synthesis of mesoprous phenolic resins and carbons. The versatility towards functionalization and the incorporation of metals and hetero-atoms in the organic mesoporous framework are considered. Finally, the broad range of potential applications for this novel class of mesoporous materials is discussed and future perspectives in this research area are given.

**Chapter 2** gives a brief introduction into the main analysis techniques to characterize mesoporous materials and mesoporous phenolic resins in particular. Additionally, this chapter gives experimental details on the different synthesis procedures of mesoporous phenolic resins used in this work.

**Chapter 3** surveys the use of mesoporous phenolic resins as support for sulphonic acid groups. The first subsection is addressed to different procedures to introduce sulphonic acid groups in the framework of mesoporous phenolic resins. As a screening test, the catalysts are evaluated for their catalytic performance in a Fisher esterification. Additionally, the stability towards leaching resistance of the sulphonic acid groups in aqueous medium is considered. Finally, these sulphonated resins are used as support for a chiral diamine catalyst and are tested in an asymmetric aldol reaction of 2-butanone with an aromatic aldehyde. The performance of the newly developed catalysts are compared to other sulphonated mesoporous materials.

**Chapter 4** focuses on the development of mesoporous phenolic resins as support for vanadium and titanium oxide catalysts. Here, the deposition of the metal precursors and the experimental parameters are described and the characterization of the functionalized catalysts is presented. Further, the novel catalysts are evaluated in three different

catalytic oxidation reactions and their catalytic performance is compared to common porous silica supported catalysts. Finally, insight in the catalytic behavior is given and a reaction mechanism is proposed.

**Chapter 5** introduces mesoporous phenolic resins as support for the covalent immobilization of a Manganese *salen* complex for asymmetric epoxidation reactions of unfunctionalized conjugated alkenes. In particular, a direct and simple covalent immobilization procedure of the Jacobsen catalysts is presented. The catalyst is evaluated for its catalytic performance in the epoxidation of diline and is compared to its homogeneous counterpart.

**Chapter 6** summarizes the most important conclusions made throughout this work and gives a future outlook in this research field.

**Chapter 7** provides a Dutch summary of this PhD research work.
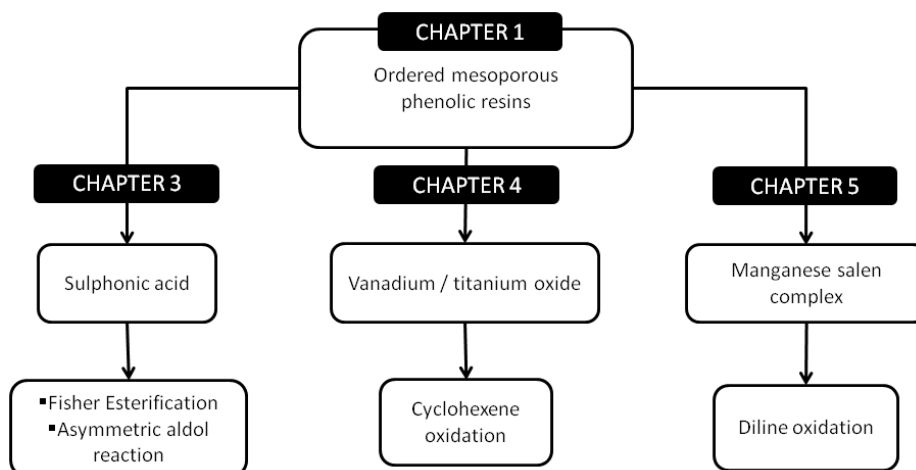


**Figure 0.2 – Schematic overview of the research subjects in this work**

## List of abbreviations

**A**
ALD     Atomic layer deposition

**B**
BET     Brunauer Emmett Teller
BJH     Barrett Joyner Halenda

**C**
COU     Ordered mesoporous carbon synthesized by the research group of
       Tanaka et. al.

**D**
DRIFT    Diffuse Reflectance Infrared Fourier Transform

**E**
*ee*      Enantiomeric excess
EISA     Evaporation induced self-assembly
EO      Ethylene oxide

**F**
FDU     Fudan University, refers to ordered mesoporous polymer synthesized by
       the research group of Zhao et. al.

**G**
GC      Gas chromatography

**H**
HMDS    Hexamethyldisilazane
HPLC    High pressure liquid phase chromatography

**M**

MCM            Mobil Composition of Matter
MW              Molecular weight

**N**

NMR            Nuclear Magnetic Resonance

**O**

OMC            Ordered mesoporous carbon
OMP           Ordered mesoporous polymer

**P**

PEO            Poly(ethylene oxide)
PMO           Periodic Mesoporous Organosilica
PO               Propylene oxide
PPO            Poly(propylene oxide)
PSD            Pore Size Distribution

**S**

SAXS          Small Angle X-ray Scattering
SBA            Santa Barbara Amorphous material
SDA            Structure Directing Agent
SEM           Scanning Electron Microscopy
SMPO         Styrene monomer propylene oxide process

**T**

TEM           Transmission Electron Microscopy
TEOS          Tetraethyl orthosilicate
$Tf_2O$           Triflic acid anhydride
TGA            Thermo Gravimetric Analysis
THF            Tetrahydrofurane
TMB           1,3,5-trimethylbenzene
TOF            Turn-Over Frequency
TON           Turn-Over Number

**X**

XPS            X-ray photoelectron spectroscopy
XRD           X-ray diffraction
XRF            X-ray fluorescence spectroscopy

**Table of contents**

**List of tables and figures**

**Figure 3.7** – Synthesis of amino acid (L-phenylalanine) derived chiral diamine catalyst. (i) Boc-protected amino acid L-phenylalanine, DCC, amine, 0°C-RT overnight; (ii) TFA/DCM, 2-5 hours RT; (iii) LiAlH$_4$/THF, 5 hours reflux.

**Figure 4.1** – Simplified representation of the three main morphologies of vanadium oxide species supported on a surface. Type A: isolated monomeric species of tetrahedral VO$_4$ units; type B: dimeric/oligomeric species containing V-O-V bridges; type C: crystalline clusters of octahedral VO$_6$ units

**Figure 4.2** – Gas phase deposition of VOCl$_3$ on mesoporous phenolic resin in the home-made reactor (1: filter; 2: metal precursor; 3 + 5: Schlenk valve; 4: connection to vacuum; 6: furnace)

**Figure 4.3** – LEFT: Powder reactor for atomic layer deposition of titanium and vanadium oxide on mesoporous materials. RIGHT: Deposition of one monolayer by the atomic layer deposition technique.

**Figure 4.4** – Hydrophobization of surface hydroxyls with hexamethyldisilazane

**Figure 4.5** – Overview of the selection of catalytic oxidation tests: (A) oxidation of cyclohexene 1 with *tert*-butylhydroperoxide towards the main reaction products: (a) epoxidation to cyclohexene oxide 2 and consecutive ring opening to cyclohexane-1,2-diol 3, (b) radical pathway to *tert*-butyl-2-cyclohexenyl-1-peroxide 4 and (c) allylic oxidation to 2-cyclohexene-1-one 5; (B) Simplified reaction mechanism of the oxidation of toluene 1 towards benzoic acid 4 via benzyl alcohol 2 and benzaldehyde 3; (C) The heart of the SMPO process: the epoxidation of propylene to propylene oxide over a silica supported titanium oxide catalyst.

**Figure 4.6** – Overview of the catalytic performance in the epoxidation of cyclohexene with *tert*-butylhydroperoxide: (a) mesoporous silica SBA-15 and (b) mesoporous resin supported vanadium and titanium oxide catalysts. The bars represent the selectivity of the catalyst towards cyclohexene epoxide (after 8 hours reaction). The 5% line represents the blanc level. The catalyst numbers correspond with the numbers in Table 4.1.

**Figure 4.7** – LEFT: Wide angle XRD pattern of (a) mesoporous phenolic resin supported vanadium oxide catalyst and (b) V$_2$O$_5$. The asterisk indicates the background signal of the sample holder, 2 θ = 32.9°). RIGHT: V2p$_{3/2}$ region in the XPS spectra of (a) V$_2$O$_5$, (b) NH$_4$VO$_3$, (c) VO(acac)$_2$ and (d) Vanadium oxide supported on mesoporous phenolic resin.

**Figure 4.8** – (a) original mesoporous phenolic resin and (b) after vanadium oxide deposition with VOCl$_3$. LEFT: Diffuse reflection infrared spectra. RIGHT: Nitrogen sorption isotherms.

**Figure 4.9** – LEFT: Leaching resistance of mesoporous silica and phenolic resin supported vanadium oxide catalysts. RIGHT: Hot filtration experiment of a silica supported vanadium oxide catalyst in the epoxidation of cyclohexene.

**Figure 4.10** – Proposed reaction mechanism of the cyclohexene epoxidation for (a) silica supported catalyst and (b) phenolic resin supported catalyst. Breaking the support-oxygen-metal (S-O-M) bond in step 2 is assumed to be critical for the epoxidation of

cyclohexene (M = V or Ti). Step 5 is essential for full regeneration of the catalyst after catalytic run.

**Figure 5.1** – Structural skeleton and a ball and stick model of the Jacobsen catalysts. The dimensions are given in Angstrom.

**Figure 5.2** – Representation of the strategy to directly immobilize a Mn-Salen complex on the surface of mesoporous phenolic resins. Previously to the immobilization in step ii, the Mn-salen complex is synthesized.

**Figure 5.3** – X-ray fluorescence evolution of the immobilization of the Mn-complex on mesoporous phenolic resin: (a) original phenolic resin support, (b) after NaOH-treatment and (c) after immobilization of the Mn-complex.

**Figure 5.4** – DRIFT-spectra of (a) mesoporous phenolic resin, (b) Jacobsen catalyst immobilized on mesoporous phenolic resin and (c) homogeneous Jacobsen catalyst.

**Figure 5.5** – Asymmetric epoxidation of 1,2-dihydronaphtalene (diline) to (1R, 2S)-naphtalene oxide and (1S,2R)-naphtalene oxide

**Figure 5.6** – Split test of the Jacobsen catalyst immobilized on mesoporous phenolic resin: after 24 hours a total conversion of 58% was observed. Subsequently, the catalyst was filtrated and the conversion was again analyzed after 48h. No increase of the conversion was observed, suggesting truly heterogeneously catalytic activity of the immobilized catalyst.

**Figure 5.7** – Groves' proposed reaction mechanism of the epoxidation of alkenes via the oxygen rebound mechanism.

**Figure 5.8** – TOP: Principle skeleton of manganese *salen* complex. The arrows represent the different possible approaches of olefin substrates to reach the activated oxo-manganese center. BOTTOM: Representation of the induced side-on approach

**Figure 5.1** – Structural skeleton and a ball and stick model of the Jacobsen catalysts. The dimensions are given in Angstrom.

**Figure 5.2** – Representation of the strategy to directly immobilize a Mn-Salen complex on the surface of mesoporous phenolic resins. Previously to the immobilization in step 2, the Mn-salen complex is synthesized.

**Figure 5.3** – DRIFT-spectra of (a) mesoporous phenolic resin, (b) Jacobsen catalyst immobilized on mesoporous phenolic resin and (c) homogeneous Jacobsen catalyst.

**Figure 5.4** – X-ray fluorescence evolution of the immobilization of the Mn-complex on mesoporous phenolic resin: (a) original phenolic resin support, (b) after NaOH-treatment and (c) after immobilization of the Mn-complex.

**Figure 5.5** – Electron paramagnetic resonance (EPR) of (a) homogeneous Jacobsen catalysts and (b) Jacobsen catalysts immobilized on mesoporous phenolic resin.

**Figure 5.6** – Asymmetric epoxidation of 1,2-dihydronaphtalene (diline) to (1R, 2S)-naphtalene oxide and (1S,2R)-naphtalene oxide

**Figure 5.7** – Split test of the Jacobsen catalyst immobilized on mesoporous phenolic resin: after 24 hours a total conversion of 58% was observed. Subsequently, the catalyst was filtrated and the conversion was again analyzed after 48h. No increase of the conversion

was observed, suggesting truly heterogeneously catalytic activity of the immobilized catalyst.

**Figure 5.8** – Groves' proposed reaction mechanism of the epoxidation of alkenes via the oxygen rebound mechanism.

**Figure 5.9** – TOP: Principle skeleton of manganese *salen* complex. The arrows represent the different possible approaches of olefin substrates to reach the activated oxo-manganese center. BOTTOM: Representation of the induced side-on approach.

**Figuur 7.1** – BOVEN: Vereenvoudigde weergave van de synthese van mesoporeuze fenolharsen in aanwezigheid van een triblok copolymeer als zacht templaat. ONDER LINKS: Representatieve weergave van verschillende morfologieën van mesoporeuze materialen. ONDER RECHTS: TEM-afbeeldingen van mesoporeus fenolisch hars. [2]

**Figure 7.2** – LINKS: Stikstofsorptie isothermen van mesporeuze fenolische harsen en koolstof. RECHTS: macroscopische vorm van ongecalcineerde mesoporeuze fenolharsen. De materialen worden gesynthetiseerd volgens A: hydrothermale synthese, B: evaporation induced self-assembly methode, C: twee-fasensysteem.

**Figuur 7.3** – Overzicht van de verankering van verschillende sulphonzure groepen op een mesoporeus fenolhars.

**Figuur 7.4** – Niet-covalente immobilizatie van een L-phenylalanine gebaseerd derivaat op een gesulphoneerd fenolhars via een zuur-base interactie als chirale katalysator voor de aldol reactie van butanon en 4-(trifluoromethyl)benzaldehyde.

**Figure 7.5** – Reactiemechanisme van de cyclohexeen oxidatie met silica en fenolhars als dragermateriaal, met de cruciale breking van de drager-zuurstof-metaalbinding in stap 2 en de regeneratie van de katalysator in stap 5 (M = V of Ti).

**Figuur 7.6** – Structuurformule en bol- en staafmodel van de Jacobsen katalysator met weergave van de ruimtelijke afmetingen.

**Figuur 7.7** – LINKS: Verankering van de Jacobsenkatalysator op het oppervlak van een mesoporeus fenolhars. RECHTS: Asymmetrische epoxidatie van diline (1,2-dihydronaftaleen).

# Chapter 1

## Ordered mesoporous phenolic resins and carbons

### 1.1 Introduction

Ordered mesoporous polymers and carbons (OMP and OMC) form an advanced class of ordered mesoporous materials, combining the high porosity properties of mesoporous materials with the physico-chemical characteristics of organic polymers and carbons. These materials can be synthesized by a hard template method as first reported by Ryoo et. al. [1] However, this synthesis process is known as time-consuming and unsuitable for large-scale production. Moreover, tuning of the wall thickness and the pore diameters is limited by the choice of the hard silica template. These obstacles stimulated intensive research towards a direct synthesis method using a soft-template procedure similar to the synthesis of mesoporous inorganic silicas. [2-5]

The soft-template synthesis of ordered mesoporous polymers and carbons, however, requires well selected conditions for the carbon precursors: firstly, the polymer/carbon precursor has to be soluble in the same medium as the surfactant. Secondly, the precursor needs the be capable to interact with and organize itself around the soft template. Next, the three-dimensional rigid mesostructure has to be stable and may not be destroyed during template removal and/or carbonization process. Finally, for high quality mesoporous carbon structures, a precursor with a high carbon content which can easily be converted to high graphitized carbon is desired. [6]

Phenol-formaldehyde based resins have shown to be excellent precursors for the soft-template synthesis of ordered mesoporous phenolic resins and carbons.[7] Phenol-formaldehyde resins as non-porous bulk materials were first discovered by the Ghent scientist Leo H. Baekeland in 1907 and patented as Bakelite® in 1909. [8] In the last century, these yellow-orange colored resins have shown to be economical highly attractive starting products for the production of daily-life utensils. Recently, this 100-years old phenolic resin knows a true renaissance as advanced polymer precursor in the research field of ordered mesoporous materials. Nowadays, this area is expanding exponentially since many chemists are inspired by the promising opportunities of these innovative materials for a wide range of potential applications.

This chapter gives an extensive overview of the main principles and the recent progress made in the synthesis of these phenolic based materials. Furthermore, the versatility towards functionalization and the incorporation of metals and hetero-atoms in the organic mesoporous framework are considered. Finally, the broad range of potential applications for this novel class of mesoporous materials is discussed and future perspectives in this research area are given.

## 1.2 The concept of the soft-template synthesis

In the synthesis of mesoporous phenolic resins and carbons through a soft-template mechanism the organic precursors, the medium and the surfactant play the key factors in the composition of the ordered organic-organic mesostructure. A schematic representation of the direct synthesis concept is shown in Figure 1.1. Here, four main stages can be considered: (1) prepolymer formation by formaldehyde addition to a phenolic compound, (2) three-dimensional crosslinking or curing around the structure directing agent and mesophase induction, (3) template removal and (4) a carbonization step. All these stages will be discussed individually in the following sections. Note that step (1) and (2) may take place simultaneously. Consequently, these two different processes may overlap and can not be well distinguished as true individual stages in the synthesis procedure. Moreover, the final step (4) is only required for the synthesis of ordered mesoporous carbons.
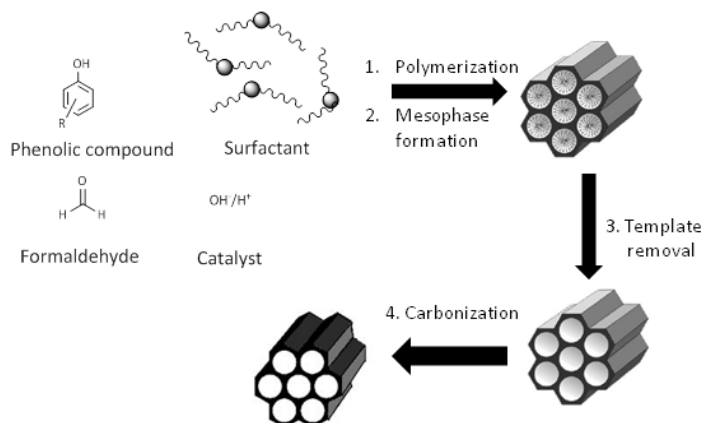


**Figure 1.1 – Schematic representation of the direct synthesis of ordered mesoporous phenolic resins and carbons using a surfactant as soft-template.**

### 1.2.1 Prepolymer formation

The prepolymer formation of phenolic resins occurs by an acid or base catalyzed step-growth polymerization of formaldehyde with a phenolic compound. [9] First, concerning the phenolic compound, three types which differ in the number of hydroxyl groups on the aromatic ring are frequently used: phenol, resorcinol and phloroglucinol. Phenol is most often chosen as starting reagent due to its low cost-price and the easy *control* over the polymerization rate (polymerization rate increases from phenol < resorcinol < phloroglucinol). It is suggested that phloroglucinol may interact better with the structure directing agent due to its higher hydroxyl density. Additionally, the synthesis of mesoporous carbon using the more condensed 1,5-dihydroxynaphtalene as carbon precursor to reduce shrinkage during the carbonization step is also reported. [10]

Secondly, to crosslink the aromatic network, formaldehyde is mostly applied. This carbonyl component is commercially available as formaline solution (aqueous 36-37wt% formaldehyde solution). Thirdly, the *pH* conditions (and the temperature) have a direct impact on the polymerization rate and the reaction mechanism between the two monomers – and consequently on the resulting products. The first step in the prepolymer formation is the formaldehyde addition to a phenolic compound. One can distinguish two different reaction mechanisms, depending on the pH. In strongly acidic medium, the addition proceeds via an electrophilic aromatic substitution reaction. In alkaline medium, the phenolic compound is rapidly deprotonated to the resonance stabilized phenoxide ion followed by formaldehyde substitution. For both, exclusively *ortho-* and *para*-alkylation is observed (*meta-* substitution is not detected).

During and after formaldehyde addition, prepolymer formation through condensation between methylolphenols or condensation with phenol occurs. In strongly acidic medium and molar excess of phenol to formaldehyde, Novolacs are obtained. These linear or slightly branched condensation products are almost exclusively linked with methylene bridges. The oligomers with a relatively low molecular weight are insoluble in organic solvents or water. On the other hand, with higher pH values and an excess of formaldehyde to phenol, resols are formed. This oligomeric network contains mainly methylene and ether bridges and is still soluble in water and organic solvents. Table 1.1 summarizes the differences in properties between the prepolymers Novolacs and Resols. As can be seen in Figure 1.2, both oligomer types can easily be transformed by a heat treatment and curing into a three dimensional interconnected *ortho-* and *para*-substituted rigid polymer network.

**Table 1.1 – Main differences in characteristics between Novolac and Resol prepolymers**

|  | Novolac | Resol |
|---|---|---|
| pH range | < 4 | > 5 |
| Molar ratio Phenol : Formaldehyde | 1 : 0.75-0.85 | 1 : 1.00-3.00 |
| Reaction rate proportional to ... | $[H^+]$ | $[OH^-]$ |
| Structure | Linear, slightly branched | Three-dimensional, crosslinked |
| Before curing | Exclusively methylene bridges | Mainly methylene and ether bridges |
| After curing | Methylene bridged 3-dimensional network | Methylene bridged 3-dimensional network |
| Molecular weight | MW = 2000 | MW = 500-5000 |
| Prepolymer type | Thermoplastic | Thermoplastic |
| Soluble in ... | Not soluble in organic solvents and water | Organic solvents and water |

## 1.2.2 Curing and mesophase induction

During crosslinking or curing, a three-dimensional interconnected network is formed by polycondensation reactions between the phenolic prepolymer units. This process can be deviated from the previous prepolymer formation by a different molecular weight progression *vs.* time curve.[11] Heat curing is by far the most important crosslinking process and it is conducted at temperatures between 100 and 200°C. Above 200°C, the framework changes into a mainly methylene connected framework. Several crosslinking reactions may take place between the building units, resulting in a non-well defined polymer with several bridging functionalities. The methylene bridge is the most stable crosslink site and at higher temperatures the prevailing building unit in cured phenolic resins. Note that here only a concise and over-simplified representation of the formation of phenolic resins is presented. For a more in depth review about the chemistry in the synthesis of phenolic resins, the research work of Knop and Pilato is highly recommended. [9]
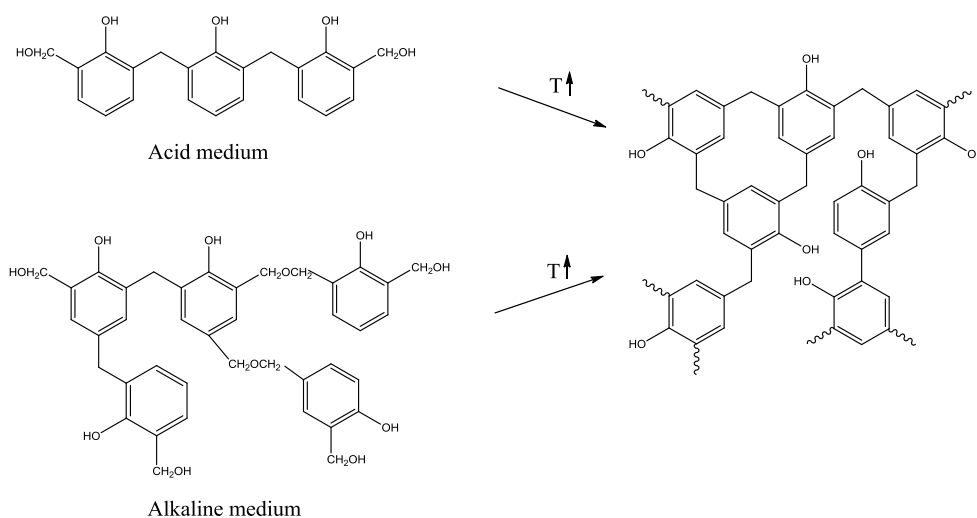


**Figure 1.2 – Simplified representation of the curing of Novolacs (acid medium) and Resols (alkaline medium) into a three-dimensional aromatic network containing mainly methylene bridges (> 300°). The phenolic aromatic rings are *ortho*- and/or *para*-substituted.**

If the crosslinking of the prepolymer occurs in presence of a structure directing agent, this may result in a co-assembled organic-organic nanostructured material, induced by the self-assembly of the structure directing agent.[12] These surfactants assemble into micelles, spherical or cylindrical structures directing the hydrophilic parts of the surfactant in the polar phase while withdrawing the hydrophobic parts within the apolar micellar core. Further increasing the surfactant concentration and/or temperature results in the self-organization into periodic hexagonal, cubic or lamellar mesophases, as can be seen in Figure 1.3. This process is based on the spontaneous organization of asymmetric molecules into well-defined supramolecular assemblies through non-covalent interactions (hydrogen bonding, Van Der Waals forces, electrostatic forces, π-π interactions, etc.) above the critical micelle concentration (cmc) and the critical temperature. Most common used surfactants are amphiphilic triblock copolymers (Pluronic $EO_xPO_yEO_x$) (EO = ethylene oxide, PO = propylene oxide), which are low-cost, non-toxic and commercially available.
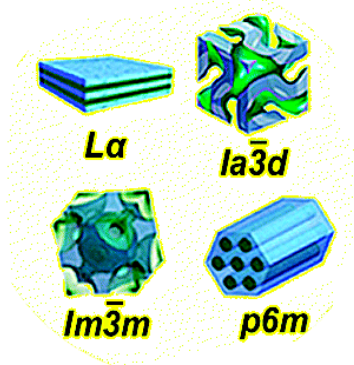


**Figure 1.3 – Schematic representation of hexagonal (p6m), cubic (Im3m and Ia3d) and lamellar (Lα) mesophases**

### 1.2.3 Template removal

The creation of porosity by template removal occurs *via* a calcination step or solvent extraction. [13] For mesoporous phenolic resins and carbons, it is necessary that – contrary to inorganic mesoporous materials –the removal of the template takes place under inert atmosphere (nitrogen). [14] TGA, ^{13}C NMR and FTIR analyses show that the template is entirely removed at a temperature of 350°C in nitrogen atmosphere. A small amount of oxygen (0.5-1%) in the atmosphere may improve the oxidation of the template, while keeping the polymer network intact. [15] Additionally, one should note that during calcination, releasing gasses can cause stress in the pores together with damage of the pore structure. In order to maintain stresses below the critical damage value, the heating

rate has to be controlled. Normally, a heating rate between 1-5°C/min is chosen. [13, 16] Note that during calcination, the unit cell parameter $a_0$ may decrease significantly due to shrinkage of the polymer network. In order to avoid or minimize this shrinkage process, a mild solvent extraction is sometimes applied. Here, thicker pore walls and larger pore sizes are obtained. Notice however that the pore volume and specific surface area are lower in comparison to a calcination procedure. [15] Sulphuric acid is reported as a good extraction agent and FT-IR measurements revealed that the organic groups were maintained after extraction. [17]

### 1.2.4 Carbonization

Finally, a carbonisation step by heating under inert atmosphere to elevated temperatures slowly converts the mesoporous organic resin into an amorphous mesoporous carbon framework. This carbonization process starts around 400°C, together with a slow shrinkage of the structure framework. From 600°C, no further significant shrinkage is observed and from then on the heating rate can be accelerated to 10°C/min. [15] Between 600 and 800°C, the generation of micropores takes place, simultaneously with the raise of the specific surface area. Above 800°C, there was no significant additional contraction, although the ordered structure may further distort according to the XRD peak width. Also TEM images showed the evolution from circular pores (400°C) to asymmetric (600°C) and slightly more asymmetric (800-1000°C) pores. [18] Finally, it is reported that the carbon matrix is stable at least up to 1400°C, indicating an ultra high thermal stability of the carbon structure. [7, 15]

### 1.3 Stability of Mesoporous Phenol/Formaldehyde Resins and Carbons

The potential implementation of mesoporous phenol/formaldehyde resins in practical applications is directly related to their (long-term) stability. Although phenolic resins as bulk material are extensively studied in literature, little studies report on the stability of the nanoporous structures. Compared to their non-porous variant, it is evident that the general stability reduces significantly according to the inclusion of porosity. However, Brinker et al. previously showed for silica that the introduction of a nanostructured morphology may significantly improve the modulus and maximizes the mechanical properties at a given density. [19]

### 1.3.1 Thermal Stability

Although all thermochemical and physical properties should be considered and even though most of them are temperature and time dependent, the term *thermal stability of a*

*polymer* generally refers to the temperature at which a polymer starts to decompose under dynamic thermogravimetric measurements. [9]

Under oxidative atmosphere, these polymers are stable up to 300-350°C. Above this temperature, the resin rapidly decomposes in three stages, mainly based on the weight loss and the volume change. The mechanism of this thermal degradation is still under debate since several proposed mechanisms are incomplete and/or contradictory to one another.[20] The main degradation products that release during thermal decomposition are water, formaldehyde, phenol, benzene, toluene, cresols, xylenols, methane, carbon monoxide and carbon dioxide.[9, 21]

Under inert atmosphere, these materials are stable up to 350-400°C. Above 400°C, carbonization or pyrolysis converts the polymer matrix of primarily methylene bridged phenolic units to coalesced carbon rings with a high amorphous carbon yield. It is generally accepted that during the carbonization process of phenolic resins, a thermo-oxidative process takes place regardless if the thermal treatment occurs in an oxidative or inert atmosphere since the degradation products provide a source of oxygen. [9, 20] During carbonization, the physico-chemical and porosity properties of these materials change drastically.

### 1.3.2 Mechanical and Hydrothermal Stability

One of the essential properties of a first-class catalytic support is its stability towards hydrothermal conditions (water and heat). Standard mesoporous silica materials as MCM-x and SBA-x families are known for their average hydrothermal stability, mainly due to hydrolysis of the siloxane bridges in their framework. Figure 1.4 shows that the specific surface drastically decrease with more than 50% after a hydrothermal treatment. In comparison, mesoporous phenolic resins, are more hydrothermally stable. Only a decrease of 17% in specific surface area is observed.

Next, preliminary mechanical stability tests, performed by keeping the porous solids for a certain time under lateral pressure showed that the mesoporous phenolic resins can easily withstand pressures of more than 700MPa without significant loss in porosity (Figure 1.4). [22] The high stability of the mesoporous resins can be attributed to the three-dimensional covalently connected C-C bonded framework and its resistance to hydrolysis. Furthermore, Meng et al. showed that the mesoporous FDU-15 carbon material is more rigid than its replicated carbon CMK-3 analogue prepared by using sucrose as a carbon source and SBA-15 as a hard template. [15] However, no study is published today reporting a general overview of the mechanical stability of these mesoporous materials in terms of modulus, hardness, tensile and compressive strength, etc. Furthermore, the abrasion and friction resistance is not reported.
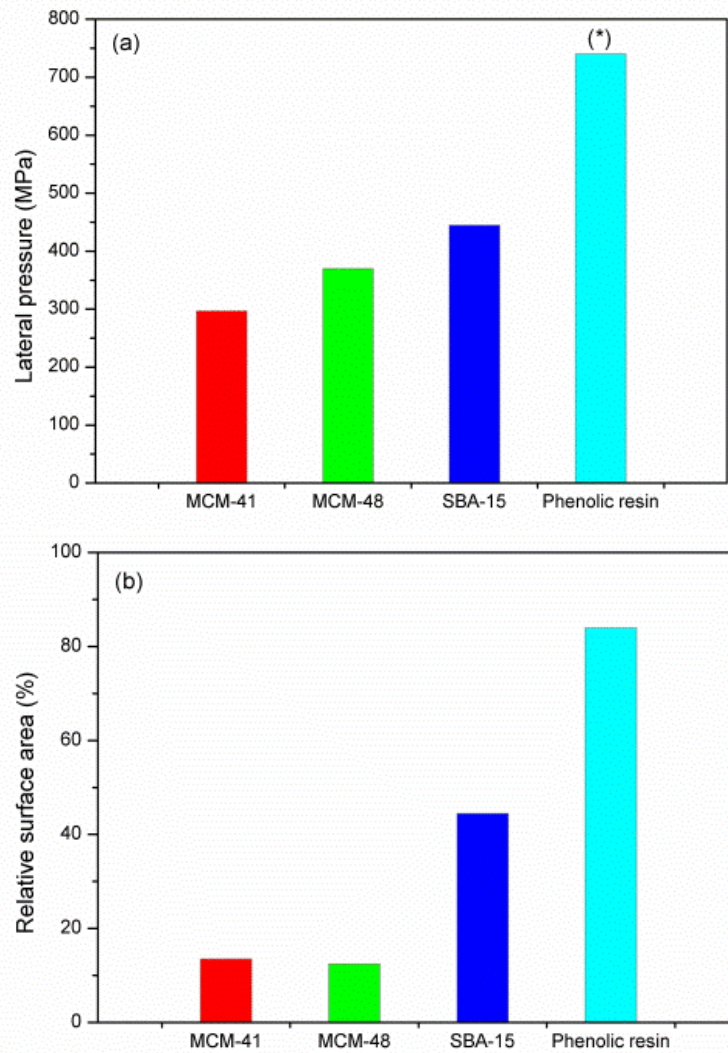
**Figure 1.4 – (a) Mechanical stability: Minimal lateral pressure (2 min) at which the porous structure collapses (> 55% decrease in specific surface area; *maximum lateral pressure obtainable in the lab) and (b) Hydrothermal stability: Relative surface area of the mesoporous material maintained after hydrothermal treatment in autoclave with steam at 100°C during 24h at autogeneous pressure (MCM-x and SBA-x are mesoporous silica materials). [22]**

**1.4 Ordered Mesoporous Phenolic Resins and Carbons: a State-of-the-Art Overview**

Since the first publication of the synthesis of mesoporous phenolic resins through a soft-synthesis method, many research groups have shown an exponential growth of interest in these materials.

Today, three main different synthesis pathways based on the macroscopic morphology are reported in literature: (A) a hydrothermal aqueous procedure [13, 16, 23], (B) an evaporation induced self-assembly [7] and (C) a two-phase system based pathway [24]. As can be seen in Figure 1.5, three different macroscopic morphologies are obtained according to the synthesis procedure: a powder, a membrane and a monolith using procedure (A), (B) and (C) respectively. A detailed comparison of the synthesis methods is given in Table 1.2. Synthesis route (A), the hydrothermal aqueous procedure, leads to a light yellow-orange powder. This synthesis pathway is a batch process with long synthesis times (>100 hours without calcination) and has often reproducibility issues. These Type A materials exhibit high surface areas of 350-400 m²/g and high micropore volumes up to 0.18 cm³/g. As can be seen in Figure 3A, these resins exhibit a type I isotherm (also called Langmuir isotherm). Note that the isotherm of the polymer is not closed at low relative pressures. This is explained by the swelling ability of polymers in liquid nitrogen during the measurement.[25] After carbonization, the framework is entirely three-dimensionally crosslinked and the compact non-swelling nanostructured carbon material shows a closure of the adsorption and desorption branch at p/p° = 0.42. The pores of the resin are relatively small, being in the microporous range (< 2nm). Only a limited percentage of the total pore volume can be assigned to small mesopores of 2-2.5 nm. During carbonization the pores shrink drastically and a microporous material with a type I isotherm with Langmuir surface areas in the range of 800-900 m²/g is obtained.

Type B materials are synthesized with identical carbon precursors, structure directing agent, catalyst and synthesis temperature as Type A materials; they only differ from each other in synthesis time, solvent type and molar ratios of the components. Here, the solvent is evaporated during the synthesis, yielding a transparent membrane. [26] The synthesis time of Type B materials is reduced to more than half the synthesis time of Type A materials, however, this pathway is more labor intensive due to the several individual synthesis steps. Additionally, up-scaling towards larger batch sizes is hard since there is a need for large surface substrate discs for evaporation. Type B materials exhibit a type IV isotherm with a typical $H_2$ hysteresis loop. The desorption is delayed to p/p° = 0.42, suggesting a cage-like pore structure with small entrance sizes. Type B materials have larger pores than Type A, although the pore size distribution is rather broad with pores between 2 to 7 nm. Contrary to Type A and Type B materials, the third class of mesoporous phenolic resins and carbons, denoted as Type C materials, are synthesized with the more reactive but also the more expensive resorcinol/formaldehyde system as carbon source. Here, the polymer precursors are polymerized in an acidic water/ethanol mixture. In a typical synthesis, the mixture is kept standing for a certain time resulting in a

two-layer system with a transparent ethanol-water rich upper phase and a yellow polymer-rich lower phase. The polymer resin is obtained after discarding the upper phase and thermopolymerizing the polymer-rich phase into a monolith resin. In case of Type C materials, the synthesis steps are easy to handle and the total synthesis time is significantly reduced to approximately 40 hours, which makes this pathway attractive for process up-scaling. The mesoporous phenolic resins obtained after calcination have excellent porosity properties with high specific surface areas (600-650 $m^2$/g), large pore volumes (0.6-0.7 $cm^3$/g) and large and uniform pores. These material properties are also maintained after carbonization, showing these materials high thermal stability. The $N_2$ isotherms of both the mesoporous resin and carbon show a type IV hysteresis curve with a steep capillary condensation step at p/p° = 0.7-0.8, indicating uniform pore size distributions. The isotherm exhibits a H1 hysteresis loop, indicating cylindrical open pores which are interconnected with a substantial amount of irregular micropores (0.08-0.12 $cm^3$/g).
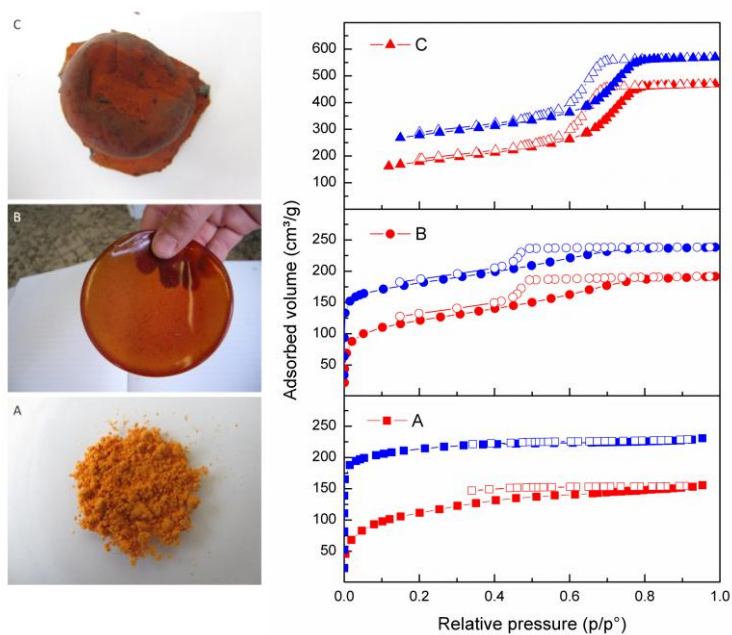


**Figure 1.5 – LEFT: Macroscopic morphology of the *as*-synthesized red-orange colored phenolic resins. RIGHT: Nitrogen sorption isotherms of calcined porous phenolic resins (lower) and carbons (upper); (a) Hydrothermal aqueous procedure, (b) evaporation induced self-assembly and (c) two-phase system based pathway.**

**Table 1.2 – Overview of the synthesis and porosity characteristics of porous phenolic resins and carbons synthesized by the three different synthesis pathways.**

|  | Type A | Type B | Type C |
|---|---|---|---|
| Carbon source | Phenol/Formaldehyde | Phenol/Formaldehyde | Resorcinol/Formaldehyde |
| Structure directing agent | F127 | F127 | F127 |
| Medium | Alkaline (NaOH) | Alkaline (NaOH) | Acidic (HCl) |
| Solvent | $H_2O$ | EtOH | $EtOH/H_2O$ |
| Synthesis temperature | 65 – 70°C | (1) 70°C; (2) RT | RT |
| Total synthesis time [h] [#] | 100 – 125 | 45 – 50 | 35 – 40 |
| Isotherm type / Hysteresis loop | Type I / no | Type IV / H1 loop | Type IV / H2 loop |
| $S_{BET}$ [m²/g] | 350 – 400* | 400 – 500 | 600 – 650 |
| Pore diameter [nm] | < 2 | 2 – 7 | 5.5 – 8.5 |
| Total pore volume [cm³/g] | 0.15 – 0.2 | 0.4 – 0.5 | 0.6 – 0.7 |
| Micropore volume [cm³/g] | 0.10 – 0.18 | 0.08 – 0.12 | 0.08 – 0.12 |
| Polymer morphology | Powder | Membranes | Monolith |

Type A: hydrothermal aqueous procedure, Type B: evaporation induced self-assembly and Type C: two-phase system based pathway; Porosity data is given of the corresponding polymer materials; [#] *as*-synthesis mesoporous polymer (calcination step excluded), * Langmuir surface area: 650 – 700m²/g.

Next to the macroscopic morphology, research groups also attempt to control the mesoscopic morphology of these materials. In order to obtain insight in the specific forces playing a role in the formation of such mesoscopic morphologies, one should note that all reaction partners (i.e. temperature, pH, molar ratios, solvents, etc.) and additionally their specific intermolecular interactions with each other influence the final mesoscopic morphology of the mesoporous material. Today, all these relations and their impact are not well understood and research is further exploring this subject matter. Here, an attempt to provide a state-of-the art overview is made. The mesoscopic morphology is mostly denoted as FDU-x, where FDU refers to the Fudan University, the place where they were firstly developed and x referring to a specific mesoscopic ordering. Note that other research groups sometimes refer to the same materials as COU-x, OMP, OMC, etc. [27-29] Table 1.3 gives an overview of the different morphologies.

Following the hydrothermal synthesis procedure, FDU-14 (Ia$\bar{3}$d), FDU-15 (p6m) and FDU-16 (Im$\bar{3}$m) have been prepared. All these materials were synthesized using neutral triblock copolymers as soft-template. Using cationic surfactants as soft-template lamellar and disordered micelle/polymer composite mesophases were also synthesized. [5, 30] However, it was reported that the electrostatic interactions between the organic polymer precursors and the amphiphilic cationic surfactants are not strong enough to form an ordered assembly. Furthermore, note that the pore size of the FDU-15 was tailored by addition of either hexadecane or decane as swelling agent. [31] Hexadecane and decane interact with the hydrophobic PPO part of the copolymer resulting in the swelling of the hydrophobic core of the micelles. The smaller the used swelling agent, the stronger the interaction with the template, the larger the pores and the larger the unit cell parameter. Decane is the smallest usable swelling agent. Using smaller swelling agents such as trimethylbenzene, hexane, heptane, only a non-controlled mesostructure is being obtained.[16]

According to the evaporation induced-self assembly method, the synthesis of mesoporous phenolic resins was firstly reported by Dai et. al. in 2004. [32] He succeeded in the synthesis of a mesoporous carbon film (COU-type materials) starting from resorcinol as carbon source and polystyrene block poly(4-vinylpyridine) (PS-P4VP) as structure directing agent. However, PS-P4VP is commercially not available and is therefore not appropriate for industrial up scaling. Tanaka et al. were successful in using triblock copolymer Pluronic F127 as surfactant. [33] They worked in strong acid medium with resorcinol/formaldehyde and with triethylorthoacetate (EOA) as carbon co-precursor. He called these materials COU-1 carbons. [10, 34]

In order to obtain more insight in the mesoscopic formation and the specific interaction between the polymer (phenol/formaldehyde precursor) and the structure directing agent (surfactant) during the evaporation induced-self assembly process, Meng et. al. developed

a mesophase diagram. [7, 15] [16] The final mesostructure mainly depends on the choice of template and the ratio of carbon precursor to surfactant. Controlling these parameters, phase transformations from lamellar to bicontinuous cubic, hexagonal and body-centered cubic were obtained. Here, higher carbon precursor to template ratios increase the hydrophilic/hydrophobic balance, which explained the observed phase transformations. Today, FDU-14 ($Ia\bar{3}d$), FDU-15 (p6m), FDU-16 ($Im\bar{3}m$), FDU-17 ($Fd\bar{3}m$) and FDU-18 ($Fm\bar{3}m$) were successfully synthesized using the evaporation induced self-assembly pathway.

Next to the conventional EISA method, the aerosol-assisted EISA method and the suspension-assisted EISA method have also been developed. The former produces small particle diameters (100 nm to 5 $\mu$m) [35-37] and the latter yields particles with larger macroscopic diameter scale (50 to 500 $\mu$m). [38] Furthermore, the addition of rigid inorganic constituents into phenolic resins to produced hybrid porous materials by a co-assembly is also reported. [39, 40] The addition enhances the toughness of polymers and carbons and resists the thermal shrinkage. Composites with high homogeneity were obtained. The ratio of silica/carbon source was ranged from 0 to infinite. A reinforced concrete model is proposed to understand the structure of the nanocomposites in which silica and carbon components are microphase separated and homogeneously dispersed inside the pore walls. Etching the silica with a HF solution or combustion of the carbon in air can remove silica or carbon components in the carbon-silica nanocomposite to form pure mesoporous carbon and silica, respectively. The former process can build pores in the carbon pore walls, the dimension depending on the size of the silicate oligomers. This new procedure is also called Evaporation Induced triconstituent Co-Assembly (EICA).

**Table 1.3 – Summary of synthesized structures with space group, synthesis parameters and comparison of pore diameter (D), pore volume (V$_p$) and BET surface (S$_{BET}$). The carbonization temperature for all carbon materials is 800°C, except for MP-CS-46 carbon-silica (900°C).**

| Synthesis procedure | Symmetry Group | Surfactant | Carbon Precursor | Solvent | D (nm) | V$_p$ (cm$^3$) | S$_{BET}$ (m$^2$/g) | Ref. |
|---|---|---|---|---|---|---|---|---|
| Hydrothermal | | | | | | | | |
| FDU-14 | $Ia\bar{3}d$ | P123 | Phenol | $H_2O$ | 3.8 | 0.40 | 550 | [16] |
| C-FDU-14 | $Ia\bar{3}d$ | P123 | Phenol | $H_2O$ | 2.8 | 0.50 | 1000 | [16] |
| FDU-15 $C_{10}/C_{16}$[a] | p6m | P123 | Phenol | $H_2O$ | 6.8/5.0 | 0.40/0.41 | 500/460 | [16] |
| C-FDU-15 $C_{10}/C_{16}$ | p6m | P123 | Phenol | $H_2O$ | 4.1/3.8 | 0.40/0.55 | 750/1040 | [16] |
| FDU-16 | $Im\bar{3}m$ | F127 | Phenol | $H_2O$ | 3.5 | 0.34 | 670 | [16] |
| C-FDU-16 | $Im\bar{3}m$ | F127 | Phenol | $H_2O$ | 3.2 | 0.50 | 1030 | [16] |
| EISA | | | | | | | | |
| COU-1 | p6m | F127 | Resorcinol, EOA | $H_2O$ / EtOH | 5.9 | 0.74 | 1354 | [33] |
| D-COU-1 | p6m | F127 | 1,5-DHN | $H_2O$ / EtOH | n.a. | n.a. | n.a. | [10] |
| FDU-14 | $Ia\bar{3}d$ | P123 | Phenol | EtOH | 3.1 | 0.10 | 130 | [15] |
| C-FDU-14 | $Ia\bar{3}d$ | P123 | Phenol | EtOH | 2.0 | 0.34 | 690 | [15] |
| FDU-15 | p6m | F127 or P123 | Phenol | EtOH | 5.4 | 0.40 | 430 | [15] |
| C-FDU-15 | p6m | F127 or P123 | Phenol | EtOH | 3.1 | 0.40 | 720 | [15] |
| FDU-16 | $Im\bar{3}m$ | F127 or F108 | Phenol | EtOH | 6.6 | 0.34 | 460 | [15] |
| C-FDU-16 | $Im\bar{3}m$ | F127 or F108 | Phenol | EtOH | 3.8 | 0.47 | 820 | [15] |
| C-FDU-17 | $Fd\bar{3}m$ | $PO_{53}$-$EO_{136}$-$PO_{53}$ | Phenol | EtOH | 3.5/5.8 | 0.47 | 780 | [27] |
| C-FDU-18 | $Fm\bar{3}m$ | $EO_{125}$-b-$St_{305}$ | Phenol | THF | 3.3 | 0.87 | 922 | [41] |
| | $Fm\bar{3}m$ | PEO-b-PMMA | Phenol | THF | 10.5 | 0.57 | 1050 | [42] |
| EICA | | | | | | | | |
| MP-CS-46 polymer-silica | p6m | F127 | Phenol | EtOH | 8.1 | 0.80 | 610 | [39] |
| MP-CS-46 carbon-silica | p6m | F127 | Phenol | EtOH | 6.7 | 0.46 | 350 | [39] |

P123: $EO_{20}$-$PO_{70}$-$EO_{20}$, F127: $EO_{106}$-$PO_{70}$-$EO_{106}$, F108: $EO_{132}$-$PO_{50}$-$EO_{132}$, DHN: dihydroxynaphthalene. [a] Addition of decane or hexadecane.

## 1.5 Functionalization and incorporation of metals and hetero-atoms in mesoporous phenolic resins and carbons and their applications

Due to the unique chemical polymer characteristics, mesoporous phenolic resins are ideal starting materials to further modify with functional groups or to incorporate metal elements, compounds or nanoparticles. Hetero-atom containing resins and carbons can be directly obtained by involving a metal precursor in the self-assembly or by polymerization using a carbon source containing the metal or compound (*in situ* methods) or can be obtained during a post-synthesis treatment (impregnation, adsorption, grafting or ion exchange methods). Since the first publication of the synthesis of mesoporous phenolic resins, different publications report on the modification of mesoporous phenolic resins and carbons. Table 1.4 gives an brief overview of the functionalization and incorporation of metals and hetero-elements in mesoporous phenolic resins and carbons.

### 1.5.1 Catalysis

Mesoporous phenolic resins, but more in particular the mesoporous carbon analogues, have already been reported as excellent support for a variety of catalytic active species. To show their potentials as support, a few examples are here discussed. Li et. al. prepared platinum catalysts by a post-synthesis incorporation with a solution of $H_2PtCl_6$. [43] It was reported that the synthesis parameters such as the molar compositions and the order of addition of the ingredients have a significant impact on the metal particle sizes and the sintering of the nanoparticles. Gao et al. synthesized a ruthenium catalyst by impregnation of mesoporous carbons with a $H_2IrCl_6$ solution. He investigated the impact of the molar ratio of resorcinol to formaldehyde and concluded that a too low resorcinol to formaldehyde ratio yielded large Irridium particles.[44] [24] Liu et. al. prepared titanium oxide catalysts and reported that the selection of the nanoparticulate titanium precursor influences the final size of the titanium nanoparticles.[45]

Furthermore, ordered mesoporous carbon-alumina (OMCA) nanocomposites have been reported to improve the interaction between the support and the catalytic active species and can promote highly dispersed metal particles. These OMCA nanocomposites have shown to be excellent supports for platinum catalysts and showed high activity in the cellulose conversion to hexitols.[46] Another example using a multi-component co-assembly support material was reported by Wan et. al. who synthesized a palladium catalyst on a hybrid silica/carbon matrix. Here the palladium particles were uniformly dispersed in the pore walls because the palladium ions selectively adsorb on the hydrophilic silica parts of the structure. The hydrophobic carbon parts of the structure are the driving force to avoid palladium aggregation.[47]

Li et. al. reported the synthesis of a $ZrO_2$/FDU-15 catalyst with a relatively high zirconia content (up to 47%). [48] However, for higher loadings pore blockage and metal incorporation in the walls have to be considered as side-phenomena, since the availability

of active site for reactants must be guaranteed. Indeed, Ji et al. prepared an active and non-active ruthenium/carbon catalyst. For the latter, the ruthenium nanoparticles were mostly embedded in the carbon walls, prohibiting contact with the reactants. [49] Next, mesoporous phenolic resins have also been successfully functionalized with sulphonic acid groups and used as efficient and re-usable heterogeneous solid acid catalysts with superior performance compared to conventional resins and microporous zeolites. [50, 51] Finally, the incorporation of amine functionalities have also been reported and tested for Knoevenagel condensation reactions. [50] This brief list gives an general idea about the versatility of mesoporous phenolic resins as support for a variety of catalytic active species.

### 1.5.2 Electrochemistry

Next to support for catalytic species, ordered mesoporous carbons with uniform and tuneable pore sizes have also been used as electrode. These materials show fast accessibility for large electrolyte ions. For example, fluorinated mesoporous carbons have been tested in cyclic voltammetry with $Fe(CN)_6^{4-}$/ $Fe(CN)_6^{4-}$.[52] Next, modest reversible capacities were reported for mesoporous carbon-titania nanocomposites formed by the triconstituent self-assembly.[53] Recently Dai et al. were successful in fabricating vanadium and cobalt containing mesoporous carbon films. There materials showed high conductivity and specific capacitance, which was respectively 5 to 7 times higher compared to the neat carbon capacitance even after 500 cyclic voltammetry cycles.[54] Mesoporous carbon have also been reported as electrochemical double-layer capacitor (EDLC).[55] Finally, incorporation of hetero-atoms as boron and phosphor in mesoporous carbons prepared via the soft template synthesis, showed an increase in electrical conductivity compared to other conventional carbon electrodes.[56]

### 1.5.3 Adsorption

Ordered mesoporous carbons, the FDU-type materials, have been reported as adsorbent for versatile target molecules. Here, some examples are discussed. For instance, Wu et al. showed that these materials are highly efficient adsorbents for the immobilization of heavy metal ions or biomolecules. [57] Furthermore, an ethylenediamine functionalized carbon showed good adsorption capacity for Cu(II) and to a lesser extent for Cr(VI). [58] Next, ordered mesoporous thiol-functionalized silica/carbon hybrid material demonstrated high capacity in adsorbing heavy metal ions Ag(I) and Pb(II). [59] Mesoporous carbon/nanoparticle nickel composites showed good adsorption properties for bulky dye fuchsine base. [60] Recently Zhao et al. prepared mesoporous MgO/carbon composites and showed its excellent solid base properties by $CO_2$. [61] Finally, a one-pot generated mesoporous carbon/calciumoxide hybrid material showed high capacities in $CO_2$ physisorption and high initial activities in $CO_2$ chemisorption. [62]

**Table 1.4 - Overview of incorporation of elements and functional groups and different test reactions**

| | Precursor | Incorporation | Support | C-precursor | Pluronic | Reaction types | Reactants | Ref. |
|---|---|---|---|---|---|---|---|---|
| **Compounds** | | | | | | | | |
| CaO | Ca(NO$_3$)$_2$. 4H$_2$O | *in situ* | OMC | PF | F127 | Physi- and chemisorptions | CO$_2$ | [62] |
| F | p-fluorophenol | *in situ* | OMC | PF | F127 | Cyclic voltammetry | Fe(CN)$_6$$^{4-}$/ Fe(CN)$_6$$^{4-}$ | [52] |
| Ir | H$_2$IrCl$_6$ | *in situ* | OMC | RF | F127 | Decomposition | Hydrazine | [44] |
| Fe | Fe(NO$_3$)$_3$.9H$_2$O | post-synthesis | OMC | RF | F127 | Catalytic wet peroxide oxidation | Phenol + H$_2$O$_2$ | [63] |
| | Fe(NO$_3$)$_3$.9H$_2$O | *in situ* | OMC | RF | F127 | - | - | [64] |
| MoC | (NH$_4$)$_6$Mo$_7$O$_{24}$.4H$_2$O | *in situ* | OMC | RF | F127 | Decomposition | Hydrazine | [65] |
| Mo$_2$C | (NH$_4$)$_6$Mo$_7$O$_{24}$.4H$_2$O | post-synthesis | OMC | RF | F127 | Decomposition | Hydrazine | |
| Ni | Ni(NO$_3$)$_2$ | *in situ* | OMSC | RF | F127 | - | - | [66] |
| | Ni(H$_2$O)$_6$(NO$_3$)$_2$ | *in situ* | OMC | RF | F127 | - | - | [67] |
| Pd | PdCl$_2$ | post-synthesis | OMSC | PF | F127 | Heck coupling  Ulmann coupling | Chlorobenzene + styrene  Chlorobenzene | [47] |
| | H$_2$PdCl$_4$ | post-synthesis | OMSC | PF | F127 | Hydrodechlorination | Chlorophenol | [68] |
| Pt | H$_2$PtCl$_6$ | post-synthesis | OMP | PF | P123 | Hydrogenation | Benzaldehyde + H$_2$ | [43] |
| | H$_2$PtCl$_6$ | post-synthesis | OMCA | PF | F127 | Conversion | Cellulose | [46] |
| | H$_2$PtCl$_6$/Pt(NH$_3$)$_4$Cl$_2$ | post-synthesis | OMC$^a$ | PF | P123 | Asymmetric hydrogenation | Ethyl pyruvate | [69] |
| Ru | RuCl$_3$.3H$_2$O | *in situ*$^b$ | OMC | PF | F127 | Hydrogenation | Benzene + H$_2$ | [49] |
| | RuCl$_3$ | *in situ* | OMC | RF | F127 | Hydrogenation | Cinnamaldehyde | [24] |
| | RuCl$_3$ | post-synthesis | OMP | PF | F127 | Hydrogenation | Benzaldehyde | [70] |
| Ti | TiCl$_4$ | *in situ* | OMC | PF | F127 | Photocatalytic decomposition | Rhodamine | [71] |
| | Ti(OBu)$_4$ | *in situ* | OMC | PF | F127 | - | - | [45] |
| V | a)VOCl$_3$-vapor  b)10%VOCl$_3$-solution | post-synthesis | OMP | PF | F127 | - | - | [22] |
| ZrO$_2$ | ZrOCl$_2$.8H$_2$O | *in situ* | OMC | PF | F127 | Oxidative dehydrogenation | Ethylbenzene | [48] |
| **Functional group** | | | | | | | | |
| -NH$_2$ | ED | post-synthesis | OMP | PF | F127 | Synthesis | Nitro-alkene | [72] |
| -NHCH$_3$  -N(CH$_3$)$_2$  -NH$_2$ | a) MA  b) DMA  c) ED | post-synthesis | OMP | PF | P123/F127 | Knoevenagel condensation | Benzaldehyde + ethyl cyanoacetate | [50] |
| -SO$_3$H | 50% SO$_3$/H$_2$SO$_4$ vapor | post-synthesis | OMP | PF | P123 | Beckmann  Condensation  Esterification | Cyclohexanone oxime  Aldehyde + alcohol  Palmitic acid | [51] |
| -SO$_3$H | | post-synthesis | OMP | PF | P123 | Transesterification | Soybeen oil | [73] |
| **Combination** | | | | | | | | |
| -NH$_2$ + Pd | 1) ED, 2) H$_2$PdCl$_4$ | post-synthesis | OMP | PF | P123/F127 | Heck coupling  Hydrogenation | Aryl halide + ethyl acrylate  Allyl alcohol | [74] |

OMSC = Ordered Mesoporous Silica-Carbon based Material; OMCA = Ordered Mesoporous Alumina-Carbon Nanocomposite; PF = Phenol-Formaldehyde; RF = Resorcinol-Formaldehyde; ED = ethylene diamine; MA = methylamine; DMA = dimethylamine. $^a$ chirally modified with cinchonidine; $^b$ both the EISA and EICA (Evaporation Induced Tri-Constituent Co-Assembly) route was followed

### 1.6 Concluding remarks and future perspectives

In this chapter, it was demonstrated that ordered mesoporous phenolic resins are an advanced class of ordered mesoporous materials. They combine the high porosity characteristics with the polymer properties. Phenolic resins exhibit high thermal, chemical and mechanical stability and have shown their potential in several applications.

The functionalization of the phenolic resins with functional groups is also promising for the development of highly selective and stable adsorbents for removal and recycling of specific potentially toxic elements. Adsorbent-based processes may also lead to efficient ways for energy storage and bio-applications.[75] In order to reduce the dependence on phenol as carbon source, alternatives have been explored to incorporate natural polymers such as lignin and lignin derivatives.[76] Finally, multi-component co-assembly gives rise to tunable surface properties (e.g. carbon-silica, carbon-alumina, carbon-titania) and has more opportunities than traditional single component materials for tuning the activities and selectivity when they are used as supports for metal catalysts.

### 1.7 References

[1] R. Ryoo, S.H. Joo, S. Jun, *J Phys Chem B*, **1999**, 103, 7743-7746.
[2] D.Y. Zhao, Q.S. Huo, J.L. Feng, B.F. Chmelka, G.D. Stucky, *J Am Chem Soc*, **1998**, 120, 6024-6036.
[3] C.T. Kresge, M.E. Leonowicz, W.J. Roth, J.C. Vartuli, J.S. Beck, *Nature*, **1992**, 359, 710-712.
[4] A. Thomas, *Angew Chem Int Edit*, **2010**, 49, 8328-8344.
[5] Y. Wan, Y.F. Shi, D.Y. Zhao, *Chem Mater*, **2008**, 20, 932-945.
[6] P. Van Der Voort, C. Vercaemst, D. Schaubroeck, F. Verpoort, *Phys Chem Chem Phys*, **2008**, 10, 347-360.
[7] Y. Meng, D. Gu, F.Q. Zhang, Y.F. Shi, H.F. Yang, Z. Li, C.Z. Yu, B. Tu, D.Y. Zhao, *Angew Chem Int Edit*, **2005**, 44, 7053-7059.
[8] Baekelandt, US Patent, 1909, 942, 699.
[9] Knop A, Pilato L, Phenolic resins, Chemistry, Applications and Performance, 1985, Springer-Verlag.
[10] F.H. Simanjuntak, J. Jin, N. Nishiyama, Y. Egashira, K. Ueyama, *Carbon*, **2009**, 47, 2531-2533.
[11] Vollmert, Polymer Chemistry, Berlin, Heidelberg, New York, Springer, 1973.
[12] H.Y. Fan, S. Reed, T. Baer, R. Schunk, G.P. Lopez, C.J. Brinker, *Micropor Mesopor Mat*, **2001**, 44, 625-637.
[13] F.Q. Zhang, Y. Meng, D. Gu, Y. Yan, C.Z. Yu, B. Tu, D.Y. Zhao, *J Am Chem Soc*, **2005**, 127, 13508-13509.
[14] F. Berube, S. Kaliaguine, *Micropor Mesopor Mat*, **2008**, 115, 469-479.

[15] Y. Meng, D. Gu, F.Q. Zhang, Y.F. Shi, L. Cheng, D. Feng, Z.X. Wu, Z.X. Chen, Y. Wan, A. Stein, D.Y. Zhao, *Chem Mater*, **2006**, 18, 4447-4464.

[16] F.Q. Zhang, Y. Meng, D. Gu, Y. Yan, Z.X. Chen, B. Tu, D.Y. Zhao, *Chem Mater*, **2006**, 18, 5279-5288.

[17] X. Zhuang, X.F. Qian, J.H. Lv, Y. Wan, *Appl Surf Sci*, **2010**, 256, 5343-5348.

[18] (a) X.X. Li, A.B. Larson, L. Jiang, L.Y. Song, T. Prichard, N. Chawla, B.D. Vogt, *Micropor Mesopor Mat*, **2011**, 138, 86-93; (b) Vogt et. al, *Langmuir*, 27, **2011**, 5607

[19] H.Y. Fan, C. Hartshorn, T. Buchheit, D. Tallant, R. Assink, R. Simpson, D.J. Kisse, D.J. Lacks, S. Torquato, C.J. Brinker, *Nat Mater*, **2007**, 6, 418-423.

[20] K.A. Trick, T.E. Saliba, *Carbon*, **1995**, 33, 1509-1515.

[21] J.M. Lin, C.C.M. Ma, *Polym Degrad Stabil*, **2000**, 69, 229-235.

[22] I. Muylaert, M. Borgers, E. Bruneel, J. Schaubroeck, F. Verpoort, P. Van Der Voort, *Chem Commun*, **2008**, 4475-4477.

[23] A.H. Lu, B. Spliethoff, F. Schuth, *Chem Mater*, **2008**, 20, 5314-5319.

[24] P. Gao, A.W. Wang, X.D. Wang, T. Zhang, *Catal Lett*, **2008**, 125, 289-295.

[25] N.B. McKeown, P.M. Budd, K.J. Msayib, B.S. Ghanem, H.J. Kingston, C.E. Tattershall, S. Makhseed, K.J. Reynolds, D. Fritsch, *Chem-Eur J*, **2005**, 11, 2610-2620.

[26] F. Hoffmann, M. Cornelius, J. Morell, M. Froba, *Angew Chem Int Edit*, **2006**, 45, 3216-3251.

[27] Y. Huang, H.Q. Cai, T. Yu, F.Q. Zhang, F. Zhang, Y. Meng, D. Gu, Y. Wan, X.L. Sun, B. Tu, D.Y. Zhao, *Angew Chem Int Edit*, **2007**, 46, 1089-1093.

[28] Y. Huang, H.Q. Cai, T. Yu, X.L. Sun, B. Tu, D.Y. Zhao, *Chem-Asian J*, **2007**, 2, 1282-1289.

[29] P. Li, Y. Song, Q.G. Guo, J.L. Shi, L. Liu, *Mater Lett*, **2011**, 65, 2130-2132.

[30] I. Moriguchi, A. Ozono, K. Mikuriya, Y. Teraoka, S. Kagawa, M. Kodama, *Chem Lett*, **1999**, 1171-1172.

[31] Y. Wan, Y.F. Shi, D.Y. Zhao, *Chem Commun*, **2007**, 897-926.

[32] (a) C.D. Liang, K.L. Hong, G.A. Guiochon, J.W. Mays, S. Dai, *Angew Chem Int Edit*, **2004**, 43, 5785-5789; (b) Dai et al., *J Am Chem Soc* **2006**, 128, 5316; (c) Dai et al., *Angew Chem Int Edit*, **2008**, 47, 3696

[33] S. Tanaka, N. Nishiyama, Y. Egashira, K. Ueyama, *Chem Commun*, **2005**, 2125-2127.

[34] J. Jin, N. Nishiyama, Y. Egashira, K. Ueyama, *Micropor Mesopor Mat*, **2009**, 118, 218-223.

[35] Y. Yan, F.Q. Zhang, Y. Meng, B. Tu, D.Y. Zhao, *Chem Commun*, **2007**, 2867-2869.

[36] C.J. Brinker, Y.F. Lu, A. Sellinger, H.Y. Fan, *Adv Mater*, **1999**, 11, 579

[37] N. Andersson, P.C.A. Alberius, J.S. Pedersen, L. Bergstrom, *Micropor Mesopor Mat*, **2004**, 72, 175-183.

[38] D.H. Long, F. Lu, R. Zhang, W.M. Qiao, L. Zhan, X.Y. Liang, L.C. Ling, *Chem Commun*, **2008**, 2647-2649.

[39] R.L. Liu, Y.F. Shi, Y. Wan, Y. Meng, F.Q. Zhang, D. Gu, Z.X. Chen, B. Tu, D.Y. Zhao, *J Am Chem Soc*, **2006**, 128, 11652-11662.

[40] N. Hao, Z.X. Wu, P.A. Webley, D.Y. Zhao, *Mater Lett*, **2011**, 65, 624-627.

[41] Y.H. Deng, T. Yu, Y. Wan, Y.F. Shi, Y. Meng, D. Gu, L.J. Zhang, Y. Huang, C. Liu, X.J. Wu, D.Y. Zhao, *J Am Chem Soc*, **2007**, 129, 1690-1697.

[42] Y. Deng, C. Liu, D. Gu, T. Yu, B. Tu, D. Zhao, *J Mater Chem*, **2008**, 18, 91-97.

[43] X.H. Li, Y.L. Shen, L.Y. Song, H.N. Wang, H.H. Wu, Y.M. Liu, P. Wu, *Chem-Asian J*, **2009**, 4, 699-706.

[44] P. Gao, A. Wang, X. Wang, T. Zhang, *Chem Mater*, **2008**, 20, 1881-1888.

[45] D. Liu, J.H. Lei, L.P. Guo, K.J. Deng, *Micropor Mesopor Mat*, **2011**, 139, 87-93.

[46] J.M. Xu, A.Q. Wang, X.D. Wang, D.S. Su, T. Zhang, *Nano Res*, **2011**, 4, 50-60.

[47] Y. Wan, H.Y. Wang, Q.F. Zhao, M. Klingstedt, O. Terasaki, D.Y. Zhao, *J Am Chem Soc*, **2009**, 131, 4541-4550.

[48] Q. Li, J. Xu, Z.X. Wu, D. Feng, J.P. Yang, J. Wei, Q.L. Wu, B. Tu, Y. Cao, D.Y. Zhao, *Phys Chem Chem Phys*, **2010**, 12, 10996-11003.

[49] Z.H. Ji, S.G. Liang, Y.B. Jiang, H. Li, Z.M. Liu, T. Zhao, *Carbon*, **2009**, 47, 2194-2199.

[50] R. Xing, H.H. Wu, X.H. Li, Z.L. Zhao, Y.M. Liu, L. Chen, P. Wu, *J Mater Chem*, **2009**, 19, 4004-4011.

[51] R. Xing, N. Liu, Y.M. Liu, H.W. Wu, Y.W. Jiang, L. Chen, M.Y. He, P. Wu, *Adv Funct Mater*, **2007**, 17, 2455-2461.

[52] Y. Wan, X. Qian, N.Q. Jia, Z.Y. Wang, H.X. Li, D.Y. Zhao, *Chem Mater*, **2008**, 20, 1012-1018.

[53] Y. Ishii, Y. Kanamori, T. Kawashita, I. Mukhopadhyay, S. Kawasaki, *J Phys Chem Solids*, **2010**, 71, 511-514.

[54] M.Z. Dai, L.Y. Song, J.T. LaBelle, B.D. Vogt, *Chem Mater*, **2011**, 23, 2869-2878.

[55] Q. Li, R.R. Jiang, Y.Q. Dou, Z.X. Wu, T. Huang, D. Feng, J.P. Yang, A.S. Yu, D.Y. Zhao, *Carbon*, **2011**, 49, 1248-1257.

[56] X.C. Zhao, A.Q. Wang, J.W. Yan, G.Q. Sun, L.X. Sun, T. Zhang, *Chem Mater*, **2010**, 22, 5463-5473.

[57] Z.X. Wu, P.A. Webley, D.Y. Zhao, *Langmuir*, **2010**, 26, 10277-10286.

[58] T. Chen, T. Wang, D.J. Wang, J.Q. Zhao, X.C. Ding, S.C. Wu, H.R. Xue, J.P. He, *Acta Phys-Chim Sin*, **2010**, 26, 3249-3256.

[59] X. Zhuang, Q.F. Zhao, Y. Wan, *J Mater Chem*, **2010**, 20, 4715-4724.

[60] Y.P. Zhai, Y.Q. Dou, X.X. Liu, S.S. Park, C.S. Ha, D.Y. Zhao, *Carbon*, **2011**, 49, 545-555.

[61] L. She, J. Li, Y. Wan, X.D. Yao, B. Tu, D.Y. Zhao, *J Mater Chem*, **2011**, 21, 795-800.

[62] Z.X. Wu, N. Hao, G.K. Xiao, L.Y. Liu, P. Webley, D.Y. Zhao, *Phys Chem Chem Phys*, **2011**, 13, 2495-2503.

[63] J.S. Li, J. Gu, H.J. Li, Y. Liang, Y.X. Hao, X.Y. Sun, L.J. Wang, *Micropor Mesopor Mat*, **2010**, 128, 144-149.

[64] T.M. Zhang, D.L. Zhao, L. Yin, Z.M. Shen, *J Alloy Compd*, **2010**, 508, 147-151.

[65] H. Wang, A.Q. Wang, X.D. Wang, T. Zhang, *Chem Commun*, **2008**, 2565-2567.

[66] (a) L. Sterk, J. Gorka, M. Jaroniec, *Colloid Surface A*, **2010**, 362, 20-27; (b) Jaroniec et al. *Angew Chem Int Ed* **2008**, 112, 11657; (c) Jaroniec et al., *J Phys Chem C*, 2008, 112, 11657; (d) Jaroniec et al., *J Phys Cem C* **2010**, 114, 6298

[67] J.Y. Yao, L.X. Li, H.H. Song, C.Y. Liu, X.H. Chen, *Carbon*, **2009**, 47, 436-444.

[68] Z.H. Jin, C. Yu, X.Y. Wang, Y. Wan, D. Li, G.Z. Lu, *J Hazard Mater*, **2011**, 186, 1726-1732.

[69] Y.L. Shen, X.H. Li, L.Y. Song, H.N. Wang, P. Wu, *Chem J Chinese U*, **2009**, 30, 1375-1379.

[70] L.Y. Song, X.H. Li, H.N. Wang, H.H. Wu, P. Wu, *Catal Lett*, **2009**, 133, 63-69.

[71] R. Liu, Y. Ren, Y. Shi, F. Zhang, L. Zhang, B. Tu, D. Zhao, *Chem Mater*, **2008**, 20, 1140-1146.

[72] S.Y. Yan, Y. Gao, R. Xing, Y.L. Shen, Y.M. Liu, P. Wu, H.H. Wu, *Tetrahedron*, **2008**, 64, 6294-6299.

[73] L. Fang, R. Xing, H.H. Wu, X.H. Li, Y.M. Liu, P. Wu, *Sci China Chem*, **2010**, 53, 1481-1486.

[74] R. Xing, Y.M. Liu, H.H. Wu, X.H. Li, M.Y. He, P. Wu, *Chem Commun*, **2008**, 6297-6299.

[75] Z.X. Wu, D.Y. Zhao, *Chem Commun*, **2011**, 47, 3332-3338.

[76] M.V. Alonso, M. Oliet, J.C. Dominguez, E. Rojo, F. Rodriguez, *J Therm Anal Calorim*, **2011**, 105, 349-356.

# Chapter 2

## Analysis techniques and synthesis strategies

### 2.1 Analysis techniques

Ordered mesoporous materials – and mesoporous phenolic resins and carbons in particular – require advanced techniques to investigate their morphology and characteristics. A brief introduction to the principal analysis methods for mesoporous phenolic resins and carbons is described below.

### 2.1.1 Powder X-ray diffraction

Ordering in solid materials can be visualized by means of X-ray diffraction (XRD). When collecting an X-ray diffraction pattern, an incoming X-ray beam is scattered through the atoms of the material (primary through the atoms' electrons) and is re-radiated in all dimensions. This phenomenon is called elastic scattering. If atoms are arranged in a regular and repetitive way, the reradiation is constructively in specific directions, as determined by Bragg's law: $2dsin\theta = n\lambda$, with $d$ the spacing between the diffracting planes, $\theta$ the incident angle of the beam, $n$ an integer and $\lambda$ the wavelength. The principle of X-ray diffraction is shown in Figure 2.1. Given a certain wavelength, the angle $\theta$ becomes very small for large $d$ values. As a consequence, the unscattered radiation – the primary radiation bundle which is much more intensive – may interfere with the scattered signal. Therefore, small angle X-ray diffraction (SAXS) is recommended for materials with large $d$ values (> 0.5 nm).

Ordered porous materials are amorphous meaning the walls of these solids are not ordered on atomic scale. Here, the ordering of the materials regards the repetitive structure of the pores on mesoscale. Several ordered pore morphologies have been reported and the most common are shown in Figure 2.1.

The X-ray powder diffraction patterns presented in this work were collected on a Siemens D5000 diffractiometer and on a ThermoScientific ARL X'tra diffractometer with a Cu K$\alpha$ radiation with a 0.15418 nm wavelength.
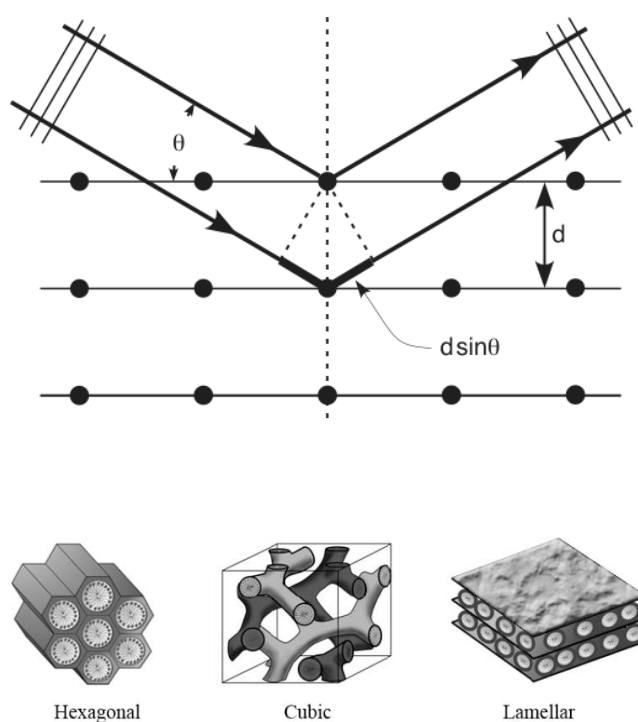


**Figure 2.1 – TOP: Principle of X-ray diffraction. BOTTOM: Main morphologies of ordered mesoporous materials.**

### 2.1.2 Nitrogen sorption

Nitrogen sorption is an analysis technique used to characterize the surface and pore features of porous solids. The main characteristics that can be qualified by physical sorption include surface area, pore volume and pore size distribution. [1]

The physical adsorption technique consists of exposing a porous solid to an inert gas. As a gas molecule randomly encounters the solid, the molecule is attracted to the surface by the surface energy and is adsorbed at least momentarily on the surface. The adsorption of the gas on the solid is a result of the forces of attraction and repulsion between the individual gas molecules and the atoms and ions composing the solid. As the gas pressure increases, the number of molecules per unit time striking the surface and correspondingly the quantity adsorbed molecules increases. In other words, the number of molecules adsorbed at any time increases as a function of increasing pressure. The quantity of molecules adsorbed or desorbed as a function of the relative pressure is known as the adsorption and desorption isotherm respectively.

Figure 2.2 shows a typical nitrogen sorption isotherm of a mesoporous silica SBA-15. At low relative pressure, gas molecules begin to adsorb on the surface. With increasing pressure, a first adsorption layer starts to build up and micropores are being filled, observed by point A in Figure 2.2. As the relative pressure continues to increase, adsorption takes place in multilayers. This is reflected by the linear region of the isotherm between point A and B. Further increasing the pressure, mesopores are filled and capillary condensation occurs, observed by the steep increase of the isotherm between point B and C in Figure 2.2. Ultimately, the absolute pressure approaches the saturation pressure and adsorption is maximized, observed by the plateau between point C and D. After point D, interparticular adsorption of gas molecules occurs.

According to the Brunauer, Deming, Deming and Teller classification, five types of adsorption isotherms can be distinguished relating to the different textures of the solids. An overview of the different isotherms is depicted in Figure 2.3. For porous materials, Type I and Type IV are the most essential isotherms. Type I, also known as the Langmuir adsorption isotherm, is related to microporous materials. The micropores are filled by low relative pressure and shows a nearly horizontal plateau at higher relative pressures. Once the pores are filled, there is mainly adsorption at the exterior of the porous material. Typically, microporous materials like zeolites, activated carbon and metal organic frameworks exhibit Type I isotherms with very high (Langmuir) surface areas of more than 1000–1500m²/g. Type IV isotherms are identified with mesoporous materials with pores between 2 and 50 nm diameter. Here, the knee in the isotherm represents the near-completion of the first monolayer and the steep capillary condensation step at higher relative pressure indicates the increased uptake of gas molecules in the pores. The best known mesoporous materials giving typical Type IV isotherms are the M41S-family and SBA-type materials.
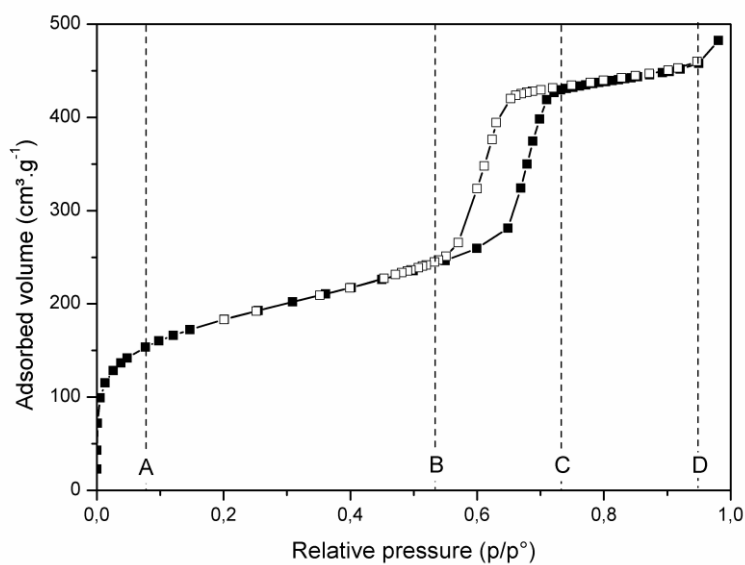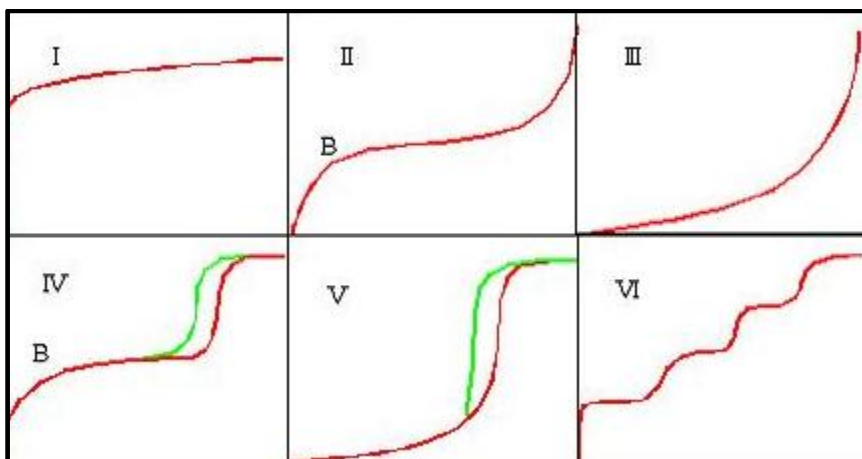
**Figure 2.2 – TOP: different types of isotherms. BOTTOM: Nitrogen adsorption and desorption isotherm of a mesoporous SBA-15.**

The energy involved in physical adsorption is very low and does not exceed 45 kJ/mol. As a consequence, the adsorbed molecules can easily be removed or desorbed by decreasing the pressure over the sample. If pressure is systematically reduced, desorption will occur. Since this desorption process has a different path than adsorption, the desorption branch

is observed at lower relative pressure, showing a hysteresis loop. The shape of the hysteresis reflects a fingerprint of the pore texture of the solid. Figure 2.4 represents the four different types of hysteresis loops classified by IUPAC. Type H1 hysteresis reflects cylindrical pores, open at both sides. Type H2 hysteresis results from ink bottle pores. Type H3 and H4 hysteresis loops are associated with slit-shaped pores or spaces between parallel plates.

Thermodynamically, the hysteresis loops have to close at a relative pressure 0.42. Porous materials with a capillary condensation step at relative pressure < 0.42 do not exhibit hysteresis loops (e.g. microporous materials, M41S family, …). However, the isotherm of mesoporous phenolic resins is often not closed at low relative pressures. This is explained by the swelling ability of polymers in liquid nitrogen during the measurement.
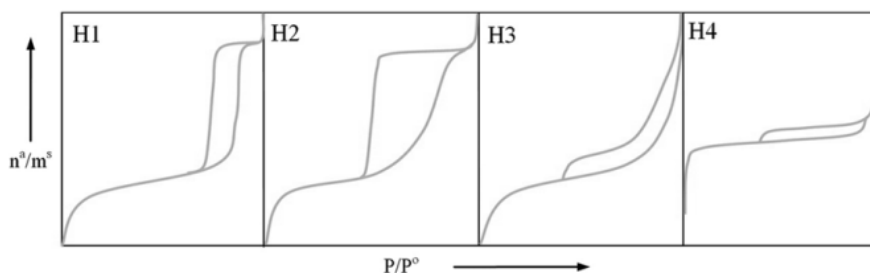


**Figure 2.3 – IUPAC classification of hysteresis loops.**
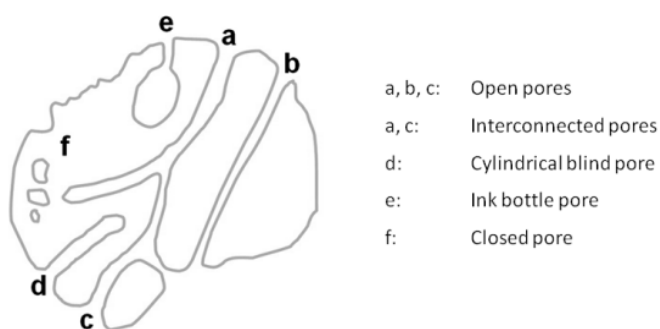


**Figure 2.4 – Overview of different pore types.**

*Specific surface area*

The specific surface area of microporous materials is determined based on the Langmuir theory. The Langmuir equation in its linear form is presented as:

$$\frac{p_A}{V_A} = \frac{1}{KV_m} + \frac{p_A}{V_m} \quad (2.1)$$

With $V_A$ the adsorbed volume at pressure $p_A$, $V_m$ the volume of gas that is adsorbed at the saturation pressure $p°$ and $K$ the adsorption coefficient. Plotting $\frac{p_A}{V_A}$ versus $p_A$ yields a straight line with intercept $\frac{1}{KV_m}$ and slope $\frac{1}{V_m}$. Here $V_m$ can be determined. The specific surface area is then calculated as:

$$S\left(\frac{m^2}{g}\right) = \frac{V_m}{2400} N_A \, A \, 10^{-18} \quad (2.2)$$

with $N_A$ the number of Avogadro and $A$ the mean cross sectional of nitrogen = 0.162nm².

The specific surface area of mesoporous materials is determined by the BET equation (theorie of Brunauer, Emmet and Teller) commonly known as the BET-method. The BET equation in its linear form is:

$$\frac{p_A}{V_A p° - p_A} = \frac{1}{V_m C} + \frac{C-1}{V_m C} \frac{p_A}{p°} \quad (2.3)$$

with $C$ the value for the strength of interaction between the gas molecule and the solid. If $\frac{p_A}{V_A p° - p_A}$ is plotted versus $\frac{p_A}{p°}$, a linear relation is obtained (mostly in the region with relative pressure $0.05 - 0.30$). Then, $V_m$ can be determined and the specific surface area is calculated using equation (2.2).

*Total pore volume*
The total pore volume is calculated at maximized adsorption at relative pressure p/p° = 0.97-0.99 using:

$$Vtot = \frac{V_A}{22400} . 34.6 cm^3 \quad (2.4)$$

*Pore size distribution*

The pore size distribution is calculated by the Barrett, Joyner, Halende (BJH)method.[2]

### 2.1.3 Diffuse reflectance infrared fourier transform spectroscopy (DRIFT)

Infrared (IR) spectroscopy is one of the most important and popular tools for structural elucidation and compound identification.[2] At temperatures above absolute zero, all the atoms in molecules are in continuous vibration. When the frequency of a specific vibration is equal to the frequency of the IR radiation directed on the molecule, the molecule absorbs the radiation. As a result, different functional chemical groups absorb characteristic frequencies of IR radiation. Those that produce a net change in the dipole moment may result in an IR activity. The total number of observed absorption bands is generally different from the total number of fundamental vibrations. On the one hand, it is reduced because some vibrations are not IR active and on the other hand, additional bands are generated by the appearance of overtones or coupling interactions of two fundamental absorption frequencies. The major types of molecular vibrations are stretching and bending and are illustrated in Figure 2.5. Although, the absorption involves discrete, quantized energy levels, no discrete lines in the spectrum are observed. This can be explained by accompanying rotational motions of the atoms, resulting in broader absorption bands.
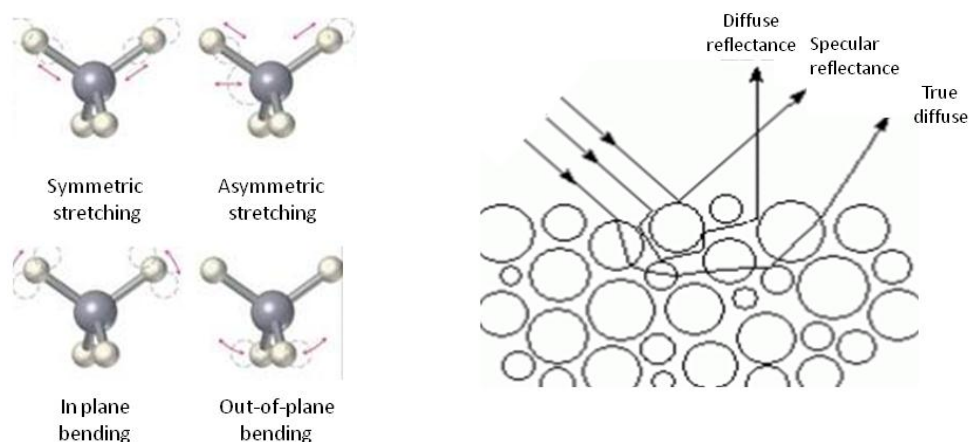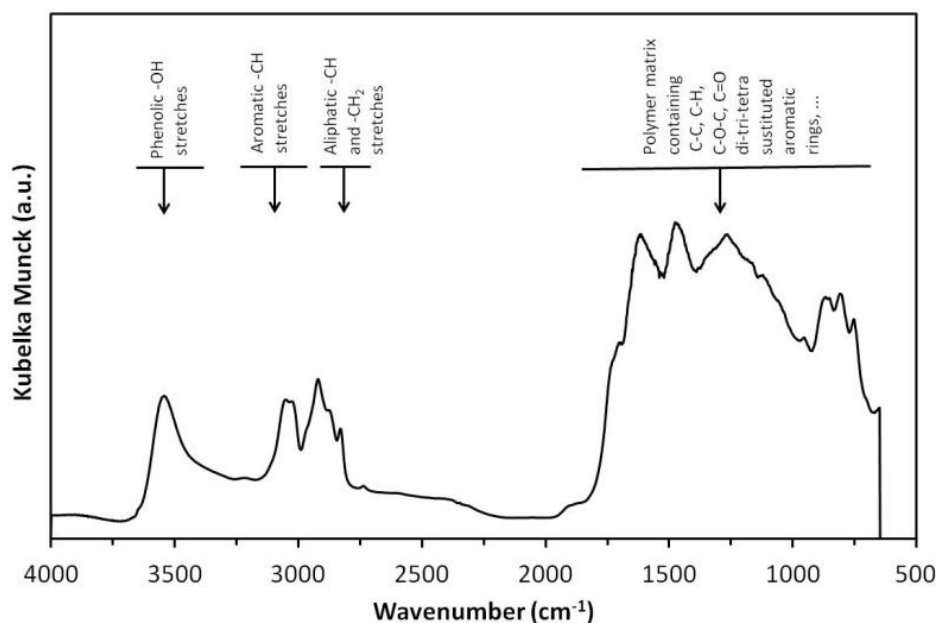
**Figure 2.5 – TOP LEFT: Various types of vibrations of molecules. TOP RIGHT: Diffuse reflectance infrared spectroscopy. BOTTOM: DRIFT-spectrum of ordered mesoporous phenolic resins**

The diffuse reflectance technique is a powerful tool for acquiring IR spectra of powders. Here, IR radiation is focused onto the surface of a solid sample and results in two types of reflections: specular reflectance, which directly reflects off the surface and has equal angles of incidence and reflectance, and diffuse reflectance, which penetrates into the sample and then scatters in all directions. Special reflection accessories are designed to collect and refocus the resulting diffusely scattered light by large ellipsoidal mirrors, while minimizing or eliminating the specular reflectance, which complicates and distorts the IR spectra. The sample can be analyzed as dispersions in IR-transparent matrices such as KBr. Dilution of analyte in a non-absorbing matrix increases the proportion of diffuse reflectance. The spectra are plotted in Kubelka–Munk units, which relates sample concentration to diffuse reflectance and applies a scattering factor. Diffuse reflectance spectroscopy allows the in situ measurements at elevated temperature, pressure and/or atmosphere. For IR measurements, water has to be avoided. Prior to analysis, the samples are dried at 90°C under vacuum overnight and scratched to a fine powder. KBr powder was used as blank. The DRIFT-spectra presented in this work were measured on a EQUINOX-55 of Bruker and on a Nicolet 6700 FT-IR spectrometer of ThermoScientific.

### 2.1.4 UV/VIS and RAMAN spectroscopy

Mesoporous phenolic resins and carbons are dark brownish-black coloured. This makes spectroscopic studies of these materials highly challenging. UV/VIS spectroscopy has shown not to be an appropriate tool to study these solids due to the intrinsic interaction of light with a dark solid (100% absorption). In case of RAMAN spectroscopy, sample heating due to the phenomenon of black body radiation is responsible for a broad band in the RAMAN spectrum. This broad 'support band' dominates the RAMAN spectrum completely. It was not possible to avoid or minimize this interference by changing the laser type from FT-RAMAN (1064 nm laser) to dispersive RAMAN equipment (532 nm and 780 nm laser). As a result, RAMAN measurements did not allow us to give more insight in the nature of these mesoporous solids.

### 2.1.5 X-ray photoelectron spectroscopy (XPS)

X-ray photoelectron spectroscopy (XPS) is a quantitative spectroscopic technique for determining the electronic state of the metals present in a solid sample.[3] XPS spectra are obtained by irradiating a material with an X-ray beam while simultaneously measuring the kinetic energy and number of electrons that escape from the upper layer (1 to 10 nm) of the sample. Because the energy of an X-ray with particular wavelength is known, the electron binding energy of the emitted electrons can be determined by using following equation:

$$E_{binding} = E_{photon} - (E_{kinetic} + \varphi) \quad (2.5)$$

where $E_{binding}$ is the binding energy (BE) of the electron, $E_{photon}$ is the energy of the X-ray photons being used, $E_{kinetic}$ is the kinetic energy of the electron as measured by the instrument and $\varphi$ is the work function of the spectrometer. XPS requires ultra-high vacuum conditions. In this study, XPS measurements were recorded on a X-ray photoelectron spectroscopy S-Probe XPS spectrometer with monochromated Al (1486 eV) exciting radiation from Surface Science Instruments (VG). Before the measurement, ion beam etching is performed to clean off some of the surface contamination. Since the metal concentration supported on the mesoporous phenolic resins in this work were very low, ultra-long measurements (> 48 hours) were performed. These ultra-long measurements under ultra-high vacuum conditions may have an effect on the interpretation of the XPS-data. Additionally, the materials show charging or partial charging during the measurements, which leads to double or partial double XPS-peaks. This phenomenon is attributed to the insulator properties of phenolic resins.

**2.1.6 Scanning electron microscopy (SEM) and transmission electron microscopy (TEM)**

SEM and TEM measurements are performed to visualize the particle size on micrometer scale and the pores on nanometer scale of ordered mesoporous phenolic resin respectively. Figure 2.6 and 2.7 show some representative images. Note that the SEM-measurements of mesoporous phenolic resins are not very clear and show white spots. This is attributed to the insulating property of phenolic resins. Gold sputtering to enhance the conductivity of the samples was not able to avoid or reduce this side-effect.
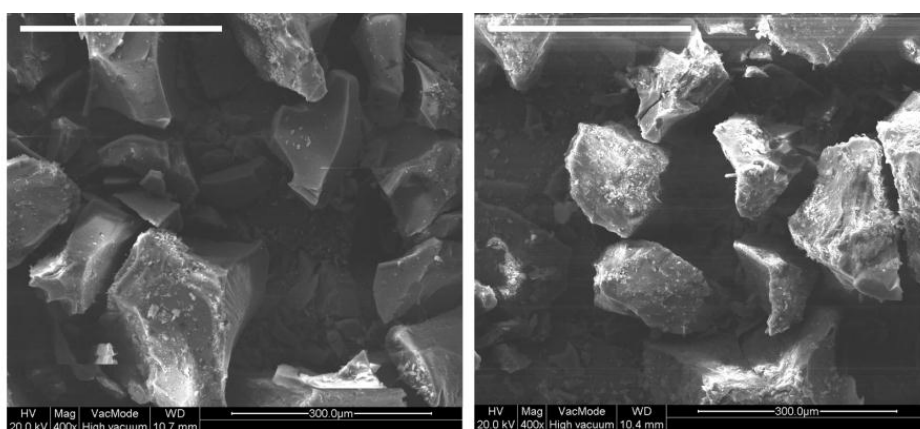


**Figure 2.6 – SEM images of mesoporous phenolic resins calcined at 350°C. The length of the scale bar represents 300 $\mu$m.**
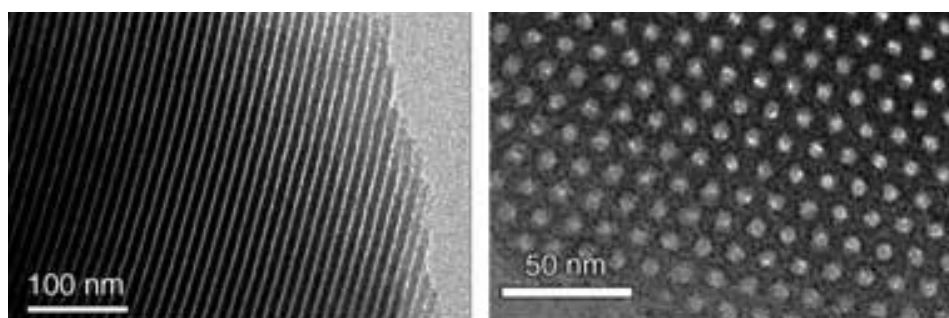


**Figure 2.7 – TEM images of mesoporous phenolic resins calcined at 350°C. Left: FDU-15 viewed at the [110] direction. RIGHT: FDU-16 viewed at the [111] direction. [4]**

**2.2 Synthesis strategies**

Ordered mesoporous phenolic resins can be synthesized according to three main procedures, resulting in their different morphologies. Below, the three different synthesis recipes are described; they mainly differ in conditions (pH, T) of the polymerization of the carbon precursors.

**2.2.1 Hydrothermal aqueous procedure**

Type A materials are synthesized using phenol/formaldehyde as carbon source in alkaline medium.[5] In a typical synthesis, phenol (2.0 g) and formaldehyde (Formaline, 37wt% formaldehyde in water) are dissolved in a NaOH solution. Then the mixture is stirred at 70°C for 30 minutes. Next, this mixture was added to an aqueous solution of F127 at room temperature and stirred to obtain a clearless solution. Subsequently, the mixture was stirred for 75 hours at 65°C and finally for 24 hours at 70°C. The obtained red-brown product was collected by filtration, washed with water, dried in air and finally calcined.

**2.2.2 Evaporation induced self-assembly**

Type B materials are synthesized using phenol/formaldehyde as carbon source in alkaline medium.[4] In a typical synthesis, phenol (1.6 g) is melted at 40°C and NaOH solution is slowly added to the solution. Formaldehyde (Formaline, 37wt% formaldehyde in water) is added dropwise to the solution. Next, the mixture is stirred at 70°C for 1 hour. After cooling down, the mixture is neutralised with HCl-solution to pH 7 and water was removed under vacuum at 45°C. Subsequently, the final product was dissolved in ethanol and added to an ethanol solution of F127 and stirred for 10 minutes to a homogeneous phase. Then, the mixture was transferred to a dish and the solvent was evaporated overnight at room temperature. The dish was placed in an oven at 100°C for 24h to polymerize the phenolic resin. Finally, the thin film was scraped and transferred to the tubular furnace for calcination.

**2.2.3 Two-phase system based pathway**

Type C materials are synthesized using resorcinol/formaldehyde as carbon source in acid medium.[6] In a typical synthesis, resorcinol (2.1 g) is added to an ethanol/water solution of F127 and stirred for 30 minutes at room temperature. Then, formaldehyde (Formaline, 37wt% formaldehyde in water) is added and stirred for 30 minutes. Finally, HCl is added dropwise and the solution is stirred for 2 hours at room temperature. While keeping the solution untouched, the mixture separated into two-phases: the transparent upper phase was ethanol-water rich and the yellow lower phase was polymer-rich. Subsequently, the

upper phase was removed and the lower phase was heated in an oven at 100°C for 24 h followed by calcination.

### 2.2.4 Calcination and carbonization

Calcination is performed in a tubular furnace under nitrogen atmosphere at 350 or 400°C (heating rate: 1.0°C/min).[7] After calcination the yellow-orange-red samples are dark-black colored and are abrasive. For carbonization, the samples are heated to 800°C under nitrogen atmosphere.

### 2.3 References
[1] R. Xu, W. Pang, J. Yu, Q. Huo, J. Cheng, Chemistry of zeolites and related porous materials - Synthesis and Structure, 2007, Wiley
[2] V. Valtchev, S. Mintova,  M. Tsapatsis, Ordered porous solids - recent advances and prospects, 2009, Elsevier.
[3] P. Van Der Heide, X-ray photoelectron spectroscopy - An introduction to principles and practices, 2012, Wiley.
[4] Y. Meng, D. Gu, F.Q. Zhang, Y.F. Shi, H.F. Yang, Z. Li, C.Z. Yu, B. Tu, D.Y. Zhao, *Angew Chem Int Edit*, **2005**, 44, 7053-7059.
[5] F.Q. Zhang, Y. Meng, D. Gu, Y. Yan, C.Z. Yu, B. Tu, D.Y. Zhao, *J Am Chem Soc*, **2005**, 127, 13508-13509.
[6] L.Y. Song, K.X. Li, X.H. Li, P. Wu, *React Kinet Mech Cat*, **2011**, 104, 99-109.
[7] X.X. Li, A.B. Larson, L. Jiang, L.Y. Song, T. Prichard, N. Chawla, B.D. Vogt, *Micropor Mesopor Mat*, **2011**, 138, 86-93.

# Chapter 3

## Mesoporous phenolic resins as support for sulphonic acid catalysts

### 3.1 Introduction

Sulphonic acid-catalyzed reactions are frequently required in industrial processes for the production of hydrocarbons, fine chemicals and pharmaceutical products.[1] Although sulphuric acid has shown its benefits as acid catalyst in the earlier stages, this liquid acid as homogeneous catalyst brings along corrosion, catalyst waste, separation and regeneration issues in industrial processes. For these reasons, solid sulphonic acid based catalysts are strongly desirable provided that they exhibit large stability and can be simply separated and regenerated after catalytic cycles.[2, 3] In the 1960s, ion exchange resins containing sulphonic acid groups were introduced as heterogeneous solid acid catalysts and nowadays a number of ion exchange resin families are commercially available.[4] The Amberlyst® family, produced by the Rohm and Haas company, consists of polystyrene crosslinked with divinylbenzene containing aryl sulphonic acid Ar-SO$_3$H groups.[5] The swelling capacity of this macroporous gel depends on the degree of crosslinking. Other similar and commercially available families of sulphonic acid polystyrene-divinylbenzene based ion-exhange resins are Dowex® of Dow Chemicals, Indion® from Ion exchange ltd. India, Lewatit® of Lanxess, etc. All these resin types have shown their benefits. However, these materials have limited thermal stability (< 150°C) and exhibit low specific surface area (< 50m²/g). The stronger acidic ion-exchange resin Nafion®, produced by DuPont, is more stable at higher temperatures (< 280°C) and consists of a copolymer of

tetrafluoroethylene and perfluoro-3,6-dioxa-4-methyl-7-octenesulphonyl fluoride with strong acidic $-CF_2CF_2SO_3H$ sites.[6] Nevertheless, this fluorinated resin also exhibits very low specific surface areas and rather low acidity loadings.

In 2007, the research group of Xing et. al. first introduced ordered mesoporous phenolic resins, as novel solid sulphonic acid catalysts.[7] These sulphonated FDU-14 and FDU-15 were evaluated as new catalysts for the liquid phase Beckmann rearrangement of cyclohexanone oxime and for the condensation of bulky aldehydes with alcohol. Very recently, FDU-15 and FDU-16 were reported as solid acid catalyst for Fisher esterification reactions.[8, 9] All these catalysts showed high acidity loadings (~ 2 mmol $H^+$/g) and good catalytic performance in the first catalytic run. However, regeneration tests were not reported. Tian et. al. showed that the catalytic conversion significantly decreased after the first run.[10] This was explained among others by the hydrolysis of the $-SO_3H$ groups (26% of the catalytic sulphonic acid sites were released after the first run)[11]; the catalytic conversion remained relatively stable in the second run. The sulphonation of the mesoporous phenolic resins is only reported by a post-synthetic sulphonation of the methylene bridged aromatic rings by stirring the support in a concentrated $H_2SO_4$ solution or *via* a gas phase reaction with fuming sulphuric acid.[7-10, 12]

In this study, the mesoporous phenolic resins are sulphonated by four different sulphonation pathways, based on the anchoring points in the framework of the resin support (aromatic rings *vs*. hydroxyl groups) and the nature of the sulphonic acid functionalities (aromatic *vs*. aliphatic). These novel solid acid catalysts contain different acidity loadings ranging from 0.5 to 2 mmol $H^+$/g. The leaching resistance in aqueous medium was evaluated. Finally, the catalysts were tested in the Fisher esterification of propanol with acetic acid. As an additional proof of concept, the novel sulphonated mesoporous phenolic resins were also used as support for the non-covalent immobilization of a chiral diamine organocatalysts and the catalytic performance in the asymmetric aldol reaction of 2-butanone with an aromatic aldehyde is evaluated.

## 3.2 Sulphonation methods

Figure 3.1 shows a schematic representation of the four sulphonation procedures of mesoporous phenolic resins. The aromatic framework of the resins was functionalized by: (i) a direct sulphonation introducing aromatic sulphonic acid functionalities on the aromatic ring and (ii) an alkyl sulphonation of the aromatic ring yielding methylene sulphonic acid groups. On the other hand, the phenolic hydroxyl surface was functionalized by using (iii) an aryl silane, *viz*. 2-(4-chlorosulphonyl phenyl)ethyl trichlorosilane and (iv) a propyl silane, 3-mercaptopropyltrimethoxysilane.
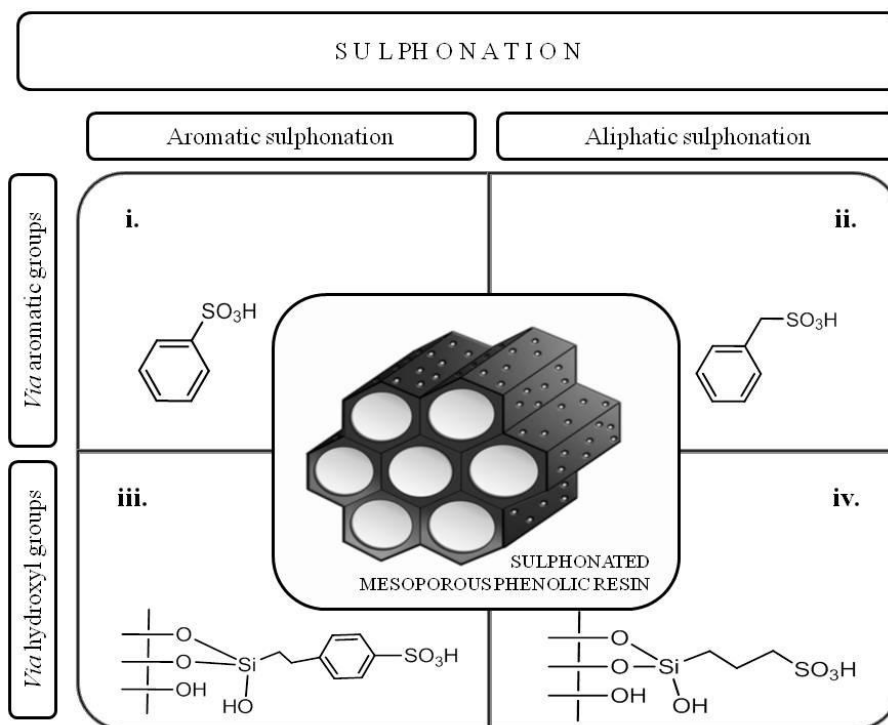
**Figure 3.1 – Overview of the different sulphonation pathways of mesoporous phenolic resins yielding aliphatic and aromatic sulphonic acid functionalities.**

The first pathway (i) represents an electrophilic aromatic substitution of an aromatic H-atom by a $SO_3H$-group. The reaction mechanism is shown in Figure 3.2a. Note that the reactive species is $SO_3$ and that this direct sulphonation is reversible (equilibrium arrows). In this study, this reaction was performed using four different sulphonic acid precursors: (a) aqueous sulphuric acid, (b) aqueous sulphuric acid/triflic acid anhydride, (c) fuming sulphuric acid and (d) chlorosulphonic acid. The first three precursors contain a relatively high concentration of reactive $SO_3$ gas, according to reaction (i) in Figure 3.2b. Remark that for catalyst (ib), triflic acid anhydride $((CF_3SO_2)_2O = Tf_2O)$ was added to the solution in order to generate additional $SO_3$ reactive species *in situ*. According to the principle of Le Chatelier, the equilibrium (i) in Figure 3.2b shifts to right when sulphuric acid is dehydrated by violent reaction of trifilic acid anhydride with water (Figure 3.2b, ii). Indeed, as can be seen from Table 3.1, by adding triflic acid anhydride the acidity more than doubles from 0.24 to 0.59 mmol $H^+$/g, determined by acid-base titration. The highest acidity loading was obtained when fuming sulphuric acid, containing a high $SO_3$ concentration, was used: an acidity of 1.90 mmol $H^+$/g was determined.



(a)

(b)  $H_2SO_4 \rightleftharpoons H_2O + SO_3$ (i)

$Tf_2O + H_2O \longrightarrow 2\ TfOH$ (ii)
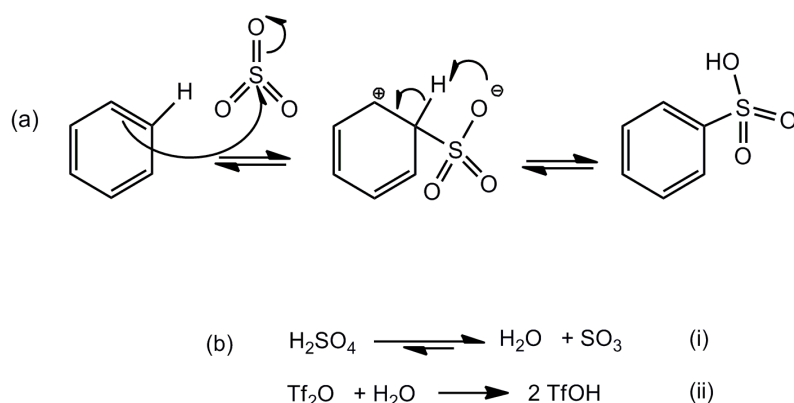
**Figure 3.2 – (a) Reaction mechanism of the sulphonation of aromatic ring with $SO_3$ and (b) proposed reaction mechanism of the *in situ* production of $SO_3$ with a sulphuric acid/triflic acid anhydride mixture (Triflic acid anhydride = $(CF_3SO_2)_2O = Tf_2O$)**

Next, sulphonation procedure (ii) occurs via a chloromethylation of the aromatic ring according to the procedure described by Samuels et. al. [13] The benzyl chloride is then converted to a sulphonic acid group by treating the support successively with an excess of sodium thiosulphate solution, a warm HCl-solution and finally an oxidizing procedure. After filtration and a washing procedure, the sulphonated resin of procedure (ii) was loaded with an acidity of 0.86 mmol $H^+$/g.

Next to aromatic functionalities, mesoporous phenolic resins also contain a high number of surface hydroxyl groups. This high density of hydroxyl functionalities can be clearly seen from the broad band at 3600-3300cm$^{-1}$ in the DRIFT-spectra, corresponding with –OH (and Ar-OH stretches) in Figure 3.3. [14] The aromatic –CH stretches are visible at 3100-3000 cm$^{-1}$ and the peaks between 3000-2800 cm$^{-1}$ can be attributed to aliphatic $CH_2$ stretches. Between 1800-800 cm$^{-1}$, the peaks are originating from the organic polymer framework. These functionalities are used as anchoring points for the silanation with a sulphonic acid silane precursor, pathway (iii) and (iv) in Figure 3.1. Note that for procedure (iv) a propyl thiol silane is used and therefore an extra oxidation step is required to convert the thiol functionality to a sulphonic acid group. The successful oxidation was proven by XPS measurements were the S 2p peak shifted from 163.7eV (S: -II) to 168.1eV (S: +VI), shown in Figure 3.3.[15] Simultaneously to the oxidation, the methoxy groups of the silane precursor were hydrolysed. After the silanation reactions, acidity loadings of 0.52 and 0.74 mmol H$^+$/g are obtained for procedure (iii) and (iv) respectively. As a reference, mesoporous silica SBA-15, was also functionalized using similar silanation procedures.[16, 17] The porosity and acidity properties of all the sulphonated supports are summarized in Table 3.1.
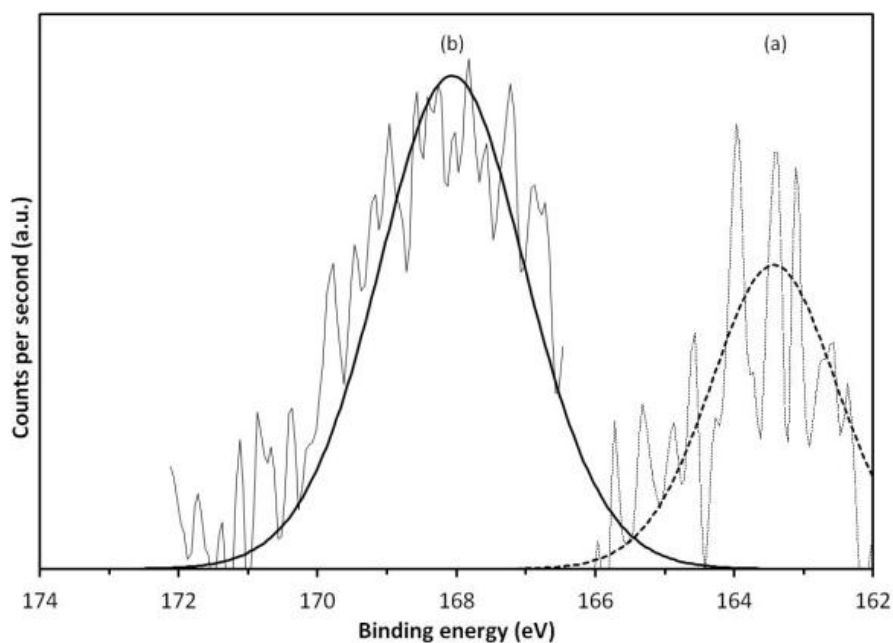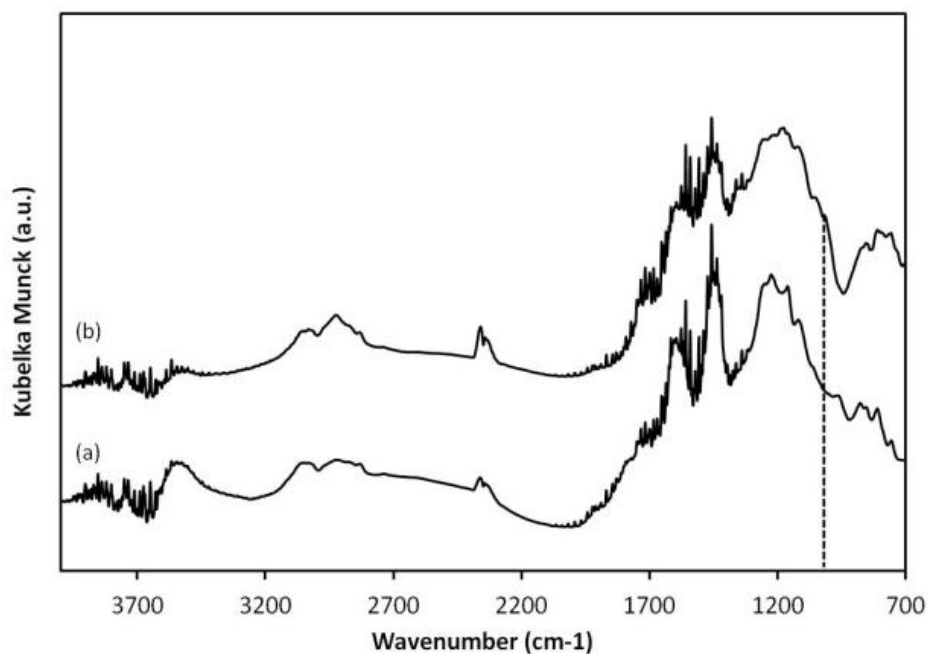
**Figure 3.3 – TOP: XPS-spectra of mesoporous phenolic resin of catalyst (iv) (a) before and (b) after oxidation procedure. The successful oxidation of the thiol function is proved by the shift of the S 2p peak from 163.7eV (-SH) to 168.1eV (-SO$_3$H). BOTTOM: DRIFT-spectra of mesoporous phenolic resin (a) before and (b) after sulphonation and oxidation (catalyst iv). The new absorption band at 1032cm$^{-1}$ in the DRIFT-spectrum can be assigned to the symmetric stretching of the S=O bond.[7]**

**Table 3.1 – Overview of the porosity properties and the acidity loadings of the sulphonated mesoporous catalysts.**

| | | | $S_{BET}$[a] [m²/g] | $V_p$[b] [cm³/g] | Acidity[c] [mmol H⁺/g] |
|---|---|---|---|---|---|
| Sulphonated phenolic resins | | | | | |
| | | Original resin | 461 | 0.61 | 0.00 |
| (i) | a | -Ar-SO$_3$H (H$_2$SO$_4$) | 453 | 0.60 | 0.24 |
| | b | -Ar-SO$_3$H (H$_2$SO$_4$ / Tf$_2$O) | 448 | 0.53 | 0.59 |
| | c | -Ar-SO$_3$H (SO$_3$/H$_2$SO$_4$) | 248 | 0.37 | 1.90 |
| | d | -Ar-SO$_3$H (ClSO$_3$H) | 432 | 0.54 | 1.31 |
| (ii) | | -Ar-CH$_2$-SO$_3$H | 412 | 0.56 | 0.86 |
| (iii) | | -O-Si-(CH$_2$)$_2$-Ar-SO$_3$H | 425 | 0.54 | 0.52 |
| (iv) | | -O-Si-(CH$_2$)$_3$-SO$_3$H | 428 | 0.60 | 0.74 |
| Reference sulphonated materials | | | | | |
| | | Amberlyst-15® | 45 | 0.20 | 4.8 |
| | | SBA-15 -O-Si-(CH$_2$)$_2$-Ar-SO$_3$H | 541 | 0.77 | 0.99 |
| | | SBA-15 -O-Si-(CH$_2$)$_3$-SO$_3$H | 532 | 0.76 | 0.75 |

[a] Specific surface area calculated using the BET-method; [b] total pore volume determined at p/p° = 0.97-0.99; [c] determined by acid-base titration; n.d. = not determined

**3.5 Catalytic performance in the Fisher esterification**

The catalytic properties of the sulphonic acid functionalized mesoporous polymers are evaluated in the esterification reaction of propanol with acetic acid. The Fisher esterification reaction corresponds to an acid catalyzed condensation of an alcohol with a carboxylic acid, producing the corresponding ester and water as by-product , see Figure 3.4. [18-20] The catalytic properties are presented in Table 3.2. Two remarks have to be made: (1) a relative high conversion of 20% after 3 hours is observed in case of the blank test. (2) The conversions are presented based on experiments with equal catalyst mass (due to limitation in batch sizes and in the amount of catalyst available). Therefore, the turn over number values give a more representative and objective indication of the catalytic performance of the catalysts. The turn over number is defined as the number of substrates molecules converted per number $H^+$. The conversion and turn over numbers (TON) are calculated after 3 hours reaction. As a reference, the catalytic performance of Amberlyst-15 and sulphonated SBA-15 materials are also depicted in Table 3.2.

From Table 3.2, it can be seen that catalyst i (a-d) is highly active in the esterification reaction in the first run. Conversions larger than 95% after three hours reaction are observed. However, in the second run, the catalytic activity decreases significantly with more than 50%. Catalyst ii showed rather low catalytic activity in the first run and a small decrease of 11% in the second run. For catalyst iii and iv, average catalytic activity is observed in the first run and decreases with 50% and 34% for catalyst iii and iv respectively. Based on the TON values, catalyst ia shows the highest catalytic activity with a TON value of 2.38. This is a direct consequence of the rather low acidity loading of 0.24 mmol $H^+$/g (see Table 3.1). The other catalysts exhibit TON values between 0.31 and 0.98. Finally, remark that the commercial reference catalyst, Amberlyst-15 exhibits a very low TON value of 0.12, representing a poor catalyst efficiency. This is attributed to the high acidity loading and the swelling of the catalyst.
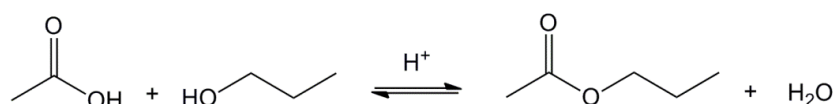


**Figure 3.4 – Acid catalyzed Fisher esterification of acetic acid with propanol to propyl acetate and water as by-product.**

**Table 3.2 – Overview of the catalytic performance of the sulphonated mesoporous catalysts in the esterification of acetic acid with propanol**

| | | | 1st run | | 2nd run |
|---|---|---|---|---|---|
| | | | Conversion [a] | TON [b] | Conversion [a] |
| | | | [%] | | [%] |
| Sulphonated phenolic resins | | | | | |
| | | Original resin | 20 | - | n.d. |
| (i) | A | -Ar-SO$_3$H (H$_2$SO$_4$) | 95 | 2.38 | 42 |
| | B | -Ar-SO$_3$H (H$_2$SO$_4$ / Tf$_2$O) | 96 | 0.98 | 41 |
| | C | -Ar-SO$_3$H (SO$_3$/H$_2$SO$_4$) | 98 | 0.31 | 39 |
| | D | -Ar-SO$_3$H (ClSO$_3$H) | 97 | 0.44 | 35 |
| (ii) | | -Ar-CH$_2$-SO$_3$H | 52 | 0.36 | 41 |
| (iii) | | -O-Si-(CH$_2$)$_2$-Ar-SO$_3$H | 76 | 0.88 | 38 |
| (iv) | | -O-Si-(CH$_2$)$_3$-SO$_3$H | 68 | 0.55 | 45 |
| Reference sulphonated materials | | | | | |
| | | Amberlyst-15® | 95 | 0.12 | 67 |
| | | SBA-15 -O-Si-(CH$_2$)$_2$-Ar-SO$_3$H | 92 | 0.56 | 68 |
| | | SBA-15 -O-Si-(CH$_2$)$_3$-SO$_3$H | 93 | 0.74 | 72 |

In a typical catalytic run, 30 mmol propanol, 100 mmol acetic acid and 30 mmol toluene (internal standard) were refluxed in a two-neck Schlenk flask under vigorous stirring at 90°C. Subsequently, 50 mg dried catalyst was added. [a] Propanol conversion determined by GC after 3 hours reaction; [b] TON calculated after 3 hours reaction based on the H$^+$-loading, the TON values in the first run are calculated based on the original acidity loadings in Table 3.1; n.d. = not determined.

**3.4 Leaching resistance in aqueous medium**

During the Fisher esterification water is produced as by-product and therefore the solid acid catalysts have to be stable in aqueous medium (Figure 3.4). [21] In order to evaluate the stability of the newly developed sulphonated mesoporous materials, leaching tests were performed. Here, the freshly synthesized sulphonated catalysts are stirred for one day in warm water (24h, 80°C) and the acidity loadings are determined before and after the stress procedure. An overview of the results are shown in Figure 3.5. It can be seen that all the catalysts lose a significant amount of acidity after the first leaching treatment (for catalyst iii and iv more than half of the initial amount is lost). After a first leaching treatment, the acidity loadings of catalyst id, iii and iv further decreases with additional leaching treatment. After three runs, catalysts iii does not remain any acidity loading, determined by acid-base titration. In contrast, catalyst ii shows an constant acidity after the first leaching procedure (0.5 mmol H$^+$/g). The differences in leaching behavior between the catalysts can be explained by the nature of the sulphonic acid functionalities. For catalyst i (and iv), the aryl sulphonic acid group is directly bounded on the aromatic ring. As can be seen in Figure 3.2a, the equilibrium easily shifts to left in acidic medium. As a consequence, the sulphonation of the aromatic ring is undone and the catalyst loses its acidity. Further, the weakness of catalyst iii and iv is situated at the Si-O-C bond. The strength is comparable with an ether bond which is sensitive to hydrolysis (the hydrolysis products are 3.32 kJ/mol more thermodynamically favored than the Si-O-C bonding). In contrast, for catalyst ii, an alkyl sulphonic acid group is introduced in the material. This alkyl functionality is more stable towards hydrolysis. [22, 23] Here, a sulphonated material with a stable acidity loading of 0.5 mmol H$^+$/g after different leaching treatments was obtained by an alkylation procedure. As a summary, the alkyl sulphonated mesoporous phenolic resins (catalyst ii) seems to be the most promising and stable solid acid catalyst of the series of newly developed phenolic resin catalysts in this research work. As already reported for sulphonated periodic mesoporous organosilane materials (PMOs), esterification under water free conditions, i.e. with dean-stark set-up, may probably further increase the regeneration capability of these sulphonated phenolic resin catalysts.[23a]
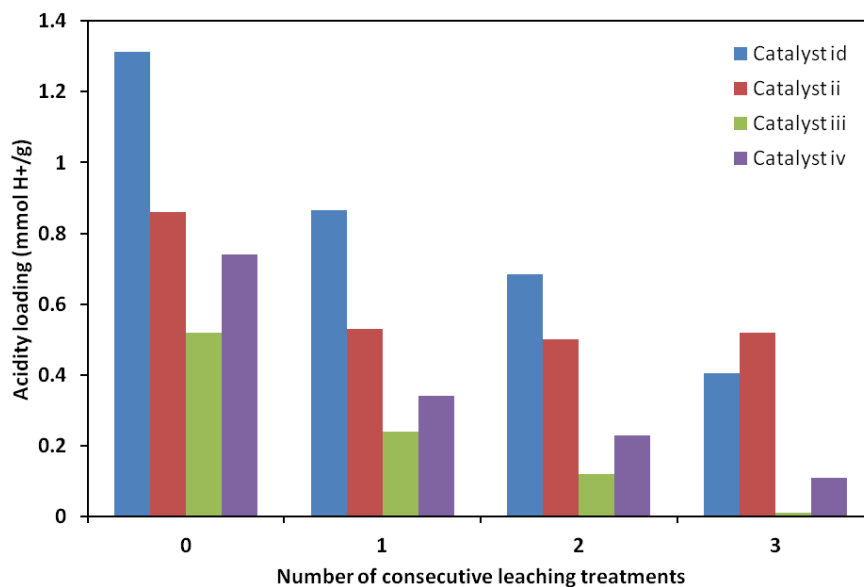
**Figure 3.5 – Leaching resistance of sulphonated mesoporous phenolic resins in aqueous medium**

## 3.5 Sulphonated mesoporous phenolic resins as support for chiral diamine organocatalysts

### 3.5.1 Introduction

Nowadays, the field of organocatalysts encounters a revival of interest due to their unique characteristics such as high catalytic performance and exceptional stereospecificity in chiral catalytic reactions.[24] In particular, recent research intensively focuses on the heterogenization of chiral organocatalysts derived from amino acids. Typically, the immobilization is achieved via a covalent attachment onto solid supports.[25] However, most of these supported organocatalysts demonstrated reduced activity and selectivity in comparison with the parent catalysts. This can be explained by the multiple synthetic steps and the structural changes to the parent catalyst structure which are required for covalent immobilization.

An alternative heterogenization strategy involves the immobilization of a homogeneous catalyst by a non-covalent linkage. This approach limits synthetic modifications of the original catalyst and offers facile immobilization with maintained or even improved catalytic activity and stereoselectivity. The non-covalent immobilization has recently been

reviewed by Fraile et. al. and was classified into four categories depending on the nature of the catalyst-support interaction.[26]

In this second study, a chiral diamine catalyst, an amino acid *L*-phenylalanine derivative with long alkyl chains is non-covalently immobilized via an acid-base interaction on sulphonated mesoporous phenolic resins as support (Figure 3.6a). This electrostatic immobilization of chiral amines has been proven to be very efficient for organocatalysts. It has been shown that the acid-base interaction not only acts as anchoring place, but it also plays a key role in the catalytic activity and stereospecificity of the catalyst. [27, 28] Here, the influence of the nature of the sulphonic acid functionality (aliphatic *vs*. aromatic) on the catalytic activity and enantioselectivity has been investigated in the asymmetric aldol reaction of 2-butanone with 4-(trifluoromethyl)benzaldehyde (Figure 3.6b).
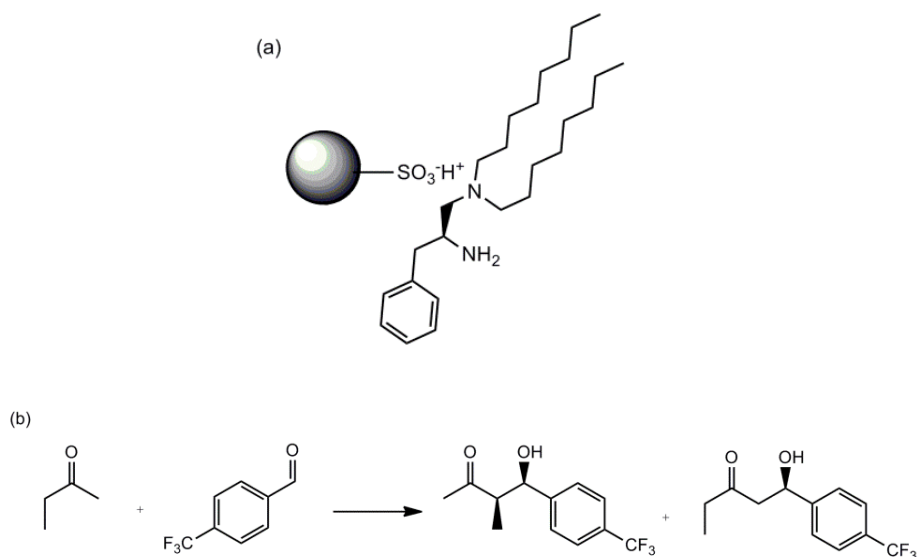


**Figure 3.6 – (a) Non-covalent immobilization through acid-base interaction of *L*-phenylalanine derived chiral catalyst on sulphonated mesoporous phenolic support. (b) Aldol reaction of 2-butanone with 4-(trifluoromethyl)benzaldehyde.**

### 3.5.2 Non-covalent immobilization of a chiral diamine catalyst and the catalytic performance in an asymmetric aldol reaction

After sulphonation of the mesoporous materials (see §3.2), the non-covalent immobilization of a chiral diamine catalyst is performed (see Figure 3.7). The chiral diamine catalyst was prepared by derivatization of the Boc-protected amino acid *L*-phenylalanine. [28, 29] This selected amino acid derived diamine, containing long hydrophobic alkyl chains, is reported as a highly *syn*-selective aldol catalyst.[29] By mixing the sulphonated solid matrix with the diamine in a 1/1 ratio, immobilization is attained by an acid-base interaction between the sulphonic acid group and the amine function. The chiral diamine, immobilized on different phenolic resins (ia-iv), is evaluated in the aldol reaction of 2-butanone with 4-(trifluoromethyl)benzaldehyde. The catalytic performance of these catalysts after 20 and 68 hours reaction, is given in Table 3.3.

As a reference, the sulphonated mesoporous materials Amberlyst-15® is loaded with the diamine catalyst and tested in the chiral aldol reaction of 2-butanone with 4-(trifluoromethyl)benzaldehyde. Amberlyst-15® is a commercial ion-exchange resin containing a sulphonated macroreticular polystyrene/divinylbenzene polymer network. It possesses an extremely high acid amount but a low surface area of 45 m²/g.[5] As can be seen in Table 3.3, Amberlyst-15® is nearly not active (less than 5% conversion after 20 hours). Considering the catalytic performance of the different sulphonated mesoporous phenolic resins, following interesting trends were observed. Firstly, when comparing catalyst (ic) and (id) containing identical sulphonic acid functionalities directly bounded on the aromatic ring, it can be seen from Table 3.3 that similar activity and selectivity are obtained, suggesting that the type of direct sulphonation method applied on the resin is not critical for the catalytic performance of the chiral diamine (catalytic data are normalized on the number of sulphonic acid groups). The results after 68 hours of reaction were also comparable, with a small benefit in selectivity for catalyst (ia) prepared using chlorosulphonic acid as precursor (*ee* = 90% *vs* 85% for catalyst (ic) and (id) respectively). Secondly, phenolic resin (ii) containing methylene sulphonic acid group attached to the aromatic ring, shows only 17% yield after 68 hours, although a high enantioselectivity of 91% is obtained. Comparing phenolic resin (i) containing an aromatic sulphonic acid group with catalyst (ii), which only differs in an aliphatic methylene bridge between the ring and the sulphonic acid functionality, it is suggested that the aromatic character of the sulphonic acid group has a positive influence on the catalytic activity of the chiral diamine organocatalyst.

**Table 3.3 – Catalytic performance of *L*-phenylalanine derived diamine catalysts in the direct asymmetric aldol reaction of 2-butanone with 4-(trifluoromethyl)benzaldehyde.**

| | | After 20 hours | | | | After 68 hours | | | |
|---|---|---|---|---|---|---|---|---|---|
| | | Yield [a] | rr [b] | dr [b] | ee [c] | Yield [d] | rr [b] | dr [b] | ee [c] |
| | | [%] | b/l | syn/anti | [%] | [%] | b/l | syn/anti | [%] |
| | Sulphonated phenolic resins | | | | | | | | |
| (ic) | – Ar-SO$_3$H (SO$_3$/H$_2$SO$_4$) | 22 | 4/1 | 5/2 | 88 | 44 | 4/1 | 5/2 | 85 |
| (id) | – Ar-SO$_3$H (ClSO$_3$H) | 18 | 4/1 | 5/2 | 89 | 48 | 4/1 | 5/2 | 90 |
| (ii) | – Ar-CH$_2$-SO$_3$H | n.d. | n.d. | n.d. | n.d. | 17 | 3/1 | 5/2 | 91 |
| (iii) | – O-Si-(CH$_2$)$_2$-Ar-SO$_3$H | 28 | 5/1 | 3/1 | 92 | 53 | 4/1 | 3/1 | 91 |
| (iv) | – O-Si-(CH$_2$)$_3$-SO$_3$H | 19 | 2/1 | 2/1 | 88 | 33 | 2/1 | 2/1 | 87 |
| | Reference sulphonated materials | | | | | | | | |
| | Amberlyst-15® | < 5 | n.d. | n.d. | n.d. | n.d. | n.d. | n.d. | n.d. |
| | CMK-3-SO$_3$H | 30 | 8/1 | 7/2 | 96 | n.d. | n.d. | n.d. | n.d. |
| | Nafion® NR50 | 86 | 4/1 | 2/1 | 91 | n.d. | n.d. | n.d. | n.d. |
| | SBA-15 – O-Si-(CH$_2$)$_2$-Ar-SO$_3$H | 28 | 5/1 | 5/2 | 89 | 60 | 3/1 | 5/2 | 91 |
| | SBA-15 – O-Si-(CH$_2$)$_3$-SO$_3$H | 19 | 4/1 | 7/2 | 92 | 41 | 4/1 | 3/1 | 91 |

All reactions were carried out under neat conditions in 2-butanone with aldehyde (0.125M), 15 mol% of diamine and 15 mol% of solid acid (data are normalized based on the number of suphonic acid groups) at room temperature. [a] Determined after 20 hours reaction; [b] Determined by chiral GC (rr = regioisomer ratio, *b/l* = ratio of branched and linear products); [c] The *ee* of the major *syn*-isomer as determined by chiral GC; [d] Determined after 68 hours reaction; n.d. = not determined.

Thirdly, with phenolic resin (iii) prepared *via* the silanation of the hydroxyl surface with an aryl sulphonic acid silane, a good yield after 20 hours and 68 hours reaction was obtained. Further, good regio- and diastereoselectivity and excellent enantioselectivity were achieved. In contrast, the alifatic propyl silane counterpart, catalysts (iv), shows a significant lower yield of aldol product after 68 hours (33%). Here as well, it seems that the aromatic character has a positive influence on the catalytic performance. Finally, a similar trend is observed for the sulphonated reference materials, mesoporous silica SBA-15: the aromatic sulphonated SBA-15 (SBA-15-O-Si-$(CH_2)_2$-Ar-$SO_3H$) shows significantly higher activity and selectivity for the *syn*-aldol condensation in comparison with the alifatic sulphonated SBA-15 (SBA-15-O-Si-$(CH_2)_3$-$SO_3H$). Taking into account all these data, one major trend can be observed: the aromatic character of the sulphonic acid group positively influences the catalytic activity and enantioselectivity of the chiral diamine catalysts whereas aliphatic sulphonic acid groups (– $CH_2$-$SO_3H$ and –$(CH_2)_3$-$SO_3H$) show lower catalytic performance. Presumably, this trend can be ascribed to the higher acidity strength of the aromatic sulphonic acid group due to the electron withdrawing nature of the aromatic ring. Finally, in order to evaluate this hypothesis, additionally a CMK-3 and Nafion®NR50 resin were evaluated as support for the chiral diamine catalyst. Sulphonated CMK-3 is a sulphonated mesoporous carbon material synthesized via an exocasting method, using mesoporous silica SBA-15 as hard template. [30] This mesoporous solid contains a conjugated network of sulphonated aromatic rings. The commercially available Nafion®NR50 is a strong acidic ion-exchange resin and consists of a copolymer of tetrafluoroethylene and perfluoro-3,6-dioxa-4-methyl-7-octenesulphonyl fluoride with strong acidic –$CF_2CF_2SO_3H$ sites (high electron withdrawing fluorine substituents).[6]

The sulphonated CMK-3 catalytic system, shows high conversion (30%) and high enantioselectivity for the *syn*-product (*ee* = 96%) after 20 hours of reaction. The catalytic results of the Nafion®NR50 polymer beads supported diamine catalyst in the aldol results of 2-butanone with 4-(trifluoromethyl)benzaldehyde are shown in Table 3.3. From these data can be clearly seen that this strong acidic fluoropolymer shows excellent catalytic performance yielding high yield (86%) and high enantioselectivity (91%). In summary, it can be concluded that the acidity – and in particular the electronic withdrawing environment – of the sulphonic acid groups influences enormously the catalytic performance of the non-covalent immobilized chiral diamine catalyst (fluorinated >> aromatic > alifatic). Hence, the catalytic performance of the sulphonated mesoporous resins as support can be ordered following Nafion®NR50 > CMK-3 > – O-Si-$(CH_2)_2$-Ar-$SO_3H$ > – Ar-$SO_3H$ > – O-Si-$(CH_2)_3$-$SO_3H$ > – Ar-$CH_2$-$SO_3H$ > Amberlyst-15®.

## 3.6 Summary and conclusions

In this study, ordered mesoporous phenolic resins are presented as novel supports for sulphonic acid groups. The sulphonation was performed by different sulphonation procedures, yielding different aromatic and aliphatic sulphonic acid functionalities.

Catalysts with different acidity loadings were obtained, ranging from 0.5 – 2 mmol $H^+$/g. The catalysts were tested in the Fisher esterification of propanol with acetic acid. Here, the aryl sulphonated and the silane based catalysts showed a good to high conversion in the first run. However, a significant decrease in catalytic activity in the second run was observed. In contrast, the alkyl sulphonated catalysts showed rather average catalytic performance, although the catalyst was stable in the second catalytic run. The catalysts were evaluated for their leaching resistance in aqueous medium. Here, alkyl sulphonated materials showed the highest stability in aqueous medium compared to the other developed catalysts.

Furthermore, the sulphonated mesoporous materials are presented as novel support for chiral diamine organocatalysts. The sulphonated supports were loaded with a chiral diamine organocatalyst via a non-covalent acid-base interaction. The resulting immobilized catalysts were evaluated for their catalytic performance in the chiral aldol reaction of 2-butanone with 4-(trifluoromethyl)benzaldehyde and compared to other sulphonated mesoporous materials. It has been shown that the electronic character of the sulphonic acid group may have a distinct influence on the catalytic activity and enantioselectivity of the chiral diamine catalyst: fluorinated and aromatic sulphonic acid functionalities show higher catalytic performance than the aliphatic counterparts due to the stronger electronic withdrawing nature of these substituents. In conclusion, these newly developed catalysts exhibit rather average catalytic performance in comparison with other commercial sulphonated materials.

## 3.7 Experimental

**Synthesis of mesoporous phenolic resin:** Mesoporous phenolic resins are synthesized according to the procedure of Song et. al. using resorcinol/formaldehyde as carbon source in acid medium.[31] In a typical synthesis, resorcinol (2.1 g) is added to an ethanol/water solution of F127 and stirred for 30 minutes at room temperature. Then, formaldehyde (Formaline, 37wt% formaldehyde in water) is added and stirred for 30 minutes. Finally, HCl is added dropwise and the solution is stirred for 2 hours at room temperature. While keeping the solution untouched, the mixture separated into two-phases. Subsequently, the transparent upper phase was removed and the yellow lower polymer phase was heated in an oven at 100°C for 24 h followed by calcination. The molar ratio resorcinol:formaldehyde:F127:HCl:EtOH:$H_2O$ = 1:1:0.0066:0.13:7.2:15.19.

**Sulphonation procedures:** *Sulphonation (ia)*: In a two-neck Schlenk flask, 0.5 g support was stirred in 10 ml dry dichloromethane and 0.15 ml chlorosulphonic acid. The mixture was stirred at 0°C for 24 hours under inert atmosphere. The powder was filtrated, successively washed with dichloromethane, acetone and water until pH 7 and finally with acetone. The catalyst was in *vacuo* dried at 90°C overnight. *Sulphonation (ib)*: 0.5 g support was treated with fuming sulphuric acid vapour at room temperature for 3 hours under atmospheric pressure. After reaction, the catalyst was degassed overnight to

remove the excess of physical adsorbed sulphuric acid. *Sulphonation (ic and id):* 0.5 g support was stirred in 10 ml 2.5M $H_2SO_4$ solution at room temperature for 3 hours. For catalyst (id) triflic acid anhydride ($Tf_2O$) is added to the 2.5M $H_2SO_4$ solution by adding 5 times 1 ml every 30 minutes. The powders were filtrated and washed thoroughly with water until pH 7 and finally with acetone. The catalysts were in *vacuo* dried at 90°C overnight. *Sulphonation (ii)*: In a 2-neck Schlenk flask, 0.5 g support, zinc chloride (0.025g) and 50 ml acetic acid/HCl (1:1) are stirred under light *in vacuo* to dissolve the zinc chloride at room temperature. Subsequently, the mixture is cooled down to 0°C in an ice bath. 1.9 g formaldehyde is added in once and sparging of a fuming hydrochloric acid vapour through the solution is performed during 4 hours. Then, the mixture is stirred overnight at room temperature, filtrated and washed with water and methanol. Finally, the product is dried *in vacuo* at 90°C. Next, the solid is stirred in a saturated solution of sodium thiosulphate and subsequently washed with a warm 0.1M aqueous HCl-solution. The sulphonation procedure is finalized by an oxidation treatment to convert the thiol group to a sulphonic acid functionality. *Sulphonation (iii) and (iv)*: In a 2-neck Schlenk flask, 0.5 g support was stirred in 10 ml dry toluene and 0.15 ml sulphonic acid precursor. The mixture was refluxed at 120°C for 24 hours under inert atmosphere. The powders were filtrated, thoroughly washed with toluene, subsequently with water until pH 7 and finally with acetone. The catalysts were *in vacuo* dried at 90°C overnight. The sulphonic acid precursors used were 2-(4-chlorosulphonylphenyl)ethyl trichlorosilane (sulphonation iii) and 3-mercaptopropyltrimethoxysilane (sulphonation iv). Concerning sulphonation (iv), the sulphonation is finalized by an oxidation treatment to convert the thiol group to a sulphonic acid functionality. *Oxidation of thiol group (-SH) to sulphonic acid group ($-SO_3H$)* – 0.5 g thiol-functionalized support is stirred in a mixture of 20 ml hydrogen peroxide (30wt% in water). To this solution, 2 ml nitric acid (68wt%) is added dropwise and stirred for 3 hours at room temperature. Next, an additional amount of 2 ml nitric acid is added dropwise and stirred for 21 hours at room temperature. The powders are filtrated and thoroughly washed with water until pH 7 and finally washed with acetone. The catalysts were *in vacuo* dried at 90°C overnight.

**Leaching resistance tests:** In order to evaluate the leaching resistance of the sulphonated materials in aqueous medium, 0.5 g sulphonated mesoporous support is stirred in 0.5 L water at 80°C for 24 hours. The catalyst is filtrated, *in vacuo* dried at 90°C overnight and the acidity is determined.

**Fisher esterification of *n*-propanol with acetic acid:** In a typical catalytic run, 30 mmol propanol, 100 mmol acetic acid and 30 mmol toluene (internal standard) were refluxed in a two-neck Schlenk flask under vigorous stirring at 90°C. Subsequently, 50 mg dried catalyst was added. The reaction was followed by sampling 0.1 ml of the reaction medium at several times. The sample was immediately diluted with 0.5 ml acetonitrile and analyzed by gas chromatography. Regeneration – At the end of the reaction, the catalyst was filtrated from the hot reaction mixture, thoroughly washed with acetone, dried and reused in a new catalytic run under the same reaction conditions.

**Synthesis of the chiral diamine catalyst 2-(S)-amino-3-phenyl-propanoic acid dioctylamine:** The chiral diamine was prepared by derivatization of the Boc-protected amino acid L-phenylalanine and a reaction scheme is given in Figure 2. [28, 29] (i) To an ice cold solution of the Boc-protected amino acid, an equimolar solution of dicyclohexylcarbodiimide (DCC), in dichloromethane (DCM) was added. After stirring for 30 minutes, an equimolar dichloromethane solution of the dioctylamine was added dropwise. The resulting mixture was warmed to room temperature and further stirred overnight. After removal of the precipitate by filtration, the filtrate was washed successively with a 2 wt% HCl solution, a saturated $NaHCO_3$ solution, water and brine and dried over $MgSO_4$. After removal of the solvent, the crude product was purified through flash column chromatography on silica gel (hexane/ethyl acetate) to afford the Boc-protected amide as a white solid. (ii) To remove the Boc-group, the *N*-protected amide was dissolved in dichloromethane and a trifluoroacetic acid/dichloromethane solution was added dropwise. The resulting mixture was stirred for 2-5 h at room temperature. Then, the mixture was diluted with MeOH and the solvent was removed under reduced pressure. The residue was diluted with ethyl acetate. The organic layer was washed three times with a 5% $NaHCO_3$ solution and dried over $MgSO_4$. The solvent was evaporated and the product was purified on silica gel (ethyl acetate/methanol) to give the corresponding amide. (iii) To an ice cold solution of $LiAlH_4$ in tetrahydrofuran (THF) a suspension of the amide in dry THF was added under inert nitrogen atmosphere using a metal syringe. The resulting mixture was refluxed during 5 h in an oil bath at 70°C. Then, the mixture was cooled down and diluted with ethyl acetate. The reaction was quenched with a saturated $Na_2SO_4$ solution. After removal of the inorganic material, the organic layer was washed with brine and dried over $MgSO_4$. The solvent was evaporated and the product was purified on silica gel (ethyl acetate/methanol) to give the amine as a slightly yellow oil.

^{1}H NMR (CDCl$_3$, 300 MHz): δ = 0.84-0.91 (t, *J* = 6.4, 6H, CH$_3$), 1.26 (s, 20H, CH$_2$), 1.34-1.46 (br. s, 4H, CH$_2$), 2.22-2.50 (m, 7H, N(CH$_2$)$_3$, C*H*$_2$C$_6$H$_5$), 2.68-2.78 (dd, *J* = 4.3 , *J* = 13.3, 1H, C*H*$_2$C$_6$H$_5$), 3.02-3.14 (septet, *J* = 4.4, 1H, α-H), 7.12 -7.34 (m, 5H, ar. H); ^{13}C NMR (CDCl$_3$, 75.5 MHz) δ = 14.1, 22.7, 27.4, 27.6, 29.4, 29.6, 31.9, 42.3, 50.7, 54.8, 61.8, 126.1,128.4, 129.2, 139.8, *m/z* 374 (M$^+$ < 1), 283 (5), 254 (100), 240 (2), 156 (38), 142 (27), 117 (12), 105 (4), 98 (6), 91 (33), 84 (6), 77 (6), 65 (8), 58 (19), 44 (31).

**Figure 3.7 – Synthesis of amino acid (*L*-phenylalanine) derived chiral diamine catalyst. (i) Boc-protected amino acid *L*-phenylalanine, DCC, amine, 0°C-RT overnight; (ii) TFA/DCM, 2-5 hours RT; (iii) LiAlH$_4$/THF, 5 hours reflux.**
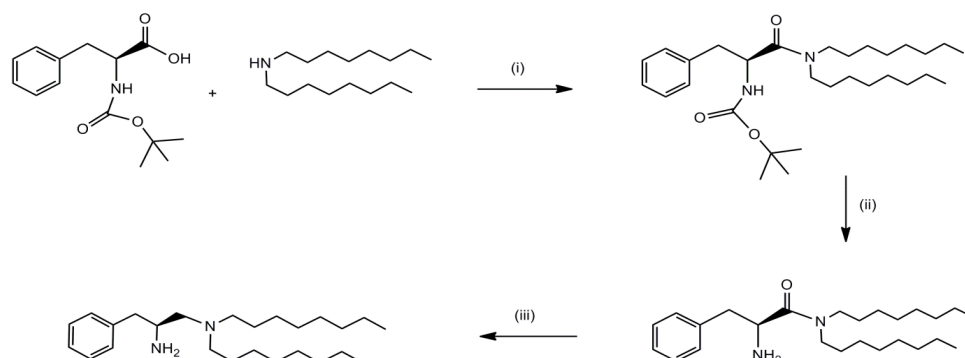
**Non-covalent immobilization of 2-(*S*)-amino-3-phenyl-propanoic acid dioctylamine:** The chiral diamine catalyst was non-covalently immobilized on the sulphonated mesoporous phenolic resins according to a method reported by Cheng et. al. [27] In a typical procedure, sulphonated mesoporous phenolic resin is suspended in dichloromethane and the reaction micture is stirred for 15 minutes at room temperature. Chiral amine is added and the resultant mixture is stirred for 2 hours at room temperature. The catalyst is separated by filtration and washed sequentially with dichloromethane and ethanol. Finally, the solid is dried *in vacuo* at room temperature overnight.

**Asymmetric aldol condensation of 2-butanone with 4-(trifluoromethyl)benzaldehyd:** To an equimolar solution of chiral diamine and sulphonic acid resin (15 mol% H$^+$) in 2-butanone, the aldehyde (0.125 M) was added. The resulting mixture was stirred at room temperature for a given time. Then, the reaction mixture was extracted with ethyl acetate and water. The organic phase was analyzed with 1H NMR and chiral GC to calculate yields and regio- and diastereomeric ratios. The enantiomeric excess (*ee*) was determined with chiral GC.

**Characterization:** Nitrogen gas sorption experiments were conducted at 77 K using a Micromeretics Tristar 3000. Samples were *in vacuo* dried at 120 °C prior to analysis. The pore size distribution (PSD) was calculated from the adsorption branch. The pore volume, $V_p$, was calculated using the BJH method. X-ray powder diffraction (PXRD) patterns were collected on ThermoFisher Diffractometer with Cu Kα radiation with 0.15418 nm wavelength. Gas chromatography – Gas chromatographic analyses were performed on a Finnigan Trace Ultra Fast GC equipped with a flame ionization detector (FID) and a 5% diphenyl / 95% polydimethylsiloxane column, with 10 m length and 0.10 mm internal diameter. Helium was used as carrier gas and the flow rate was programmed as 0.8 ml/min. Chiral GC analyses were performed on a Hewlett Packard Series 6890 chromatograph equipped with an automatic Agilent 7683 injection system, a CP-chiralsil-Dex CB column (25 m x 0.32 mm, film thickness 0.25 μm) from Varian and a flame ionization detector (FID). XPS measurements were recorded on a X-ray photoelectron spectroscopy S-Probe XPS spectrometer with monochromated Al (1486 eV) exciting

radiation from Surface Science Instruments (VG). The flood gun was set to 10 eV. A nickel grid was placed 3 mm above the samples in order to suppress charging of the samples. The acidity loading was determined by acid-base titration. 50 mg dried catalyst is stirred in 20 ml 2 M NaCl solution for 24 hours at room temperature. The solution is titrated with 0.005 M NaOH solution (in presence of the catalyst) with phenolphthalein as indicator. Previously to the titration, the concentration of the alkaline NaOH solution was determined with a 0.005 M solution of the primary standard oxalic acid dihydrate. Determination of the sulphur content – The sulphur content is determined by a CHNS-O analyser Thermo Scientific Flash 2000, with a TCD detector and using the Eager Experience software. 2 mg of the sample and a small amount of catalyst ($V_2O_5$) is placed in a tin container and heated to 1800°C to fully oxidize the sulphur to $SO_2$. The integration of the sulphur peak is calibrated using *L*-methionine as standard.

## 3.8. References

[1] G. Busca, *Chem Rev*, **2007**, 107, 5366-5410.
[2] A. Corma, H. Garcia, *Top Catal*, **2008**, 48, 8-31.
[3] J.H. Clark, *Accounts Chem Res*, **2002**, 35, 791-797.
[4] D.T. On, D. Desplantier-Giscard, C. Danumah, S. Kaliaguine, *Appl Catal a-Gen*, **2003**, 253, 543.
[5] www.rohmhaas.com/ionexchange.
[6] www.fuelcells.dupont.com.
[7] R. Xing, N. Liu, Y.M. Liu, H.W. Wu, Y.W. Jiang, L. Chen, M.Y. He, P. Wu, *Adv Funct Mater*, **2007**, 17, 2455-2461.
[8] L. Fang, R. Xing, H.H. Wu, X.H. Li, Y.M. Liu, P. Wu, *Sci China Chem*, **2010**, 53, 1481-1486.
[9] L. Mou, X.J. Qu, C.Y. Wang, *Chem J Chinese U*, **2010**, 31, 1643-1646.
[10] X.N. Tian, L.L. Zhang, P. Bai, X.S. Zhao, *Catal Today*, **2011**, 166, 53-59.
[11] J.M. Aragon, J.M.R. Vegas, L.G. Jodra, *Ind Eng Chem Res*, **1994**, 33, 592-599.
[12] S. Suganuma, K. Nakajima, M. Kitano, H. Kato, A. Tamura, H. Kondo, S. Yanagawa, S. Hayashi, M. Hara, *Micropor Mesopor Mat*, **2011**, 143, 443-450.
[13] W.D. Samuels, N.H. LaFemina, V. Sukwarotwat, W. Yantasee, X.H.S. Li, G.E. Fryxell, *Separ Sci Technol*, **2010**, 45, 228-235.
[14] X. Zhuang, X.F. Qian, J.H. Lv, Y. Wan, *Appl Surf Sci*, **2010**, 256, 5343-5348.
[15] M.L. Testa, V. La Parola, A.M. Venezia, *Catal Today*, **2010**, 158, 109-113.
[16] X.G. Wang, S.F. Cheng, J.C.C. Chan, *J Phys Chem C*, **2007**, 111, 2156-2164.
[17] C.C. Chen, S.F. Cheng, L.Y. Jang, *Micropor Mesopor Mat*, **2008**, 109, 258-270.
[18] E.I. Basaldella, M.S. Legnoverde, I. Jimenez-Morales, E. Rodriguez-Castellon, B.O. Dalla Costa, C.A. Querini, *Adsorption*, **2011**, 17, 631-641.
[19] S.J. Miao, B.H. Shanks, *J Catal*, **2011**, 279, 136-143.
[20] Z.J. Zhang, Q.W. Wang, P. Tripathi, C.U. Pittman, *Green Chem*, **2011**, 13, 940-949.

[21] B. Cinlar, B.H. Shanks, *Appl Catal a-Gen*, **2011**, 396, 76-84.

[22] P.F. Siril, N.R. Shiju, D.R. Brown, K. Wilson, *Appl Catal a-Gen*, **2009**, 364, 95-100.

[23] P.F. Siril, A.D. Davison, J.K. Randhawa, D.R. Brown, *J Mol Catal a-Chem*, **2007**, 267, 72-78.

[23a] Carl Vercaemst, PhD Isomeric olefinic periodic mesoporous organosilicas : an emerging class of versatile nanomaterials, Ghent University, **2009**

[24] S. Mukherjee, J.W. Yang, S. Hoffmann, B. List, *Chem Rev*, **2007**, 107, 5471-5569.

[25] D.E. De Vos, M. Dams, B.F. Sels, P.A. Jacobs, *Chem Rev*, **2002**, 102, 3615-3640.

[26] J.M. Fraile, J.I. Garcia, J.A. Mayoral, *Chem Rev*, **2009**, 109, 360-417.

[27] S.Z. Luo, J.Y. Li, L. Zhang, H. Xu, J.P. Cheng, *Chem-Eur J*, **2008**, 14, 1273-1281.

[28] A.L.W. Demuynck, L. Peng, F. de Clippel, J. Vanderleyden, P.A. Jacobs, B.F. Sels, *Adv Synth Catal*, **2011**, 353, 725-732.

[29] A.L.W. Demuynck, J. Vanderleyden, B.F. Sels, *Adv Synth Catal*, **2010**, 352, 2421-2426.

[30] R. Ryoo, S.H. Joo, S. Jun, *J Phys Chem B*, **1999**, 103, 7743-7746.

[31] L.Y. Song, K.X. Li, X.H. Li, P. Wu, *React Kinet Mech Cat*, **2011**, 104, 99-109.

# Chapter 4

## Mesoporous phenolic resins as support for vanadium and titanium oxide catalysts

### 4.1 Introduction

In modern heterogeneous catalysis, supported vanadium and titanium oxide catalysts represent an important class of catalytic materials. In scientific research, they have become a model for catalytic systems and today they are widely implemented as selective oxidation catalysts in a variety of economically attractive industrial processes, e.g. oxidation of hydrocarbons, epoxidation of olefins, etc.[1-3] These heterogeneous catalysts, often deposited on a porous silica support, combine the advantages of mechanical strength with easy recovery and recycling. Moreover, the high surface area and the nature of the porous support endow these advanced materials unique catalytic properties. [4, 5]

In recent years, numerous efforts have been made to determine the structure-reactivity relationship of these supported vanadium and titanium oxide catalysts.[6, 7] In particular *off line* and *in situ* spectroscopic analysis techniques have shown to be powerful tools to elucidate the molecular and electronic structure of the active catalytic sites.[8, 9] Figure 4.1 shows a simplified representation of the three main morphologies of the catalytic vanadium oxide sites that might be present on the support surface: type A are isolated monomeric species with a tetrahedral coordination ($VO_4$ units), type B are one or two dimensional oligomeric species connected by V–O–V bridges and type C are three-dimensional bulk vanadium oxide crystalline clusters present in an octahedral coordination ($VO_6$ units).[10] Nowadays, it is generally accepted that for a high catalytic efficiency, the highly dispersed and isolated catalytic sites (type A) are preferred to oligomeric species (type B) or crystalline clusters (type C).[11, 12] For the supported titanium (+IV) oxide species, similar assumptions concerning the morphologies as for the supported vanadium (+V) oxide species are considered.
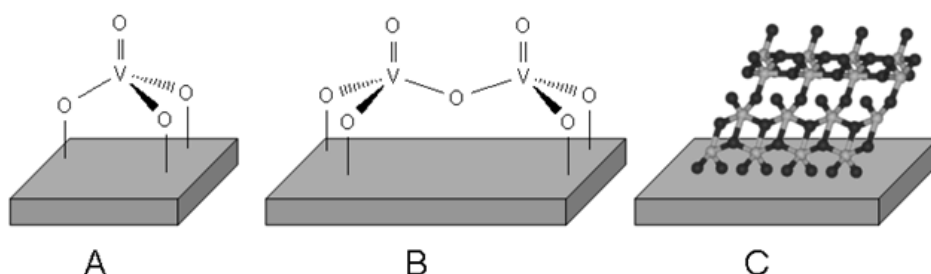
**Figure 4.1 – Simplified representation of the three main morphologies of vanadium oxide species supported on a surface. Type A: isolated monomeric species of tetrahedral VO$_4$ units; type B: dimeric/oligomeric species containing V-O-V bridges; type C: crystalline clusters of octahedral VO$_6$ units**

The morphology of the surface sites can be reasonably designed by controlling certain critical parameters like the metal loading, the choice of the metal precursor and the nature of the support.[13] Firstly, the degree of metal loading has a high impact on the morphology of the species.[14, 15] At low metal loadings the supported species are mainly present as dispersed isolated monomeric units (type A). With increasing loadings, the amount of dimeric and polymeric chains gradually increases (type B). At very high loadings, the extent of polymerization enlarges and the supported metal oxide species aggregate easily into crystalline metal oxide clusters (type C).

Secondly, the choice of the metal precursor – and in particular the side groups of the metal center – has also shown to be critical for the final morphology of the active species. Metal precursors containing easily hydrolysable side groups like -Cl, -OBu,-iPrO, etc. are – although often highly reactive with the surface – also more susceptible to oligo- and polymerization. [16] In the 1990s, the molecularly designed dispersion method was introduced by using metal precursors surrounded by large acetyl acetonate ligands, which are less sensitive to hydrolysis.[17, 18] These bulky ligands avoid coalescence and clustering of the metal centers and after ligand removal by calcination, highly isolated and dispersed metal oxide sites on the surface are obtained.

Finally, the nature of the support plays a key role in the stability of the morphology of the catalytic species.[14, 19] In heterogeneous catalysis, porous silica is very common as support. Due to the easy synthesis procedure, simple characterization, high thermal stability, relative low cost-price and high porosity properties, silica is practically considered as a standard support (other inorganic oxides sometimes used as supports are Al$_2$O$_3$, ZrO$_2$, Nb$_2$O$_5$, etc.). Here, the vanadium or titanium precursor reacts with the hydroxyl groups on the surface and is covalently bonded by a support-oxygen-metal bound.

One of the two major problems of silica supported vanadium and titanium oxide catalysts, however, is the rather weak covalent bond of the silica support with the supported metal sites. Consequently, the catalytic active species grafted on the silica surface are often

subject of coalescence and clustering. This can be explained by the stronger V-O-V and Ti-O-Ti bonds compared to Si-O-V and Si-O-Ti bonds. Secondly, silica exhibits a relatively low hydrothermal stability due to easy hydrolysis of the siloxane bridges in aqueous environment. As a result, silica supported vanadium and titanium oxide species are sensitive to leaching in liquid phase reactions.[20] Therefore, the question about the true nature of the final catalytic reaction – heterogeneous or homogeneous – is relevant.[21] In recent years, many studies have already been inspired by the improvement of the stability of supported vanadium and titanium catalysts, strongly driven by increasing environmental concerns and economic perspectives. As an illustration, partial hydrophobization of the silica surface using alkylchlorosilanes can reduce leaching by a factor 4 due to the protection of the siloxane bridges against hydrolysis.[18] Nevertheless, the search for the ideal support for vanadium and titanium oxide is not yet finished...

In this study, mesoporous phenolic resins are introduced for the first time as a novel support for vanadium and titanium oxide catalysts. These advanced solids have shown to be significantly more stable compared to porous silica materials.[22] Moreover, the combination of the organic nature of the walls with high porosity characteristics may provide these supported materials unique catalytic properties. In this research, the deposition of the metal precursors and the experimental parameters are described and the characterization of the functionalized catalysts is presented. Furthermore, the novel catalysts are evaluated in two different catalytic oxidation reactions and their catalytic performance is compared to common porous silica supported catalysts. Finally, insight in the catalytic behavior is given and a reaction mechanism is proposed.

### 4.2 Vanadium and titanium oxide deposition on mesoporous phenolic resins

Mesoporous phenolic resins are functionalized with vanadium and titanium oxide by either an one-pot synthesis method (while synthesizing the solid support) or via a post-synthesis deposition in the liquid or in the gas phase (after synthesis of the support), eventually followed by a treatment (hydrophobization or calcination). In this study, different vanadium and titanium precursors with different oxidation states are used: vanadium (III) chloride, vanadium (IV) oxyacetylacetate, vanadium (IV) oxysulfate, ammonium metavanadate (V),  vanadium (V) oxychloride, trisisopropoxy vanadium (V) oxide were applied for the vanadium catalysts and titanium (IV) chloride, titanium (IV) butoxide and tetrakis(dimethylamido)titanium (IV) for the titanium catalysts. An overview of the synthesized vanadium and titanium oxide catalysts is given in Table 4.1.

### 4.2.1 One-pot synthesis

The one-pot synthesis method includes that all reagents are added either simultaneously or one by one and remain in one flask during the full synthesis process.[23-25] The major advantage of this procedure is the simplified modus operandi of catalyst synthesis. Additionally, this method is less time consuming and less labor intensive. However, this direct synthesis pathway includes the incorporation of the active centers both on the surface as well as in the wall of the mesoporous framework. Consequently, a significant part of the catalytic centers, encapsulated in the walls, is not reachable and cannot take part in the catalytic reaction.

In this study, vanadium oxide is incorporated by a one-pot synthesis method using two types of vanadium precursors with different oxidation states, vanadium(III)chloride and vanadium(V)oxychloride. These catalysts are represented by (1) and (2) respectively in Table 4.1.

### 4.2.2 Post-synthesis deposition: liquid phase deposition

Vanadium and titanium oxide are deposited post-synthetically on the surface of mesoporous phenolic resins in liquid phase by stirring the mesoporous support for a certain time at elevated temperatures in a solution containing the metal precursor (dry toluene). This wet impregnation procedure was performed using different types of metal precursors and solvents. An overview of the different catalysts is given in Table 4.1, represented by (3) to (7) and by (10) to (11) for the vanadium and the titanium oxide catalysts respectively. Additionally, a so-called incipient wetness impregnation was performed. This last method is very common in catalyst synthesis and includes the adsorption of a volume of the metal containing solution, exactly equal to the pore volume of the support.[26, 27] Capillary forces draw the solution into the pores. As a result, a dry solid is obtained after impregnation. In this study, a vanadium oxide catalyst is synthesized by performing the dry impregnation route, represented by (4b) in Table 4.1.

### 4.2.3 Post-synthesis deposition: gas phase deposition

Gas phase deposition includes a gas-solid phase reaction between the metal precursor and the mesoporous support. Gas phase reactions are often preferred to liquid phase due to the feasibility of higher deposition temperatures, less diffusion limits, no need of solvents, waste reduction and more precise control of reaction conditions. In this study, vanadium and titanium oxide are deposited on the surface of mesoporous phenolic resins in the gas phase using two experimental set-ups: a home-made Schlenk reactor and an atomic layer deposition reactor. The advanced depositions were performed in collaboration with dr. Jan Musschoot and Prof. dr. Christophe Detavernier of the department of Solid State Science, Ghent University.

### 4.2.3.1 Home-made deposition reactor

A representation of the home-made Schlenk reactor is shown in Figure 4.2. Here, pre-dried mesoporous phenolic resin is placed on a silica grid (1). The metal oxide precursor is situated at the bottom (2). Valve (3) at the bottom is closed and a dynamic vacuum is installed by opening valve (5) and valve (3) at the top. The dotted line (6) represents a furnace to control the deposition temperature. Gas phase deposition was performed with vanadium(V)oxychloride ($VOCl_3$) and titanium(IV)chloride ($TiCl_4$). Prior to deposition, these metal precursor solutions are first treated by the freeze-pump-thaw technique, to guarantee degassing of the precursors. The catalysts synthesized using the home-made reactor are represented in Table 4.1 by (8) and (12) for the vanadium and titanium oxide catalysts respectively.
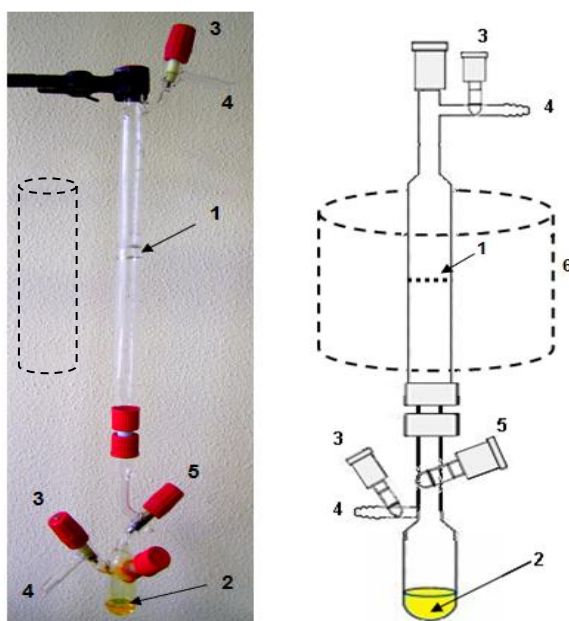


**Figure 4.2 – Gas phase deposition of $VOCl_3$ on mesoporous phenolic resin in the home-made reactor  (1: filter; 2: metal precursor; 3 + 5: Schlenk valve; 4: connection to vacuum; 6: furnace)**

### 4.2.3.2 Advanced atomic layer deposition reactor

Vanadium and titanium precursors were also deposited using the more advanced deposition reactor of the department of the Solid State Science at the Ghent University. Here, the reaction conditions as temperature, time, pressure, etc… can be precisely controlled by computer operated software. A picture of the reactor is shown in Figure 4.3. The deposition is based on the atomic layer deposition process.[28-31] Atomic layer deposition (ALD) is a powerful technique that allows a controlled gas phase deposition of metal oxide monolayers on the surface of ordered mesoporous materials. The method is based on the sequential exposure of the mesoporous support to a volatile metal-containing precursor and a reactive gas. During an ALD pulse, the gas reacts self-limitingly with the substrate. As shown in Figure 4.3, a single ALD cycle includes four steps: (1) an exposure of the hydroxyl surface of the support to the titanium or vanadium oxide precursor in the gas phase. The self-limiting nature of the reaction between the surface hydroxyl groups and the metal oxide precursor avoids metal oxide clustering and well dispersed monomer particles are obtained. (2) A degassing stage to remove the excess of metal precursor and reacted side groups. (3) A water pulse to hydrolyse the side groups and to regenerate a new reactive hydroxyl surface and (4) a second time a degassing step.

Here, vanadium and titanium oxide were deposited on the surface of mesoporous phenolic resin using vanadium(V)oxyisopropoxide (VO($i$PrO)$_3$) and tetrakis(dimethylamido) titanium (IV) (TDMAT) respectively and are represented by catalyst (9a) and (13a) respectively in Table 4.1. Additionally, catalysts were synthesized by applying consecutive ALD cycles, creating multiple oxide layers. The multiple oxide layer catalysts are represented by (9b) and (9c) for the vanadium and (13b) and (13c) for the titanium layers respectively. Finally, ALD allows also the controlled deposition of mixed metal oxide layers by performing consecutive cycles with different metal oxide precursors. The mixed oxide catalysts are represented by (14) to (17) in Table 4.1.
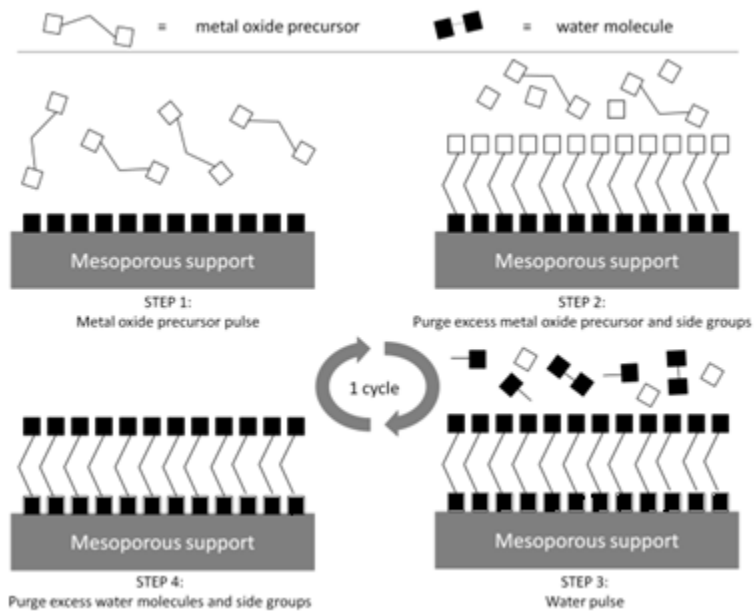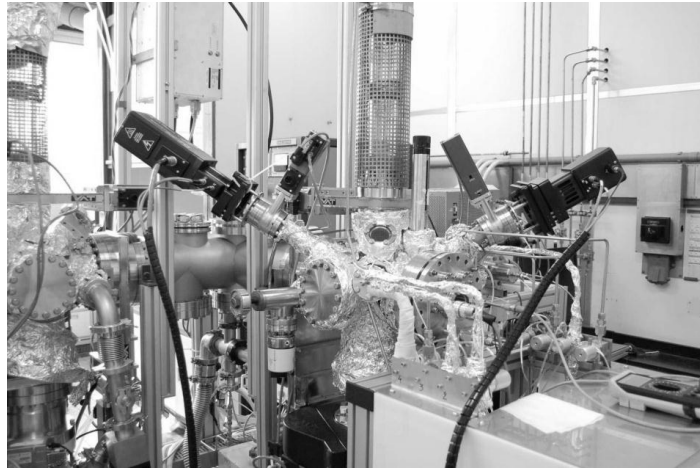
**Figure 4.3 – TOP: Powder reactor for atomic layer deposition of titanium and vanadium oxide on mesoporous materials. BOTTOM: Deposition of one monolayer by the atomic layer deposition technique.**

### 4.2.4 Oxidation treatment

The oxidation state of the metal center plays a crucial role in the catalytic performance of metal oxide supported catalysts. The main oxidation state of common titanium compounds is +IV, whereas the main oxidation states of vanadium precursors are +III, +IV or +V. Although the lower oxidation states are also reported to be catalytically active, generally, the +V form is preferred due to its higher electron acceptor ability.

This observation has direct consequences on the synthesis level of the supported catalysts. By using metal precursors with lower oxidation states, an extra oxidation step of the metal center is regularly required. If inorganic oxides are used as support, e.g. silica, the metal oxide centers can be directly and easily oxidized to the highest oxidation state by a calcination step, i. e. a post-synthetic thermal treatment of the supported catalysts. According to literature, thermal treatments at temperatures of 500-600°C in air are generally applied.[32] Simultaneously with the oxidation of the metal center, all organic ligands are removed by calcination and supported metal oxide species are obtained.

Mesoporous phenolic resins, however, start to decompose at 350°C under oxidizing atmosphere. For this reason, a post-synthetic calcination step at high temperatures is not applicable for these organic supports. Here, two strategies have been followed to post-synthetically oxidize the supported vanadium species: (1) a calcination treatment at 300°C in air and (2) stirring the supported catalyst in a strong oxidizing medium (acidic aqueous solutions of $HNO_3/H_2O_2$ or $KMnO_4$-solution). These supported catalysts are represented by (1b), (3b), (3c), (3d) and (6b) in Table 4.1.

### 4.2.5 Hydrophobization treatment

Water molecules, and in addition -OH groups, strongly adsorb on Ti-centers and often lead to partial deactivation of the catalyst.[33] This water poisoning is also – but more restrictively – reported for supported vanadium oxide catalysts.[34, 35] As a consequence, ultra-dry conditions are often required for catalytic reaction with supported titanium or vanadium oxide centers. Recently, Galarneau et. al. reported that for silica supported titanium oxide catalysts, a post-hydrophobization treatment of the titanium oxide surface can significantly reduce water poisoning of the catalyst.[36] This observation is very useful since it opens the way to greener oxidation chemistry by using environmental-friendly oxidants as hydrogen peroxide which produces only water as by-product [36, 37]

In this study, the influence of a post-hydrophobization treatment on the catalytic performance of phenolic resin supported titanium oxide catalysts is evaluated. This was performed using hexamethyldisilazane (HMDS) as hydrophobization reagent. As shown in Figure 4.4, HMDS reacts with two surface hydroxyl groups while ammonia is released and a hydrophobic surface is obtained. The catalyst post-treated with HMDS is represented by (10b) in Table 4.1.
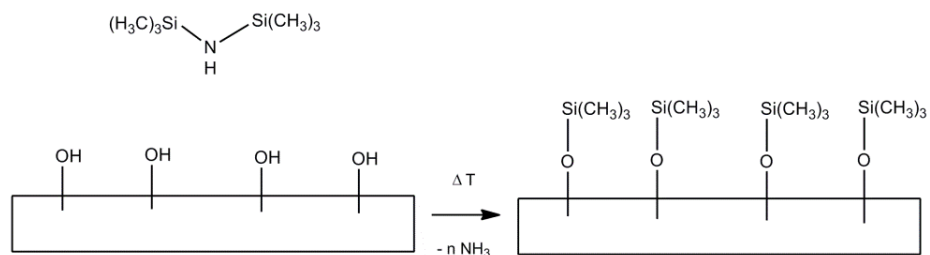
**Figure 4.4 – Hydrophobization of surface hydroxyls with hexamethyldisilazane**

### 4.2.6 Overview of the mesoporous phenolic resins supported vanadium and titanium oxide catalysts

Table 4.1 gives an overview of the vanadium and titanium oxide catalysts, synthesized under different reaction conditions. For clarity, the table is split in three parts: (a) vanadium oxide catalysts, (b) titanium oxide catalysts and (c) mixed vanadium/titanium oxide catalysts. An extra subdivision, indicated by letters (4.xa, 4.xb, 4.xc, …), is made if one single reaction parameter was varied. In addition, mesoporous silica supported vanadium and titanium oxide catalysts (SBA-15 type) are also synthesized as a reference, by applying similar deposition conditions as the corresponding mesoporous phenolic resin catalysts. These silica based catalysts are numbered equally to the numbering of the corresponding mesoporous phenolic resin supported catalysts and are marked with an accent (') in Figure 4.6.

# Table 4.1 – Overview of the synthesis conditions and porosity characteristics of the phenolic resin supported catalysts:

## (a) vanadium oxide catalysts, (b) titanium oxide catalysts and (c) mixed vanadium/titanium oxide catalysts

| Catalyst number | Synthesis method | Metal Precursor | Oxidation state | Post-synthesis treatment | Mesoporous phenolic resin Metal loading (mmol/g) | Specific surface area (m²/g) | Mean pore diameter (nm) | Total pore volume (cm³/g) | Mesoporous silica SBA-15 Metal loading (mmol/g) | Specific surface area (m²/g) | Mean pore diameter (nm) | Total pore volume (cm³/g) |
|---|---|---|---|---|---|---|---|---|---|---|---|---|
| *(a) vanadium oxide catalysts* | | | | | | | | | | | | |
| 1 a | One-pot | VCl₃ | +III | - | 0.46 | 432 | 6.2 | 0.60 | n.a. | n.a. | n.a. | n.a. |
| b | One-pot | VCl₃ | +III | Calcination | 0.43 | 463 | 6.3 | 0.62 | n.a. | n.a. | n.a. | n.a. |
| 2 | One-pot | VOCl₃ | +V | - | 0.73 | 453 | 6.1 | 0.53 | n.a. | n.a. | n.a. | n.a. |
| 3 a | Liquid phase | VO(acac)₂ | +IV | - | 1.12 | 559 | 6.1 | 0.51 | 1.10 | n.d. | n.d. | n.d. |
| b | Liquid phase | VO(acac)₂ | +IV | Calcination | 1.10 | n.d. | n.d. | n.d. | 1.10 | 632 | 6.5 | 0.76 |
| c | Liquid phase | VO(acac)₂ | +IV | HNO₃/H₂O₂ | n.d. | n.d. | n.d. | n.d. | n.d. | n.d. | n.d. | n.d. |
| d | Liquid phase | VO(acac)₂ | +IV | KMnO₄ | n.d. | n.d. | n.d. | n.d. | n.a. | n.a. | n.a. | n.a. |
| 4 a | Liquid phase | VOCl₃ | +V | - | 0.96 | 589 | 6.0 | 0.52 | 0.92 | 589 | 6.7 | 0.67 |
| b | Incipient wetness | VOCl₃ | +V | - | 0.84 | 536 | 5.9 | 0.54 | 0.94 | 625 | 6.5 | 0.65 |
| 5 | Liquid phase | NH₄VO₃ | +V | - | 0.86 | 531 | 6.2 | 0.51 | 0.97 | 613 | 6.4 | 0.63 |
| 6 a | Liquid phase | VOSO₄ | +IV | - | 0.75 | 567 | 6.0 | 0.53 | n.a. | n.a. | n.a. | n.a. |
| b | Liquid phase | VOSO₄ | +IV | Calcination | n.d. | n.d. | n.d. | n.d. | n.a. | n.a. | n.a. | n.a. |
| 7 | Liquid phase | VO(iPrO)₃ | +V | - | 0.61 | 423 | 5.2 | 0.49 | n.a. | n.a. | n.a. | n.a. |
| 8 | Gas phase- HMR | VOCl₃ | +V | - | 0.50 | 589 | 5.9 | 0.49 | 0.93 | 611 | 6.5 | 0.75 |
| 9 a | Gas phase- ALD | VO(iPrO)₃ | +V | - | 0.56 | 602 | 0.59 | 0.51 | 0.97 | 648 | 6.4 | 0.71 |
| b | Gas phase- ALD | VO(iPrO)₃ | +V | -V-O-V-OH | n.d. | n.d. | n.d. | n.d. | n.d. | n.d. | n.d. | n.d. |
| c | Gas phase- ALD | VO(iPrO)₃ | +V | -V-O-V-O-V-OH | n.d. | n.d. | n.d. | n.d. | n.d. | n.d. | n.d. | n.d. |
| *(b) titanium oxide catalysts* | | | | | | | | | | | | |
| 10 a | Liquid phase | Ti(OBu)₄ | +IV | - | 0.52 | 502 | 6.2 | 0.57 | 1.0 | 629 | 6.4 | 0.71 |
| b | Liquid phase | Ti(OBu)₄ | +IV | HMDS | n.d. | 465 | 6.0 | 0.45 | n.d. | n.d. | n.d. | n.d. |
| 11 | Liquid phase | TiCl₄ | +IV | - | 0.43 | 556 | 6.3 | 0.50 | 0.91 | 644 | 6.5 | 0.75 |
| 12 | Gas phase- HMR | TiCl₄ | +IV | - | 0.52 | 532 | 6.2 | 0.54 | 0.95 | 687 | 6.6 | 0.76 |
| 13 a | Gas phase- ALD | TDMAT | +IV | - | 0.47 | 423 | 6.1 | 0.53 | 1.08 | 654 | 6.4 | 0.74 |
| b | Gas phase- ALD | TDMAT | +IV | -Ti-O-Ti-OH | n.d. | n.d. | n.d. | n.d. | n.d. | n.d. | n.d. | n.d. |
| c | Gas phase- ALD | TDMAT | +IV | -Ti-O-Ti-O-Ti-OH | n.d. | n.d. | n.d. | n.d. | n.d. | n.d. | n.d. | n.d. |
| *(c) mixed vanadium/titanium oxide catalysts* | | | | | | | | | | | | |
| 14 | Gas phase– ALD | VO(iPrO)₃+ TDMAT | | -Ti-O-V-OH | n.d. | n.d. | n.d. | n.d. | n.d. | n.d. | n.d. | n.d. |
| 15 | Gas phase– ALD | VO(iPrO)₃+ TDMAT | | -V-O-Ti-O-V-OH | n.d. | n.d. | n.d. | n.d. | n.d. | n.d. | n.d. | n.d. |
| 16 | Gas phase– ALD | VO(iPrO)₃+ TDMAT | | -V-O-Ti-OH | n.d. | n.d. | n.d. | n.d. | n.d. | n.d. | n.d. | n.d. |
| 17 | Gas phase– ALD | VO(iPrO)₃+ TDMAT | | -Ti-O-V-Ti-OH | n.d. | n.d. | n.d. | n.d. | n.d. | n.d. | n.d. | n.d. |

HMR = homemade reactor; ALD = advanced atomic layer deposition reactor; n.a. = not applicable (not synthesized); n.d. = not determined. The specific surface area is calculated using the BET-method (Brunauer-Emmett-Teller). The total pore volume is determined at p/p° = 0.98-0.99. The mean pore size is determined by the BJH-method at the adsorption branch. The titanium and vanadium oxide catalysts are synthesized starting from different phenolic resin and silica batches. The silica based catalysts are numbered equally to the numbering of the corresponding mesoporous phenolic resin supported catalysts and are marked with an accent (') in Figure 4.6.

### 4.3 Selection of the catalytic oxidation tests

Vanadium and titanium oxide catalysts are reported in literature as excellent catalysts for a variety of catalytic oxidation processes. Here, two oxidation reactions were selected as test reaction for the newly synthesized catalysts. Initially, this selection was mainly based on the simplicity of the test reaction, e.g. easy analysis of reaction products, minimal production of by-products, uncomplicated reactor settings, etc. The two selected catalytic test reactions are: (1) cyclohexene epoxidation and (2) toluene oxidation (see Figure 4.5). In this study, the novel catalysts are mainly investigated in the cyclohexene epoxidation and the catalytic performance was compared to the silica reference catalysts.

### 4.3.1 Cyclohexene epoxidation

In recent years, the epoxidation of cyclohexene has attracted intensive attention seeing as cyclohexene epoxide is a key intermediate in the synthesis of adipic acid, a monomer for the industrial production of nylon-6,6.[38, 39] The major reaction products are shown in Figure 4.5. Three pathways can be observed: (a) epoxidation reaction, (b) radical pathway between the substrate and the oxidant *tert*-butylhydroperoxide and (c) allylic oxidation. In presence of water, the epoxide ring can open due to the nucleophilic attack of water molecules on the electrophilic carbon centre of the epoxide. Considering this consecutive reaction, the *trans*-diol isomer **3** is formed. Usually, the reaction products of reaction pathways (b) and (c) are not considered to be useful byproducts. However, they can give very useful and diagnostic insights into the catalytic pathway.[40]

### 4.3.2 Toluene oxidation

The selective oxidation of toluene to benzoic acid represents a key process in several chemical plants. Benzoic acid forms the starting product for the industrial production of different chemical compounds like ε-caprolactam.[41] Additionally, its derivative sodium benzoate finds wide applications in food and fine chemical industry.[42] Figure 4.5 shows a simplified reaction mechanism of the selective oxidation of toluene towards benzoic acid. Here, toluene is firstly oxidized to benzyl alcohol or benzaldehyde. The former can be transformed further into benzaldehyde and is finally converted into benzoic acid. Note that this simplified reaction scheme does not represent the actual elementary reactions, but directly shows the stoichiometric reactions.[43]
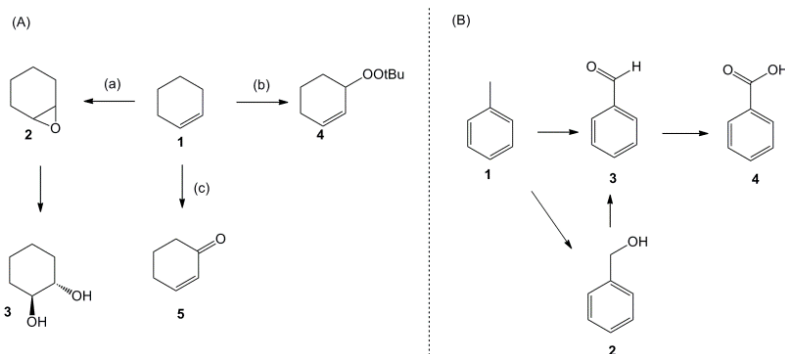
**Figure 4.5 – Overview of the selection of catalytic oxidation tests: (A) oxidation of cyclohexene 1 with *tert*-butylhydroperoxide towards the main reaction products: (a) epoxidation to cyclohexene oxide 2 and consecutive ring opening to cyclohexane-1,2-diol 3, (b) radical pathway to *tert*-butyl-2-cyclohexenyl-1-peroxide 4 and (c) allylic oxidation to 2-cyclohexene-1-one 5; (B) Simplified reaction mechanism of the oxidation of toluene 1 towards benzoic acid 4 via benzyl alcohol 2 and benzaldehyde 3.**

**4.4 Catalytic performance: results**

The novel synthesized catalysts of Table 4.1 were first of all tested in the epoxidation of cyclohexene. As a reference, the silica functionalized materials were also evaluated. An abundance of results were obtained. Here, only the most significant summary will be discussed.

Figure 4.6 shows the catalytic performance of the catalysts in the epoxidation of cyclohexene. All these silica based catalysts show relative high activity (not shown) and selectivity (> 40%) towards the epoxide. Furthermore, it can also be concluded that the titanium oxide based catalysts are more selective than the vanadium oxide catalysts (±80% for catalyst 10'-13'*versus* ±40% for catalysts 1'-9'). A small increase of selectivity for the mixed metal oxide catalysts is observed and the titanium oxide catalyst 16' with a vanadium interlayer (-V-O-Ti-OH) showed the highest selectivity of 84% towards the epoxide. Figure 4.6b shows the selectivity towards the epoxide of the mesoporous phenolic resin based catalysts. Cyclohexene conversions around 20% (after 8 hours) with high selectivity (> 80%) for the radical product *tert*-butyl-2-cyclohexenyl-1-peroxide are obtained (data not shown). This product is formed by a radical pathway which is initiated through decomposition of the oxidant *tert*-butylhydroperoxide.[40] Furthermore, in contrast to the silica based catalysts, very limited or no selectivity towards epoxide formation was observed. As can be seen in Figure 4.6b, neither the deposition method nor the choice of the metal precursor or a post-synthesis treatment have a positive impact on the catalytic performance of the solids. The selectivity towards the epoxide never exceeded the 5% level. Additionally, catalysts 3a, 3b, 4a, 4b, 8, 10a, 11 and 12 were tested

in the oxidation of toluene with hydroperoxide as oxidant. However, the catalytic performance of all the supported phenolic resin catalysts did not exceeded the blanc levels in the different test reactions.
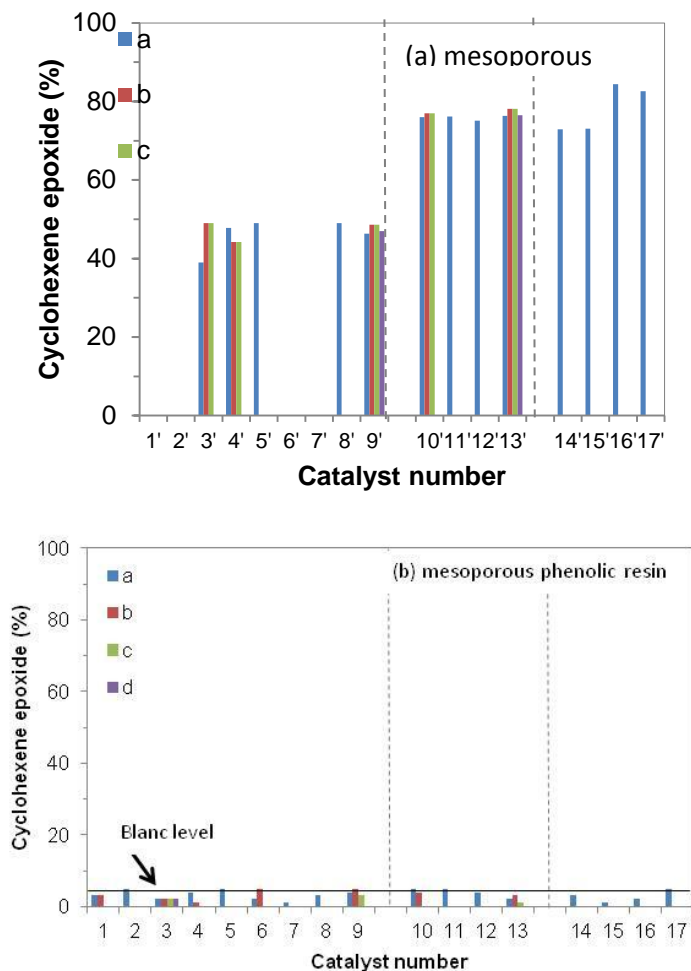


**Figure 4.6 – Overview of the catalytic performance in the epoxidation of cyclohexene with *tert*-butylhydroperoxide: (a) mesoporous silica SBA-15 and (b) mesoporous resin supported vanadium and titanium oxide catalysts. The bars represent the selectivity of the catalyst towards cyclohexene epoxide (after 8 hours reaction). The 5% line represents the blanc level. The catalyst numbers correspond with the numbers in Table 4.1.**

**4.5 Catalytic performance: characterization**

As discussed in section 4.4, the mesoporous phenolic resin supported vanadium and titanium oxide catalysts show very poor or even no significant catalytic activity in the two catalytic oxidation reactions. Moreover, it has been shown that – and this is also in contrast to the silica supported reference catalysts – neither the deposition method nor the choice of metal precursor or a post-synthesis treatment have a positive impact on the catalytic performance of the solids (Figure 4.6). In order to provide a proper explanation for this inactivity, a thorough characterization of the mesoporous supported solids by means of different analysis techniques is discussed below. The characterization is mainly based on the vanadium oxide catalyst 8, however, similar conclusions can be made for the other catalysts in Table 4.1.

The presence of clusters of crystalline $V_2O_5$ species on the surface – or the lack thereof – can generally be confirmed by RAMAN-spectroscopy or X-ray diffraction measurements.[46] Taking into account that mesoporous phenolic resins are amorphous polymers ánd dark brownish-black coloured, sample heating due to the phenomenon of black body radiation of the black support is responsible for a broad band in the RAMAN spectrum. This broad 'support band' completely dominates the RAMAN spectrum. It was not possible to avoid or minimize this interference by changing the laser type from FT-RAMAN (1064 nm laser) to dispersive RAMAN equipment (532 nm and 780 nm laser). As a result, RAMAN measurements did not allow a confirmation of the presence/absence of crystalline metal oxide clusters on the surface.

On the other hand, the absence of crystalline $V_2O_5$ clusters was successfully confirmed by means of X-ray diffraction measurements. The wide angle XRD pattern, shown in Figure 4.7, shows only a broad peak at $2\theta$ = 20-25, originating from the original phenolic resin support. As a reference, the powder-XRD pattern of crystalline $V_2O_5$ is also included in Figure 4.7. From these data, it can be concluded that no crystalline phases are present on the supports.

The oxidation state and the geometric structure of the vanadium oxide species grafted on the surface of mesoporous phenolic resins is verified by means of X-ray photoelectron spectroscopy. Figure 4.7 contains the $V2p_{3/2}$ region in the XPS spectra of the mesoporous phenolic resin after gas phase $VOCl_3$ deposition (catalyst 8) and of the reference samples $V_2O_5$, $NH_4VO_3$ and $VO(acac)_2$. Two different $V2p_{3/2}$ peaks at 514.1 eV and 511.8 eV can be distinguished for the phenolic resin after $VOCl_3$ treatment. A comparison of the binding energies of the V2p core levels for the phenolic supported sample to those for bulk polymeric $V_2O_5$ suggests the absence of crystalline clusters on the surface (this is also in agreement with the previously discussed XRD measurements). The $V2p_{3/2}$ peak at 514.1 eV of the phenolic resin accords with the $V2p_{3/2}$ peak of the reference sample $NH_4VO_3$ (513.9 eV), which indicates a tetrahedral geometry of the species with the vanadium center in the +V oxidation state. Surprisingly, a second peak at the lower binding energy of

511.8 eV is also distinguished. This peak position corresponds with the binding energy of the reference sample VO(acac)$_2$ and can be attributed to a lower +IV oxidation state, although the vanadium center in the initial vanadium precursor VOCl$_3$ exhibits the +V oxidation state. Vanadium species are, however, very sensitive to reduction and the reduction of vanadium during the XPS-measurement under hard vacuum conditions is already reported in the literature.[22] Indeed, the ratio of the +IV:+V increased from 1:2 to 1:1 after sputtering the samples with argon bombardement under ultra-high vacuum conditions.
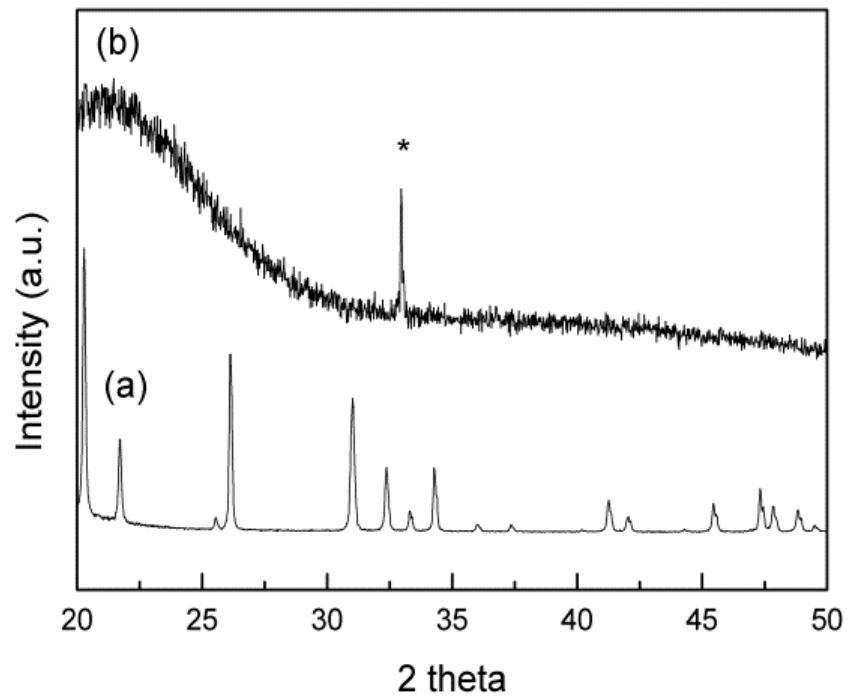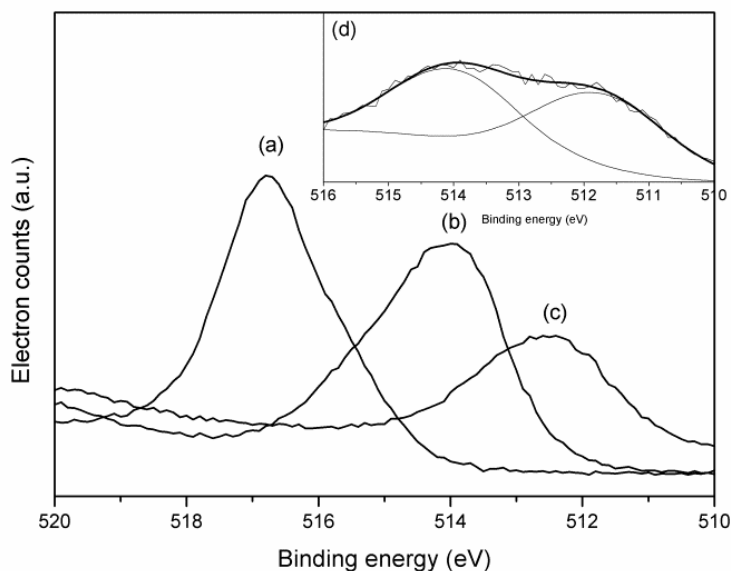
**Figure 4.7 – TOP: Wide angle XRD pattern of (a) V$_2$O$_5$ and (b) mesoporous phenolic resin supported vanadium oxide catalyst. The asterisk indicates the background signal of the sample holder, 2 θ = 32.9°. BOTTOM: V2p$_{3/2}$ region in the XPS spectra of (a) V$_2$O$_5$, (b) NH$_4$VO$_3$, (c) VO(acac)$_2$ and (d) Vanadium oxide supported on mesoporous phenolic resin.**

Furthermore, supplementary analysis techniques were applied to characterize thoroughly the novel supported catalysts. However, some have proven to be more successful and reliable than others.

Figure 4.8 shows the diffuse reflection infrared spectra of the mesoporous phenolic resins of the phenolic resin supported vanadium oxide catalyst. Here, a new absorption peak at 1010 cm$^{-1}$ was assigned to a V=O or V-O-C bond vibration.[47] Note that the intensity of the hydroxyl groups in the region 3600-3400 cm$^{-1}$ is significantly decreased, resulting from reaction with the metal precursor. Although the peaks are less resolved after deposition, the main characteristic absorption bands of the original mesoporous phenolic resin remained, indicating the stability of the support towards the deposition conditions. Next, UV/VIS spectra of supported vanadium oxide catalysts show absorbance in the 200-450 nm region.[6] This absorbance is specific for isolated (pseudo)tetrahedral +V vanadium oxide structures, generally accepted in literature as the catalytic active species (see also §4.1). When the samples are exposed to air, the ligand to metal (L → M) charge transfer band shifts to the visible region due to an increase of the metal coordination sphere by coordinating water molecules. For silica supported catalysts (SBA-15 type) the hydration

process proceeds very fast (within several minutes) and is associated with a visible colour change of the catalyst from white to light yellow. Here, however, diffuse reflectance UV/VIS spectroscopy has shown not to be an appropriate tool to study the nature of the resin supported metal species due to the intrinsic interaction of the UV/VIS light with the dark support: a 100% absorbancy in the 200-800 nm region was observed. Consequently, specific peaks to identify the nature of the supported metal oxide species could not be distinguished by UV/VIS measurements. Additionally, solid state $^{13}$C NMR of the mesoporous phenolic resin and the $^{13}$C and $^{51}$V NMR spectra of the supported resin show very broad bands. Unfortunately, the resolution of the spectra was insufficient to give more insight in the nature of the supported species. Finally, nitrogen sorption measurements of the catalysts after metal oxide deposition revealed that the porosity characteristics remained after deposition. As can be seen in Figure 4.8, also no pore blocking was observed after deposition of the metal precursor in the pores, based on the shape of the hysteresis of the isotherms. Only the nitrogen sorption isotherms of the catalysts synthesized via the one-pot synthesis method (4.1 and 4.2) showed a two-step desorption branch, indicating a small percentage of pore blocking. [22]
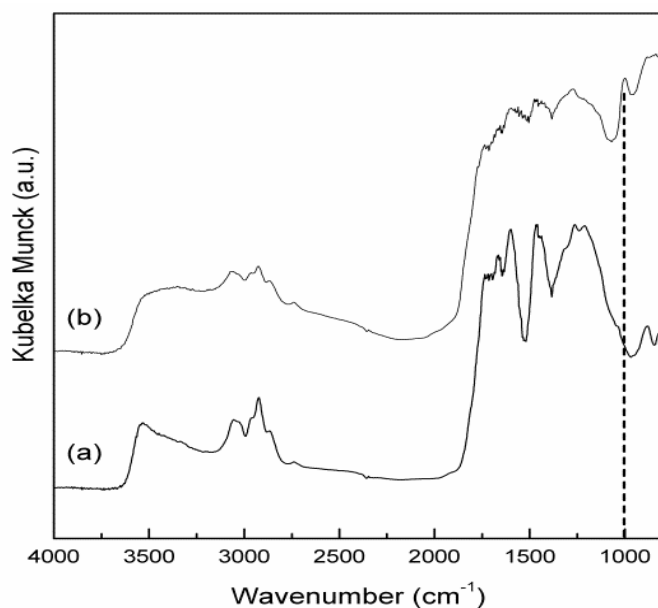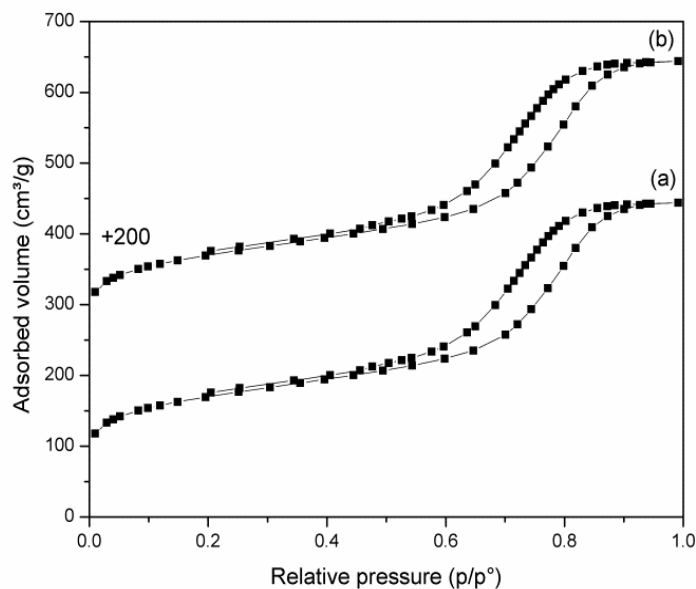
**Figure 4.8 – TOP: (a) original mesoporous phenolic resin and (b) after vanadium oxide deposition with VOCl₃. LEFT: Diffuse reflection infrared spectra. BOTTOM: Nitrogen sorption isotherms (STP conditions; for clarity, isotherm (b) is shifted to above with 200 cm³/g).**

### 4.6 Catalytic performance: discussion

As can be summarized from the discussion above, the geometric structure, the oxidation state and the loading of the supported metal oxide species on the one hand and the stability of the mesoporous phenolic resin support at the other, combine all the proper qualities needed for a vanadium or titanium oxide supported oxidation catalyst. However, compared to the silica catalysts, very limited or no catalytic activity in one of the test reactions was observed. In order to verify if the catalytic activity of the silica based catalysts is the consequence of leaching, a more in depth study by leaching and hot filtration experiments has been performed.

Figure 4.9 shows the comparison of the leaching resistance under relative severe conditions between the silica and the mesoporous phenolic resins based catalysts. Here, the fresh synthesized catalysts were consecutively treated by stirring the catalysts in (1) ice-cold water, (2) in water and (3) in a 2.5M hot sulphuric acid solution at 80°C. After filtration, the residual vanadium loading was determined. In case of the silica support, the amount of vanadium that leached during the washing procedure amounted to 60-80% and

after 3 consecutive leaching experiments more than 90% was leached. In contrast, in the case of the mesoporous phenolic resins only an amount of 20-30% of the vanadium could be found in the first washing solution. Moreover, a decreasing leaching trend line after three leaching experiments is observed and stirring the catalyst in a hot 2.5M sulphuric acid solution exhibits a leaching of merely 4-7%. These observations of strongly reduced leaching behavior can be explained by the more hydrophobic nature of the polymer surface which prevents attack of water molecules to the active sites and the less acidic character of the phenol group (phenol pKa = 10 versus silanol pKa = 2.2) which shows stronger affinity to the acidic vanadium oxide species.[22] After determination of the leaching resistance of both catalysts, the question now is whether or not the epoxide reaction proceeds heterogeneously, or in other words, are the leached species responsible for the catalytic epoxidation of the substrate in case of the silica based catalysts?

To provide a rational answer to this question, a split test (also known as a hot filtration experiment) in the cyclohexene epoxidation for the silica based catalyst was performed. Here, the catalyst was filtered from the hot reaction mixture after 4 hours reaction and the conversion was followed without the catalyst. Figure 4.9 shows the total cyclohexene conversion and the cyclohexene epoxidation formation. Although the total cyclohexene conversion continues due to the progressive radical formation of *tert*-butyl-2-cyclohex-enyl-1-peroxide, this reaction profile clearly shows that the formation of cyclohexene epoxide instantly ends after filtration. Although a considerable amount of the metal oxide centres was leached, the stagnation of the epoxide formation indicates that the leached metal centres are not responsible for the catalytic epoxidation and that the epoxidation reaction occurs heterogeneously at the supported oxide centres.
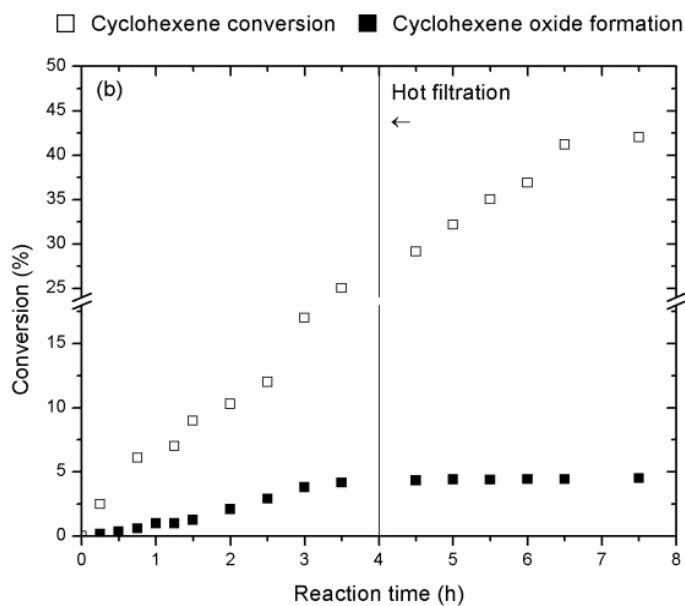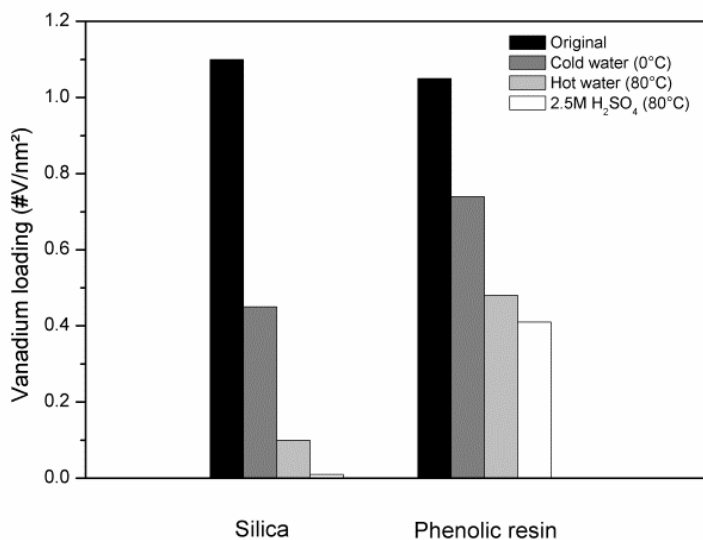
**Figure 4.9 – TOP: Leaching resistance of mesoporous silica and phenolic resin supported vanadium oxide catalysts. BOTTOM: Hot filtration experiment of a silica supported vanadium oxide catalyst in the epoxidation of cyclohexene.**

At first glance, these results seem contradictory: on the one hand, the hot filtration experiment showed that the epoxidation occurs heterogeneously and the supported metal oxide centers are responsible for the epoxidation of cyclohexene (*vide* hot filtration experiment of the silica catalysts). On the other hand, the metal oxide centres, which are (too?) strongly bound to the surface are not able to epoxidize cyclohexene (*vide* leaching experiment of the mesoporous phenolic resin based catalysts). A plausible answer is given by the proposed reaction mechanism discussed below and supports integrally the recent discussion in literature about the critical role of the support-oxygen-metal bound in oxidation reactions.[11, 12]

Figure 4.10 shows an overview of the proposed reaction cycles for the supported catalysts. In the ideal case, when the hydroxyl density on the silica surface is high, the unsaturated metal centre is triply bound to the surface in a tetrahedral coordination. Initially, the metal centre coordinates with a *tert*-butylhydroperoxide molecule (1). In the next step, one support-oxygen-metal (S-O-M) bond weakens and a proton transfer from the peroxide to the support takes place with the formation of a peroxocomplex and a free silanol group (2). Subsequently, the olefin enters the reaction cycle (3) and coordinates with the M-complex. Here, the peroxocomplex transfers an oxygen atom to the hydrocarbon substrate. The mechanism of this oxygen transfer of peroxometal complexes to nucleophilic substrates is still a matter of considerable debate. Next, the cyclohexene oxide molecule desorbs from the metal centre and the epoxide product exits the catalytic run (4). Finally, a new proton transfer occurs for the recovery of the original metal complex triply bound to the support, together with the exit of the decomposition product *tert*-butanol. The reaction cycle is closed when the metal centre coordinates with a free hydroxyl group on the substrate surface. This final step in the reaction cycle is extremely important in the regeneration of the catalyst: the initial configuration is only obtained when this final step takes place. If not, the metal centre, which was initially triply bound to the support, is only double bound to the surface. Now, the catalyst can run another two times through the catalytic cycle and will finally leach from the support. Considering this reaction pathway, the surface oxygen bond is assumed to be critical in the epoxidation reaction. This reaction cycle is in agreement with the general perspectives in literature about supported metal oxide catalysts. [11]

In case of the mesoporous phenolic resin catalysts, the reaction mechanism is depicted in Figure 4.10(b). Here, the metal oxide centers are supposed to be covalently bound by only one single bond (or at maximum one double bond), since the hydroxyl density is lower than for the hydrophilic silica surface. The oxidant *tert*-butylhydroperoxide enters the reaction cycle, however, the S-O-M bond is hard to break and as a consequence, the active peroxocomplex is not formed. This reaction mechanism, where the surface oxygen bond has to break in order to form a peroxocentre provides an answer why the strongest bonded and the leached metal centres are not catalytically active in the epoxidation of cyclohexene.

Taking into account the discussion above, two main conclusions can be made: (1) The

supported metal oxide species have to be able to form the active metal peroxocomplex by breaking the support-oxygen-metal bond in step 2. As a consequence, this bond may not be too strong. (2) Full regeneration and reduction of the leaching can only be accomplished when the support-oxygen-metal bond is reinstalled. As a result, the observed catalytic (in)activity and leaching for the mesoporous phenolic resin and the silica based catalysts can be explained by non-conformity of the catalysts with conditions (1) and (2) respectively.

## 4.7 Summary and conclusions

Vanadium and titanium oxide are widely used as oxidation catalysts in a variety of industrial production processes of chemical compounds. Mostly inorganic oxides, e.g. silica, are used as support for these metal oxides. From the viewpoint of durability, poor leaching resistance and stability issues are the main drawbacks of these common catalytic systems.

In this chapter, mesoporous phenolic resins are introduced as novel potential support for vanadium and titanium oxide. The synthesis of these new catalytic systems is described and their catalytic performance is validated in two selected oxidation test reactions. A thorough characterization study has been performed. The black color and the organic nature of the novel mesoporous support made the characterization of the supported species – mainly by spectroscopic techniques – highly challenging. Despite the geometric structure, the oxidation state and the loading of the active metal oxide species on the one hand and the stability of the mesoporous phenolic resin support at the other, combine all the proper qualities needed for a good oxidation catalyst, very limited or no catalytic activity was observed in one of the three test reactions. Efforts have been made to provide an explanation for this inactivity and the hypothesis of the critical strength of the support-oxygen-metal bond has been discussed. Despite all the attempts made, the catalytic activity of the novel systems could not be significantly improved. Finally, it was concluded that the mesoporous phenolic resin based catalysts do not exceed the activity of the silica reference catalysts and are consequently not ideal candidates to apply them as novel support for vanadium and titanium oxide in heterogeneous oxidation catalysis. Nevertheless, it has been shown that mesoporous phenolic resins are very valuable solid materials in terms of stability and leaching resistance. Moreover, the obtained results support the 'critical bond' theory and is therefore very useful information - especially from the viewpoint of advanced catalyst design – for the further improvement of actual supported metal oxide catalysts and the development of original and innovative catalytic systems.
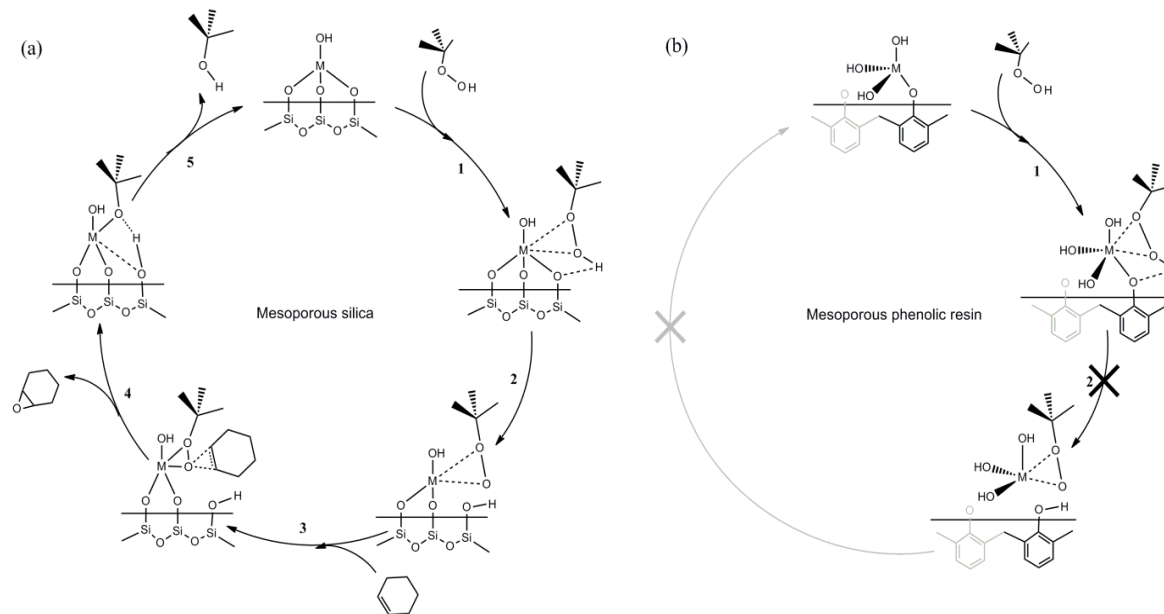
**Figure 4.10 – Proposed reaction mechanism of the cyclohexene epoxidation for (a) silica supported catalyst and (b) phenolic resin supported catalyst. Breaking the support-oxygen-metal (S-O-M) bond in step 2 is assumed to be critical for the epoxidation of cyclohexene (M = V or Ti). Step 5 is essential for full regeneration of the catalyst after catalytic run.**

**4.8 Experimental**

**Synthesis of mesoporous phenolic resins:** mesoporous phenolic resins were synthesized using the evaporation induced self-assembly method reported by Zhao et al.[48] Phenol (1.2 g) was melted at 45 °C before NaOH solution (10 mL, 6.25 M) was added slowly while stirring. Formaline solution (2.4 mL, 37 wt.% formaldehyde in water) was added dropwise. The reaction mixture was stirred at 70 °C for 1 h. After cooling to room temperature, the pH of the reaction mixture was neutralized with HCl (0.6 M). Water was removed under vacuum at 45 °C. The product was dissolved in ethanol (20 mL) and added to Pluronic F127 (3.2 g) dissolved in ethanol (30 mL). The solution was stirred for 10 min at room temperature and transferred to a dish to evaporate the ethanol. The membrane was thermopolymerized at 100 °C in air. Finally, the mesoporous structure was calcined under a nitrogen flow at 350 °C for 6 h (heating rate: 1 °C/min).

**Synthesis of SBA-15:** The SBA-15 materials were synthesized by using P123 as the surfactant and TEOS as the silica source.[49] In a typical synthesis, P123 (4 g) was dissolved in HCl (120 mL, 2 M) and distilled water (30 mL). TEOS (9.1 mL) was added, and the mixture was stirred vigorously at 45 °C for 5 h followed by an aging step at 90 °C for 20 h. Finally, the white precipitated product was collected by filtration, washed with distilled water, dried and calcined in air at 550 °C for 6 h (heating rate: 1 °C/min).

**Liquid phase deposition:** For the liquid phase impregnation, 0.5 g of the support is refluxed in a 30 mL dry saturated toluene solution of the metal precursor for 5 hours. For the vanadium precursor $NH_4VO_3$, water was used as solvent. Next, the catalyst is filtrated, washed with the solvent and acetone. Finally, the catalysts were collected by filtration, washed thoroughly, exposed to air and dried in *vacuo* at 90°C. *Incipient wetness impregnation* – The total pore volume of the mesoporous material was measured by nitrogen sorption measurements. Then, a dry toluene solution (equal amount as the calculated pore volume) of $VOCl_3$ (0.05M) was dropwise added to 0.5g support at room temperature. The catalyst was exposed to air and dried at 90°C in *vacuo*.

**Gas phase deposition – home made reactor:** Figure 4.2 shows the experimental set-up of the home-made reactor. Pre-dried mesoporous support (0.5 g) is placed on a silica grid (1). The metal oxide precursor is situated at the bottom (2). Valve (3) at the bottom is closed and a dynamic vacuum is installed by opening valve (5) and valve (3) at the top. The dotted line (6) represents a furnace to control the deposition temperature at 350°C. Gas phase deposition was performed with vanadium(V)oxychoride ($VOCl_3$) and titanium(IV)chloride ($TiCl_4$). Prior to deposition, these metal precursor solutions are first treated by the freeze-pump-thaw technique, to guarantee degassing of the precursors. After deposition, the samples are degassed for two additional hours, to ensure removal of all physically adsorbed metal excess. Finally, the samples are exposed to air, to induce hydrolysis of unreacted side groups.

**Gas phase deposition – atomic layer deposition reactor:** Prior to the deposition, the powders were stored at elevated temperature under vacuum in the ALD reactor. Vacuum

is slowly installed in the reactor through a needle valve during sample loading and slowly vented during unloading to prevent loss of the powders. A base pressure of $5\times10^{-7}$ mbar was measured. Titanium and vanadium oxide were deposited from TDMAT and VO($i$PrO)$_3$ respectively.[50-52] TDMAT and VO($i$PrO)$_3$ were heated to 40 °C, and water was stored at room temperature. The gases entered the reactor through heated lines (45 °C) to prevent condensation, and a turbomolecular pump continually evacuated the reactor. The deposition temperature was 150 °C. The reactant pulses were automated by computer controlled pneumatic valves. Both SBA-15 and mesoporous phenolic resins were functionalized with: (1) a (sub)monolayer of titanium or vanadium oxide with different loadings, (2) multiple (mono, double and triple) titanium or vanadium oxide layers and (3) mixed titanium and vanadium oxide layers (see Table 4.1).

**Post-synthesis treatment:** *Hydrophobization treatment* – 0.5 g functionalized support is refluxed at 125°C in 10 mL hexamethyldisilazane for 5 hours. Next, the catalyst is filtrated, thoroughly washed with toluene and acetone. Finally, the catalyst is dried at 90°C in *vacuo*. *Oxidation treatment with HNO$_3$/H$_2$O$_2$* – 0.5 g support is stirred in a mixture of 20 ml hydrogen peroxide (30wt% in water). To this solution, 2 ml nitric acid (68wt%) is added dropwise and stirred for 3 hours at room temperature. Next, an additional amount of 2 ml nitric acid is added dropwise and stirred for 21 hours at room temperature. The resins are filtrated and thoroughly washed with water until pH 7 and finally washed with acetone. The catalysts were *vacuo* dried at 90°C overnight. *Oxidation treatment with KMnO$_4$* – 0.5 g support is stirred in a 0.1M KMnO$_4$-solution for 4 hours at room temperature. The resins are filtrated and thoroughly washed with water and acetone. Finally, the catalysts were *vacuo* dried at 90°C overnight.

**Catalytic experiments:** *Cyclohexene epoxidation* – In a typical catalytic run, chloroform (10.0 mL), cyclohexene (1.5 mL, 15 mmol), *tert*-butyl hydroperoxide (5.5 M in decane, 5.5 mL, 30 mmol) and 1,2,4-trichlorobenzaldehyde (internal standard, 1.8 mL, 15 mmol) were heated to reflux in a two-necked round bottomed flask with vigorous stirring under argon at 80 °C and the dried catalyst (30 mg) was added.[40] The conversion of cyclohexene was followed by sampling 0.1 mL of the reaction medium. The sample was immediately diluted with ethyl acetate (0.5 mL) and analysed by GC. *Toluene oxidation* – In a typical run, acetonitrile (30.0 mL), toluene (2.0 mL, 18.9 mmol), *tert*-butylhydroperoxide (5.5 M in decane, 37.8 mmol) and dodecane (internal standard, 4.3 mL, 18.9mmol) are refluxed in a two-necked round bottomed flask with vigorous stirring under argon at 80°C and dried catalyst (50 mg) was added. [53, 54] The conversion of toluene was followed by sampling 0.1 mL of the reaction medium several times. The sample was immediately diluted with acetonitrile (0.5 mL) and analysed by GC. *Propylene epoxidation* – The catalytic tests were carried out in cooperation with dr. Jan-Karel Buijink in the research lab of Shell Chemicals (site Amsterdam) using a pilot reactor setting. Due to professional secrets, more specific details concerning the reaction conditions are not permitted to publish.

**Characterization:** Nitrogen gas sorption experiments were conducted at 77 K with a Micromeritics Tristar 3000. Samples were vacuum dried at 120 °C prior to analysis. The

pore size distribution was calculated from the adsorption branch, and the micropore volume was calculated using the *t*-plot method. X-ray powder diffraction

patterns were collected with an ARL X-TRA Diffractometer with Cu-Kα radiation with 0.15418 nm wavelength. DRIFT-spectra were measured on a EQUINOX-55 spectrometer of Bruker and on a Nicolet 6700 FT-IR spectrometer of ThermoScientific. XPS measurements were performed on S-probe monochromatized XPS spectrometer Al(KR) radiation (1486 eV) as probe of Surface Science Instruments (VG). GC was performed with a Thermo/Interscience Ultra Fast GC equipped with a flame ionisation detector and a 5% diphenyl/ 95% polydimethylsiloxane column (10 m length and 0.10 mm internal diameter). Helium was used as carrier gas and the flow rate was programmed at 0.8 mL/min. X-ray fluorescence (XRF) spectroscopy measurements were performed with a Bruker system with molybdenum X-rays. The titanium and vanadium loadings on SBA-15 were verified by XRF spectroscopy. The surface areas of the silicon, titanium and vanadium peaks were determined at 1.74 keV, 4.51 keV and 4.95 keV respectively. For the phenolic resin samples, the titanium and vanadium loadings were quantified colorimetrically by UV/VIS spectroscopy with a UV/VIS Varian spectrophotometer following the procedure described by Vogel.[55]

## 4.9 References

[1] J.A.L. da Silva, J.J.R.F. da Silva, A.J.L. Pombeiro, *Coordin Chem Rev*, **2011**, 255, 2232-2248.

[2] S. Shylesh, M.J. Jia, W.R. Thiel, *Eur J Inorg Chem*, **2010**, 4395-4410.

[3] S. Todorova, V. Parvulescu, G. Kadinov, K. Tenchev, S. Somacescu, B.L. Su, *Micropor Mesopor Mat*, **2008**, 113, 22-30.

[4] M.R. Maurya, A. Kumar, J.C. Pessoa, *Coordin Chem Rev*, **2011**, 255, 2315-2344.

[5] V. Polshettiwar, C. Len, A. Fihri, *Coordin Chem Rev*, **2009**, 253, 2599-2626.

[6] R. Bulanek, L. Capek, M. Setnicka, P. Cicmanec, *J Phys Chem C*, **2011**, 115, 12430-12438.

[7] A.E. Lewandowska, M. Calatayud, E. Lozano-Diz, C. Minot, M.A. Banares, *Catal Today*, **2008**, 139, 209-213.

[8] M. Mathieu, P. Van Der Voort, B.M. Weckhuysen, R.R. Rao, G. Catana, R.A. Schoonheydt, E.F. Vansant, *J Phys Chem B*, **2001**, 105, 3393-3399.

[9] E.L. Lee, I.E. Wachs, *J Phys Chem C*, **2007**, 111, 14410-14425.

[10] I.E. Wachs, *Catal Today*, **2005**, 100, 79-94.

[11] I. Muylaert, P. Van Der Voort, *Phys Chem Chem Phys*, **2009**, 11, 2826-2832.

[12] B.M. Weckhuysen, D.E. Keller, *Catal Today*, **2003**, 78, 25-46.

[13] M. Cozzolino, R. Tesser, M. Di Serio, E.M. Gaigneaux, P. Eloy, E. Santacesaria, *Stud Surf Sci Catal*, **2006**, 162, 697-704.

[14] D. Shee, T.V.M. Rao, G. Deo, *Catal Today*, **2006**, 118, 288-297.

[15] L. Fabian-Mijangos, L. Cedeno-Caero, *Ind Eng Chem Res*, **2011**, 50, 2659-2664.

[16] S.L. Wegener, H. Kim, T.J. Marks, P.C. Stair, *J Phys Chem Lett*, **2011**, 2, 170-175.

[17] M. Baltes, P. Van Der Voort, B.M. Weckhuysen, R.R. Rao, G. Catana, R.A. Schoonheydt, E.F. Vansant, *Phys Chem Chem Phys*, **2000**, 2, 2673-2680.

[18] P. Van Der Voort, M. Baltes, E.F. Vansant, *J Phys Chem B*, **1999**, 103, 10102-10108.

[19] R. Chlosta, G. Tzolova-Muller, R. Schlogl, C. Hess, *Catal Sci Technol*, **2011**, 1, 1175-1181.

[20] Y. Deng, C. Lettmann, W.F. Maier, *Appl Catal a-Gen*, **2001**, 214, 31-45.

[21] R.A. Sheldon, M. Wallau, I.W.C.E. Arends, U. Schuchardt, *Accounts Chem Res*, **1998**, 31, 485-493.

[22] I. Muylaert, M. Borgers, E. Bruneel, J. Schaubroeck, F. Verpoort, P. Van Der Voort, *Chem Commun*, **2008**, 4475-4477.

[23] L.Y. Song, K.X. Li, X.H. Li, P. Wu, *React Kinet Mech Cat*, **2011**, 104, 99-109.

[24] L. She, J. Li, Y. Wan, X.D. Yao, B. Tu, D.Y. Zhao, *J Mater Chem*, **2011**, 21, 795-800.

[25] P. Gao, A.W. Wang, X.D. Wang, T. Zhang, *Catal Lett*, **2008**, 125, 289-295.

[26] M. Bowker, A. Nuhu, J. Soares, *Catal Today*, **2007**, 122, 245-247.

[27] L. Delannoy, N. El Hassan, A. Musi, N.N. Le To, J.M. Krafft, C. Louis, *J Phys Chem B*, **2006**, 110, 22471-22478.

[28] J.W. Elam, G. Xiong, C.Y. Han, H.H. Wang, J.P. Birrell, U. Welp, J.N. Hryn, M.J. Pellin, T.F. Baumann, J.F. Poco, J.H. Satcher, *J Nanomater*, **2006**.

[29] J.W. Elam, D. Routkevitch, P.P. Mardilovich, S.M. George, *Chem Mater*, **2003**, 15, 3507-3517.

[30] I. Perez, E. Robertson, P. Banerjee, L. Henn-Lecordier, S.J. Son, S.B. Lee, G.W. Rubloff, *Small*, **2008**, 4, 1223-1232.

[31] R.G. Gordon, D. Hausmann, E. Kim, J. Shepard, *Chem Vapor Depos*, **2003**, 9, 73-78.

[32] S.Y. Chen, C.Y. Tang, J.F. Lee, L.Y. Jang, T. Tatsumi, S. Cheng, *J Mater Chem*, **2011**, 21, 2255-2265.

[33] M.C. Capel-Sanchez, J.M. Campos-Martin, J.L.G. Fierro, *Catal Today*, **2010**, 158, 103-108.

[34] V.I. Avdeev, V.M. Tapilin, *J Phys Chem C*, **2010**, 114, 3609-3613.

[35] D.E. Keller, T. Visser, F. Soulimani, D.C. Koningsberger, B.M. Weckhuysen, *Vib Spectrosc*, **2007**, 43, 140-151.

[36] M. Guidotti, C. Pirovano, N. Ravasio, B. Lazaro, J.M. Fraile, J.A. Mayoral, B. Coq, A. Galarneau, *Green Chem*, **2009**, 11, 1421-1427.

[37] M. Guidotti, I. Batonneau-Gener, E. Gianotti, L. Marchese, S. Mignard, R. Psaro, M. Sgobba, N. Ravasio, *Micropor Mesopor Mat*, **2008**, 111, 39-47.

[38] P. Jin, Z.H. Zhao, Z.P. Dai, D.H. Wei, M.S. Tang, X.Y. Wang, *Catal Today*, **2011**, 175, 619-624.

[39] Q.H. Tang, C. Wang, S.Q. Hu, S. Hui, C. Yuan, G.L. Haller, Y. Yang, *Catal Lett*, **2007**, 117, 25-33.

[40] K. Leus, I. Muylaert, M. Vandichel, G.B. Marin, M. Waroquier, V. Van Speybroeck, P. Van Der Voort, *Chem Commun*, **2010**, 46, 5085-5087.

[41] X.Q. Li, J. Xu, F. Wang, J. Gao, L.P. Zhou, G.Y. Yang, *Catal Lett*, **2006**, 108, 137-140.

[42] Z.H. Yuan, B.Z. Chen, J.S. Zhao, *Chem Eng Sci*, **2011**, 66, 5137-5147.

[43] J.A.A. Hoorn, J. Van Soolingen, G.F. Versteeg, *Chem Eng Res Des*, **2005**, 83, 187-195.

[44] J.K.F. Buijink, J. van Vlaanderen, A. Crocker, E.M. Niele, *Catal Today*, **2004**, 93-5, 199-204.

[45] J.K.F. Buijink, J.P. Lange, R.A.N.R. Bos, A.D. Horton, F.G.M. Niele, *Abstr Pap Am Chem S*, **2007**, 234.

[46] A.E. Stiegman, *J Phys Chem C*, **2011**, 115, 10917-10924.

[47] S.A. Trifonov, V.A. Lapikov, A.A. Malygin, *Russ J Appl Chem+*, **2002**, 75, 969-973.

[48] Y. Meng, D. Gu, F.Q. Zhang, Y.F. Shi, H.F. Yang, Z. Li, C.Z. Yu, B. Tu, D.Y. Zhao, *Angew Chem Int Edit*, **2005**, 44, 7053-7059.

[49] D.Y. Zhao, J.L. Feng, Q.S. Huo, N. Melosh, G.H. Fredrickson, B.F. Chmelka, G.D. Stucky, *Science*, **1998**, 279, 548-552.

[50] M. Ritala, M. Leskela, L. Niinisto, P. Haussalo, *Chem Mater*, **1993**, 5, 1174-1181.

[51] J. Aarik, A. Aidla, T. Uustare, M. Ritala, M. Leskela, *Appl Surf Sci*, **2000**, 161, 385-395.

[52] Q. Xie, Y.L. Jiang, C. Detavernier, D. Deduytsche, R.L. Van Meirhaeghe, G.P. Ru, B.Z. Li, X.P. Qu, *J Appl Phys*, **2007**, 102, -.

[53] X.Q. Wang, G.N. Ou, Y.Z. Yuan, *Acta Chim Sinica*, **2004**, 62, 1695-1700.

[54] A.V. Shijina, N.K. Renuka, *React Kinet Catal L*, **2008**, 94, 261-270.

[55] A.I. Vogel, *Quantitative Inorganic Analysis, Longmans, London, 3rd edn, 1961, 790–791.*

# Chapter 5

## Mesoporous phenolic resins as support for Manganese (III) salen complexes

### 5.1 Introduction

Epoxides are versatile intermediates in organic chemistry. Their inherent polarity and the strain in the three-membered ring make them interesting compounds for regioselective ring opening reactions followed by the formation of 1,2-disubstituted products.[1-3] In particular, optical pure epoxides with two vicinal chiral centres are often used as intermediate in the synthesis of biological and pharmaceutical active compounds.[4] Today, the synthesis of chiral epoxides generally occurs by oxidation of olefins. In this field, the asymmetric epoxidation of unsubstituted alkenes is not evident, since no substituents are present to control the orientation of the substrate. The Jacobsen catalysts, a Manganese (III) salen complex, have proven to be very appropriate catalysts for asymmetric alkene epoxidation reactions.[5] As can be seen in Figure 5.1, these salen type complexes have two chiral $sp^3$ hybridized carbon atoms (*) in the vicinity of the metal center.

The major drawback of these catalysts, however, is the deactivation process in homogeneous phase due to the formation of inactive dimeric $\mu$-oxo manganese(IV) species.[6] In recent years, heterogenisation through immobilization of these homogeneous enantioselective catalysts on mesoporous supports have become the object of intensive research. Due to local site isolation of the complexes on a solid matrix, dimerisation is hindered. Furthermore, the possibility of simple recyclability after catalytic run makes these expensive complexes more economical attractive. The majority of the reports on the heterogenisation of Mn(III) salen catalysts have mostly been centered on encapsulation, adsorption or covalent attachment to porous inorganic supports, such as zeolites, MCM-41, Al-MCM-41 and clays. [3][7-12] For covalent immobilization, however, the original structure of the manganese complex has often to be modified or multiple synthetic steps and structural changes to the parent catalyst structure are required. Recently, Silva and co-workers published the immobilization of the Jacobsen catalyst through a direct axial coordination of the metal centre onto the phenolate groups of a

modified commercial activated carbon.[13] This immobilization procedure involves a direct and simple reflux procedure. The newly developed catalysts showed high activity in the asymmetric epoxidation of styrene and α-methylstyrene. [14] Previously to the immobilization of the manganese complex on activated carbon, the carbon surface has to be pre-treated by an oxidation step (mostly $H_2O_2$ treatment or with an air flow) in order to generate sufficient surface phenolic hydroxyl functions as anchoring points. [13]

In this study, mesoporous phenolic resins are introduced as a novel support for a Manganese (III) salen complex. Mesoporous phenolic resins contain an abundance of phenolic hydroxyl groups in their framework. Consequently, the pre-oxidation is not required in case of mesoporous phenolic resins. The immobilization is performed by a simple direct method involving the synthesis of the complex followed by a direct attachment of the complex on the phenolic resin, as can be seen in Figure 5.2. This newly developed catalyst is then evaluated for its catalytic performance in the asymmetric epoxidation of diline (1,2-dihydronaphtalene). The results are compared to the catalytic activity of the homogeneous Jacobsen catalyst system and the complex attached to activated carbon (with the extra oxidizing pretreatment of the surface). Additionally, a second run and the leaching resistance are also evaluated. Finally, insight in the proposed reaction mechanism is presented.
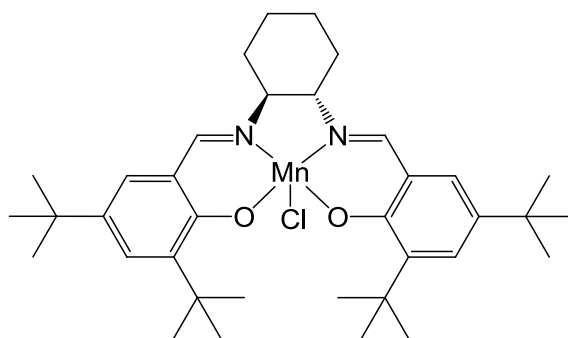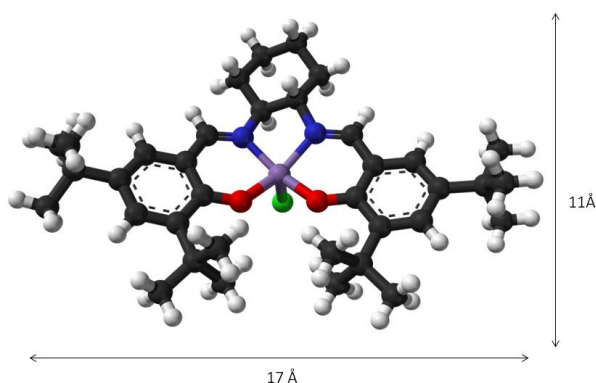
**Figure 5.1 – Structural skeleton and a ball and stick model of the Jacobsen catalysts. The dimensions are given in Angstrom.**

**5.2 Covalent immobilization of Manganese-Salen complex on mesoporous phenolic resins**

Figure 5.2 gives an overview of the synthesis strategy to immobilize the Jacobsen catalyst on the surface of the mesoporous phenolic resins. In step (i), the hydroxyl surface was activated by refluxing with an aqueous solution of sodium hydroxide (0.0138M) for one hour. A decrease in pH of the aqueous solution was observed. Then, the solid was filtrated, washed with deionised water until constant pH 8 and subsequently dried at 120°C in *vacuo*. In step (ii), 0.5 g of the activated solid was refluxed for 8 hours in 100 mL 0.5M ethanolic solution Jacobsen catalyst. It is supposed that the chlorine atom is substituted and an axial Manganese-oxygen-support bonding is formed, as shown in Figure 5.2. Finally, in order to remove the excess of physisorbed complexes, the resulting material was purified by soxhlet extraction with ethanol overnight. Finally, the solid was filtrated and dried at 120°C in *vacuo*. As a comparison, the Jacobsen catalyst was also immobilized on activated carbon. Here, a pre-oxidation step was performed with hydrogen peroxide, in order to generate surface hydroxyl functions. The additional steps are similar to these of the immobilization on the mesoporous phenolic resin. [13]
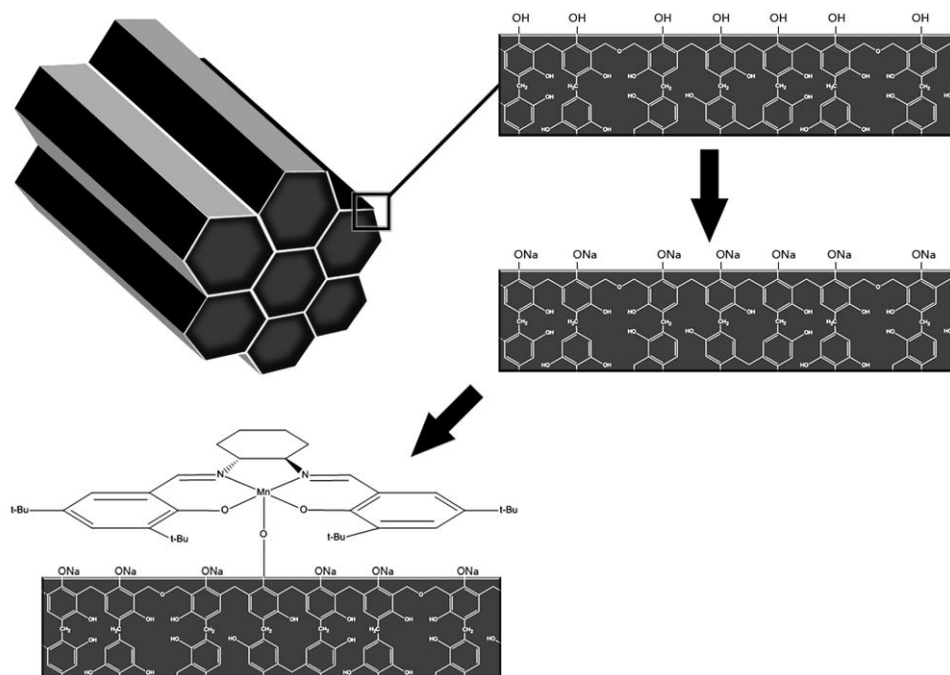
**Figure 5.2 – Representation of the strategy to directly immobilize a Mn-Salen complex on the surface of mesoporous phenolic resins. Previously to the immobilization in step 2, the Mn-salen complex is synthesized.**

### 5.3 Characterization

Table 5.1 shows the porosity characteristics of the phenolic resins before and after immobilization of the catalyst. Here only a slight decrease in porosity properties is observed after immobilization. In particular, the specific surface area and pore volume are decreased. This can mainly be attributed to the weight increase after immobilization of the large salen complex. It is suggested that the cylindrical open pores of the mesoporous phenolic resins are large enough (pore diameter is estimated around 7 nm) to give easily access to the bulky complexes (17Å x 11Å). Elemental analysis revealed that the support was loaded with a loading of 0.014 mmol Mn/g. Theoretically, a maximum 'monolayer' loading of 0.4 Mn-centers/g is calculated, suggesting the Mn-complexes are highly dispersed on the surface of the mesoporous phenolic resin. As a reference, the Jabobsen catalyst was also immobilized on the surface of activated carbon. The pore characteristics

of the activated carbon before and after immobilization of the catalysts are also shown. The manganese loading was calculated as 0.22 mmol Mn/g.

**Table 5.1 – Porosity characteristics of mesoporous phenolic resin and activated carbon before and after immobilization of the manganese complex.**

| | $S_{BET}$ [a] $(m^2/g)$ | $V_p$ [b] $(cm^3/g)$ | Pore size [c] (nm) | Manganese loading [d] | |
|---|---|---|---|---|---|
| | | | | mmol Mn/g | #Mn/nm² |
| Original phenolic resin support | 453 | 0.60 | 7.1 | - | - |
| Jacobsen catalyst @ phenolic resin | 378 | 0.44 | 7.1 | 0.014 | 0.02 |
| Original activated carbon support | 450 | n.d. | < 2 | - | - |
| Jacobsen catalyst @ activated carbon | 403 | n.d. | < 2 | 0.22 | 0.33 |

[a] $S_{BET}$= specific surface area calculated using the BET-theory; [b] $V_p$ = total pore volume, [c] mean pore size determined by the BJH method; [d] loading determined by elemental analysis; * Langmuir surface area; n.d. = not determined

Figure 5.3 shows the DRIFT spectra of the original phenolic resin support, the catalyst immobilized on the surface and the homogeneous Jacobsen catalyst. The spectrum of the phenolic resin shows a broad absorption band around 3600 - 3400 $cm^{-1}$, originating from free and perturbated phenolic hydroxyl stretches. Two bands at 3100 – 3000 $cm^{-1}$ and 3000 – 2800 $cm^{-1}$, corresponding to the aromatic and aliphatic CH and $CH_2$-stretches respectively, can also be observed. Furthermore, the spectrum contains a broad band in the 1800 – 700 $cm^{-1}$ region, consisting of not-well resolved peaks originating from different chemical functionalities present in the polymer framework: C=C vibrations of di-, tri- and tetra-substituted aromatic rings, ether- and methylene bonds, aldehyde functionalities, ... The infrared spectrum of the homogeneous Jacobsen complex shows two bands at 3100 – 3000 $cm^{-1}$ and 3000 – 2800 $cm^{-1}$, corresponding to aromatic and aliphatic CH and $CH_2$-stretches respectively. Also, a clear peak at 1690 – 1640 $cm^{-1}$, corresponding to the imine moiety of the complex, can be observed. A peak at 1538 $cm^{-1}$, corresponding to complexated Mn centers is also observed. [15-17]

The IR-spectrum of the catalyst after immobilization is also shown in Figure 5.3. From this figure, it can be clearly seen that the absorption bands of the complex completely overlap the characteristic bands of the homogeneous complex. Due to the relatively low loading of the complex, the peaks of the immobilized complex could not be observed after immobilization. Also software manipulation by substracting the two spectra did not reveal the characteristic bands of the immobilized complex.

Next, the immobilization of the Jacobsen catalyst in the phenolic resin was verified by means of XRF and EPR measurements. In the XRF spectra of the original support, two peaks at 2.622 keV and 2.817 keV, corresponding with the $K_\alpha$(Cl) and $K_\beta$(Cl) peaks respectively. This high chlorine content originates from the synthesis procedure (HCl is

used as catalyst to polymerize resorcinol and formaldehyde). After immobilization, two new additional peaks at 5.895 keV and 6.492 keV are detected, which can be assigned to the $K_\alpha(Mn)$ and $K_\beta(Mn)$ peaks respectively. In order to quantify the number of Mn-centres, elemental analysis indicated a Mn-loading of 0.014 mmol Mn/g, corressponding to 0.02 Mn complexes/nm². Theoretically, a maximum loading of 0.53 Mn complexes/nm² can be obtained. The relative low loading on the support and the presence of the large ligands avoid the formation of $\mu$-oxo-species through dimerization, the major reason for deactivation of the Jacobsen catalyst in the homogeneous phase. [18, 19]
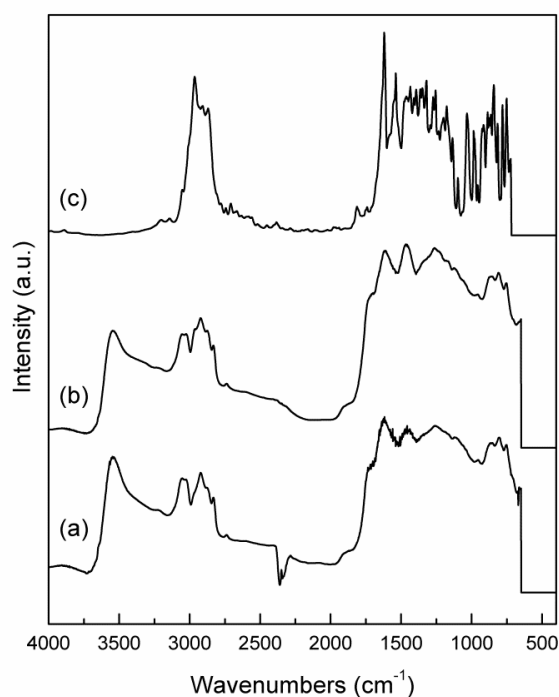


**Figure 5.3 – DRIFT-spectra of (a) mesoporous phenolic resin, (b) Jacobsen catalyst immobilized on mesoporous phenolic resin and (c) homogeneous Jacobsen catalyst.**
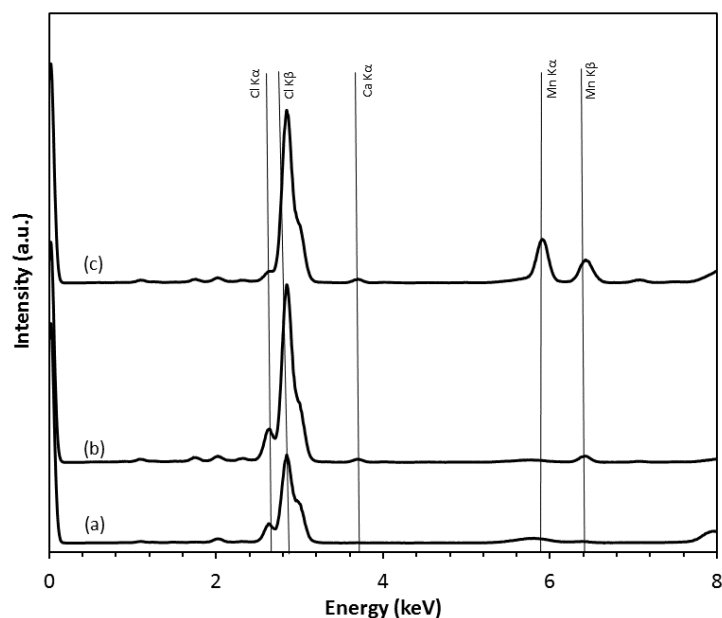
**Figure 5.4 – X-ray fluorescence evolution of the immobilization of the Mn-complex on mesoporous phenolic resin: (a) original phenolic resin support, (b) after NaOH-treatment and (c) after immobilization of the Mn-complex.**

The oxidation state of the immobilized catalyst was verified by means of electron paramagnetic resonance spectroscopy. Figure 5.5 shows the EPR spectra of the (a) homogeneous Jacobsen catalysts and (b) Jacobsen catalysts immobilized on mesoporous phenolic resin. Here, the homogeneous catalyst Mn-Jacobsen catalyst shows one broad band at a magnetic field around 400 mT, corresponding to Mn(+III) species. After immobilization 6 individual peaks of Mn (+II) centers is observed at 1200 mT. This indicates that the manganese species are reduced to Mn (+II). The reduction of Manganese (+III → +II) can probably be explained by the loss of the chlorine atom on the Manganese center (Figure 5.1).
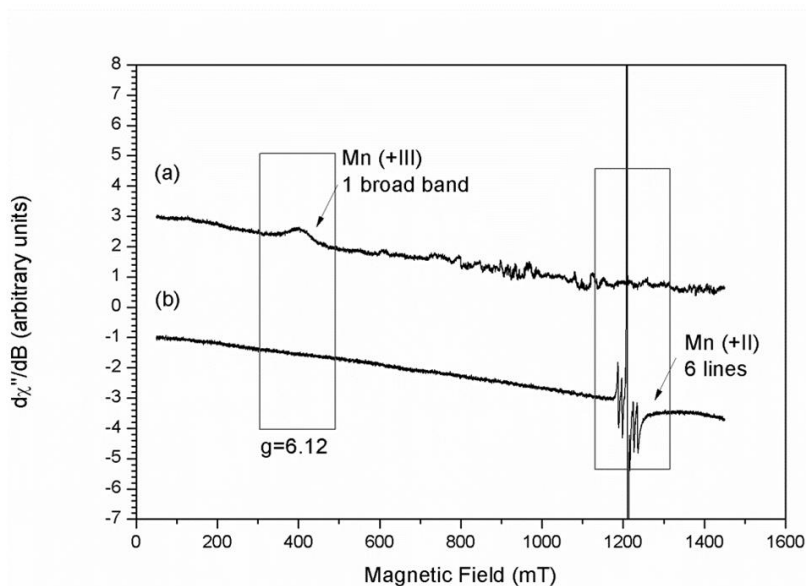
**Figure 5.5 – Electron paramagnetic resonance (EPR) of (a) homogeneous Jacobsen catalysts and (b) Jacobsen catalysts immobilized on mesoporous phenolic resin.**

**5.4 Catalytic performance of the immobilized Jacobsen catalyst in the epoxidation of diline: results**

The catalysts have been evaluated in the epoxidation of diline (1,2-dihydronaphtalene). As can be seen in Figure 5.6, the asymmetric epoxidation of this conjugated olefin yields two enantiomers: (1R, 2S)-naphtalene oxide and (1S,2R)-naphtalene oxide.
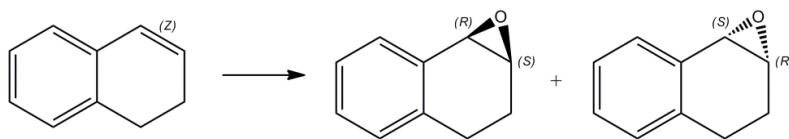


**Figure 5.6 – Asymmetric epoxidation of 1,2-dihydronaphtalene (diline) to (1R, 2S)-naphtalene oxide and (1S,2R)-naphtalene oxide**

Table 5.2 shows an overview of the catalytic performance of the different catalysts in the epoxidation of diline. The reaction mixture was analysed after 24 hours reaction at room temperature.The homogeneous catalyst shows a high catalytic activity: after 24 hours of reaction, 76.74% substrate is converted and a TON of nearly 30 is calculated. For the Jacobsen catalyst immobilized on the mesoporous phenolic resin, also a high conversion of nearly 58% is obtained, corresponding with a turn over number of 23.51. For the reference support, activated carbon, a conversion below the blank level was observed (< 5%).

Next, preliminary attempts were made to determine the enantioselectivity of the catalysts by means of chiral HPLC measurements. The enantiomeric excess *ee* is calculated as

$$ee = \frac{A-B}{A+B}.100$$

with A enantiomer 1 and B enantiomer 2. A chiral catalyst is considered as an appropriate catalyst if at least an enantioselectivity of more than 95% to one of the products is observed. Here, combined chiral HPLC, ^{1}H NMR and VCD (vibrational circular diochroism) experiments were not able to qualitatively determine the enantioselectivity of the new developped catalyst. Therefore, further research is necessary to unambigeously assign the enantiomeric peaks in the chromatogram and the corresponding enantiomeric excess of the products.

Next, the heterogeneity of the newly developed catalyst, was evaluated by means of a so-called split test (or hot filtration test). Here, the catalyst was filtrated from the reaction mixture after 24 hours of reaction. Subsequently, the reaction mixture was analyzed after an extra 24 hours (48hours in total: 24 hours in presence of the catalyst and an additional period of 24 hours without catalyst). Figure 5.7 shows that the conversion remained constant after filtration of the catalyst, indicating the catalytic activity occurs truly heterogeneously (As a comparison, for the homogeneous Jacobsen catalyst, the conversion further increased from 76.74% to 80.10% if the catalytic activity homogeneous catalyst).
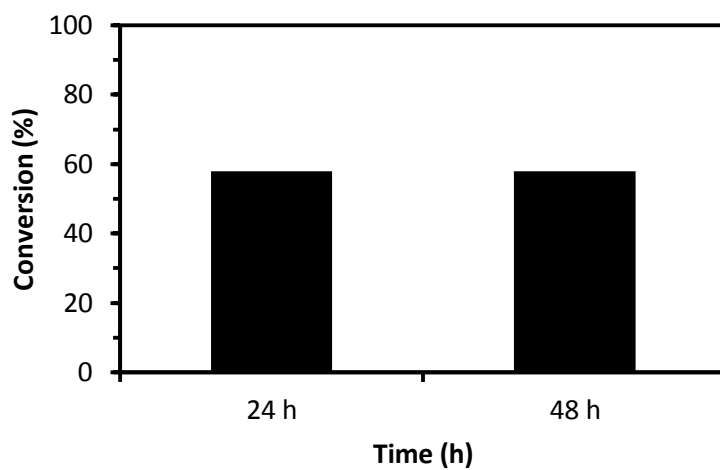
**Figure 5.7 – Split test of the Jacobsen catalyst immobilized on mesoporous phenolic resin: after 24 hours a total conversion of 58% was observed. Subsequently, the catalyst was filtrated and the conversion was again analyzed after 48h. No increase of the conversion was observed, suggesting truly heterogeneously catalytic activity of the immobilized catalyst.**

**Table 5.2 – Overview of the catalytic performance of the immobilized Mn-Salen catalysts in the epoxidation of diline**

|  | Manganese loading | | RUN I | | RUN II | |
|  | mmol Mn/g | #Mn/nm² | Conversion (%) [a] | TON | Conversion (%) [a] | TON |
| --- | --- | --- | --- | --- | --- | --- |
|  | - | - | <5 | - | - | - |
|  | 0.396* | 0.53 | 76.74 | 29.99 | - | - |
| ed carbon | 0.22 | 0.33 | < 5 | n.d. | n.d. | n.d |
| c resin | 0.014 | 0.02 | 57.40 | 23.51 | 25 | 25.40 |

[a] Conversion determined after 24 hours, an equal amount of Mn-centers are used for each catalytic reaction; n.d. = not determined; theoretically monolayer of Jacobsen catalyst; the catalytic experiments are carried out with identical manganese centers in each experiment.* Theoretical monolayer of the Jacobsen complex on a surface.

**5.5 Catalytic performance of the immobilized Jacobsen catalyst in the epoxidation of diline: discussion**

Previously to the epoxidation of an olefin, the manganese *salen* complex has to be activated through an appropriate oxidant. The activated manganese complex can donate subsequently oxygen to an approaching olefin substrate. During oxidation of the olefin, the manganese center reduces to its original oxidation state. This concept is known as the oxygen rebound mechanism of Groves and is shown in Figure 589. [20]
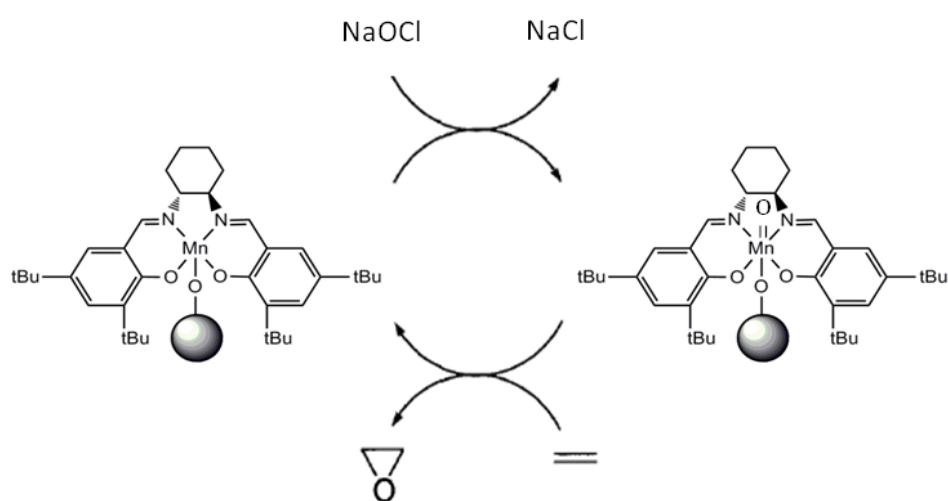


**Figure 5.8 – Groves' proposed reaction mechanism of the epoxidation of alkenes via the oxygen rebound mechanism.**

Figure 5.9 shows the principle skeleton of the manganese *salen* complex; the arrows indicate the possible approaches of olefin substrates to the activated oxo-metal complex. Considering that the manganese complex is anchored on the support via a direct axial bonding, pathway *e* is excluded. Also, the bulky tert-butyl groups on positions A and B avoid the approach of substrate molecules via pathway *d* and *d'*; also pathway *c* and *c'* are not easily accessible due to sterical hindrance. As a consequence, the substrate is forced to follow pathway *a*, *b* and *b'*. These pathways are called the side-on approach and is presented in Figure 5.9 (bottom).[21] It is generally accepted that this forced approach is mainly responsible for the observed high enantioselectivity of the Jacobsen catalyst.

Considering the above described forced side-on approach, the Mn=O bond is assumed to be the critical bond in the catalytic olefin epoxidation. The observed high catalytic activity at the one hand and the stability of this newly developed manganese *salen* catalysts at the

other, can now be understood by the insights obtained in previous chapter. Indeed, it was shown in Chapter 4 that the phenolic support-oxygen-metal bond is highly stable. Immobilization of the Jacobsen catalyst through such a direct axial bond leads to a strongly covalently bonded complex on the surface of a mesoporous phenolic resin. Additionally, through substitution of the chlorine atom by the support-oxygen bond, the manganese center is still unsaturated and can coordinate an extra oxygen in its coordination sphere after activation through an appropriate oxidant. Moreover, the immobilization of the catalyst forces the substrate to approach via a side-on approach (pathway *a*, *b* and *b'* in Figure 5.9), inducing high activity and enantioselectivity of the catalyst. Finally, note that the above described hypothesis corresponds with recent literature and is able to explain the obtained results and observations in this research work. However, more experiments will be required in the future to completely characterize the newly developed catalysts and to elucidate the true reaction mechanism of these newly developed catalysts.
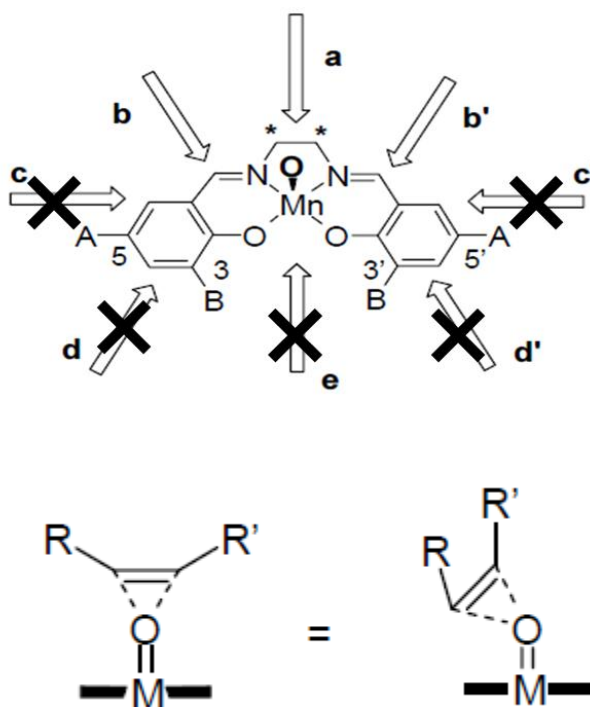


**Figure 5.9 – TOP: Principle skeleton of manganese *salen* complex. The arrows represent the different possible approaches of olefin substrates to reach the activated oxo-manganese center. BOTTOM: Representation of the induced side-on approach (left**

**figure corresponds with approach a, the right figure corresponds with approach b and b').**

## 5.6 Conclusions

The Jacobsen catalyst is a very efficient epoxidation catalyst for the asymmetric epoxidation of conjugated non-substituted olefins. The main drawback of this catalytic system is deactivation through formation of dimeric $\mu$-oxo-species during catalytic run. This dimerization process can be avoided through immobilization of the manganese complex on a support material. In this study, the Jacobsen catalyst was immobilized on mesoporous phenolic resins. Indications of the successful immobilization of the manganese complex was given by means of XRF, EPR, XPS and elemental analysis. However, unambiguous spectroscopic confirmation was not obtained due to low loadings. Finally, the newly developed catalyst was evaluated for its catalytic performance in the asymmetric epoxidation of diline and compared to its homogeneous variant. A first catalytic run showed high epoxide yields with a turn over number which is competitive with the turn over number of the homogeneous Jacobsen catalyst. A split test showed that the catalytic activity of the phenolic resin supported manganese catalyst occurs truly heterogeneously. Moreover, the catalysts remained highly active in a second catalytic run. Unfortunately, the enantiomeric excess of the reaction products was not determined. Finally, insight in the reaction mechanism is given. It is assumed that the oxidation occurs via a side-on approach of the substrate to the Mn=O center following Groves' oxygen rebound mechanism.

In conclusion, the results obtained in this research work are very promising. Today, the enantioselectivity of the newly developped catalysts is still unclear. Further optimization of this catalyst – and from the viewpoint of the development of more stable and reusable selective catalysts – can initially be expected in the expansion of the potential application of this manganese based catalyst to alternative oxidants (e.g. $H_2O_2$) and olefin substrates (e.g. styrene).

## 5.7 Experimental

**Synthesis of mesoporous phenolic resins** – Mesoporous phenolic resins are synthesized according to the procedure of Song et. al. using resorcinol/formaldehyde as carbon source in acid medium.[22] In a typical synthesis, resorcinol (2.1 g) is added to an ethanol/water solution of F127 and stirred for 30 minutes at room temperature. Then, formaldehyde (Formaline, 37wt% formaldehyde in water) is added and stirred for 30 minutes. Finally, HCl is added dropwise and the solution is stirred for 2 hours at room temperature. While keeping the solution untouched, the mixture separated into two-phases. Subsequently, the transparent upper phase was removed and the yellow lower polymer phase was

heated in an oven at 100°C for 24 h followed by calcination. The molar ratio resorcinol:formaldehyde:F127:HCl:EtOH:H$_2$O = 1:1:0.0066:0.13:7.2:15.19.

**Immobilization of the Jacobsen catalyst on the mesoporous support** – 0.5 g of the support is refluxed in a sodium hydroxide solution (0.014M), during 6 hours at 95°C. The product is filtrated, washed and dried *in vacuo* overnight. Next, the activated support was stirred in an ethanolic solution (100 ml) of the Jacobsen catalyst (0.05g), during 6 hours at 80°C. Finally, a soxhlet extraction was carried out with ethanol to remove the excess of physisorbed manganese complex. The catalyst was filtrated and dried *in vacuo*. For the activated carbon (Norit, activated charcoal, Sigma Aldrich), the carbon is firstly pretreated with hydrogen peroxide solution to generate surface phenolic hydroxyl functions. 0.5 g of activated carbon is stirred in an aqueous 30wt% H$_2$O$_2$ solution for 5 hours at room temperature.

**Epoxidation of 1,2-dihydronaphtalene (diline)** - In a typical procedure, dichloromethane (solvent, 1.4 mL), sodium hypochlorite (oxidant, 0.077 mmol), 1,2-dihydronaphtalene (substrate, 0.077 mmol) and the catalyst (4.7µmol Mn) are stirred at room temperature. After 24 hours, the reaction mixture is carefully concentrated in vacuo and the residue is purified by column chromatography (SiO$_2$, hexane:ethyl acetate = 4:1 − 1:1) and followed by thin layer chromatography (hexane: ethyl acetate = 1:1). The conversion is determined by gas chromatography using decane as internal standard. The formation of the epoxide is confirmed by 1H NMR. The optical purity of the product is determined by vibrational circular diochroism. The enantioselectivity is determined by HPLC.

**Characterization** – Nitrogen gas sorption experiments were conducted at 77 K using a Micromeretics Tristar 3000. Samples were *in vacuo* dried at 120 °C prior to analysis. The pore size distribution (PSD) was calculated from the adsorption branch. The pore volume, V$_p$, was calculated using the BJH method. XPS measurements were recorded on a X-ray photoelectron spectroscopy S-Probe XPS spectrometer with monochromated Al (1486 eV) exciting radiation from Surface Science Instruments (VG). The flood gun was set to 10 eV. A nickel grid was placed 3 mm above the samples in order to suppress charging of the samples. Elemental analysis was performed by a CHNS-O analyser Thermo Scientific Flash 2000, with a TCD detector and using the Eager Experience software. 2 mg of the sample is placed in a tin container and heated to 1800°C to fully oxidize sample. The integration of the peaks is calibrated using *L*-methionine as standard. DRIFT-spectra were measured on a EQUINOX-55 spectrometer of Bruker and on a Nicolet 6700 FT-IR spectrometer of ThermoScientific. KBR powder was used as blank. The measurements were performed *in vacuo* at 120°C. Electron paramagnetic resonance (EPR) spectra of dry powders were recorded at 20K with a Bruker ESP300E X-band (9.77 GHz) spectrometer, equipped with a HP5350B frequency counter and a ER035 M gaussmeter. Gas chromatographic analyses were performed on a Finnigan Trace Ultra Fast GC equipped with a flame ionization detector (FID) and a 5% diphenyl / 95% polydimethylsiloxane column, with 10 m length and 0.10 mm internal diameter. Helium was used as carrier gas and the flow rate was programmed as 0.8 ml/min. The reaction products were identified by ^{1}H NMR.

Dihydronaphtalene oxide. ^{1}H NMR (300 MHz, CDCl$_3$): d 7.4e7.2 (4H, m, Ar), 3.85 [1H, d, J 4.5 Hz, CH(O)CHCH2], 3.73 [1H,dd, J 4.3, 3.0 Hz, CH(O)CHCH2], 2.80 (1H, m), 2.55 (1H, dd, J 6.0, 15.5 Hz), 2.43 (1H, m), 1.78 (1H, m).[23] Chiral HPLC was performed using a DAICEL Chiralpak AJ-H column (250 x 4.6 mm, 5 μm dp) and a pre-column security guard with phenomenx lux cellulose-1,4 cartridge. Injection volume = 3 μL, mobile phase hexane:isopropanol = 9:1 at room temperature. The products were detected at 220 nm. IR- and VCD-spectra were recorded on a ChiralIR-2X Dual PEM spectrometer (BioTools, Inc.). The epoxide solution in CDCl3 (99,8%, Aldrich) was measured in a BaF2 cell using 100μm spacers and a 4 cm$^{-1}$ resolution. Solvent and solution were recorded separately.

## 5.8 References

[1] J.G. Smith, *Synthesis-Stuttgart*, **1984**, 629-656.

[2] P. Besse, H. Veschambre, *Tetrahedron*, **1994**, 50, 8885-8927.

[3] R.C. Ewins, H.B. Henbest, M.A. Mckervey, *Chem Commun*, **1967**, 1085-&.

[4] M. Wu, C.X. Miao, S.F. Wang, X.X. Hu, C.G. Xia, F.E. Kuhn, W. Sun, *Adv Synth Catal*, **2011**, 353, 3014-3022.

[5] K. Srinivasan, P. Michaud, J.K. Kochi, *J Am Chem Soc*, **1986**, 108, 2309-2320.

[6] B. Cardoso, J. Pires, A.P. Carvalho, I. Kuzniarska-Biernacka, A.R. Silva, B. de Castro, C. Freire, *Micropor Mesopor Mat*, **2005**, 86, 295-302.

[7] I. Kuzniarska-Biernacka, C. Pereira, A.P. Carvalho, J. Pires, C. Freire, *Appl Clay Sci*, **2011**, 53, 195-203.

[8] L.L. Lou, S. Jiang, K. Yu, Z.C. Gu, R.A. Ji, Y.L. Dong, S.X. Liu, *Micropor Mesopor Mat*, **2011**, 142, 214-220.

[9] X.C. Zou, X.K. Fu, Y.F. Luo, *Acta Chim Sinica*, **2011**, 69, 431-437.

[10] R.N. Ji, K. Yu, L.L. Lou, Z.C. Gu, S.X. Liu, *J Inorg Organomet P*, **2010**, 20, 675-683.

[11] T.C.O. Mac Leod, M.V. Kirillova, A.J.L. Pombeiro, M.A. Schiavon, M.D. Assis, *Appl Catal a-Gen*, **2010**, 372, 191-198.

[12] I. Kuzniarska-Biernacka, A.R. Silva, A.P. Carvalho, J. Pires, C. Freire, *Catal Lett*, **2010**, 134, 63-71.

[13] A.R. Silva, C. Freire, B. de Castro, *Carbon*, **2004**, 42, 3027-3030.

[14] P. Das, A.R. Silva, A.P. Carvalho, J. Pires, C. Freire, *Catal Lett*, **2009**, 129, 367-375.

[15] M.P. Feth, C. Bolm, J.P. Hildebrand, M. Kohler, O. Beckmann, M. Bauer, R. Ramamonjisoa, H. Bertagnolli, *Chem-Eur J*, **2003**, 9, 1348-1359.

[16] J. Cubillos, I. Montilla, C.M. de Correa, *Appl Catal a-Gen*, **2009**, 366, 348-352.

[17] T. Ben Zid, I. Khedher, A. Ghorbel, *React Kinet Mech Cat*, **2010**, 100, 131-143.

[18] EN Jacobsen, MH Wu. Comprehensive asymmetric catalysis. Berlin: Springer-Verslag, 1999, 649-77.

[19] T. Katsuki, *Coordin Chem Rev*, **1995**, 140, 189-214.

[20] J.T. Groves, W.J. Kruper, *J Am Chem Soc*, **1979**, 101, 7613-7615.

[21] J.T. Groves, T.E. Nemo, *J Am Chem Soc*, **1983**, 105, 5786-5791.

[22] L.Y. Song, X.H. Li, H.N. Wang, H.H. Wu, P. Wu, *Catal Lett*, **2009**, 133, 63-69.

[23] J.M. Vega-Perez, I. Perinan, M. Vega-Holm, C. Palo-Nieto, F. Iglesias-Guerra, *Tetrahedron*, **2011**, 67, 7057-7065.

# Chapter 6

## Summary and general conclusions

In the past decades, porous silica supports were often used as support for catalytic species. Although these supports have proven their benefits for a wide range of catalytic species and for different catalytic reactions, supported silica catalysts have one main drawback: these materials are highly sensitive towards hydrolysis and consequently leaching of the supported catalytic species is a main issue. As a consequence, silica based catalysts show a decrease in catalyst efficiency in function of time and therefore a limited life-time. For these reasons, scientists are continuously looking for new stable supports – and stable support-catalyst interaction – with a never-ending regenerability capacity and stability.

Mesoporous phenolic resins combine the porosity characteristics of mesoporous silica, with the stability and the nature of the organic polymer. Phenolic resins – firstly discovered in 1907 as the first plastic Bakelite® synthesised from phenol and formaldehyde as carbon precursors - consist of an aromatic carbon network, which is more hydrophobic and consequently more stable towards hydrolysis. The main goal of this research work was to evaluate mesoporous phenolic resins as alternative support candidate for different catalytic species and for different catalytic reactions.

In a first part, mesoporous phenolic resins were functionalized with sulphonic acid groups. Here, the funtionalization was performed by different sulphonation procedures. The alkyl sulphonic groups showed higher stability in comparison with an aryl sulphonic functionality. Secondly, these sulfonated mesoporous materials were used to non-covalently immobilize a chiral diamine catalyst for asymmetric aldol reactions. The catalysts showed rather average to good catalytic performance in comparison with the

commercial Nafion®-support. Next, titanium and vanadium oxide were deposited on the surface of mesoporous phenolic resins. Here, the catalysts showed limited or no catalytic activity in two oxidation test reactions. Further characterization revealed that the strength of the support-oxygen-metal bonding was critical for its non-catalytic behaviour. Finally, a Manganese (III) Salen complex, also known as the Jacobsen catalysts, was covalently immobilized on the surface of mesoporous phenolic resins. Here, a highly active and stable catalyst was obtained for the asymmetric epoxidation of diline. This newly developed catalyst is presented here as an alternative for the homogeneous complex who deactivates rapidly due to the formation of inactive oxo-species during a catalytic run.

In conclusion, this research is a pioneering work in the screening and exploration of mesoporous phenolic resins as alternative support for catalytic active species. In the up-coming years, it may be expected that this research field will further expand. In particular, progress in the functionalization of mesoporous phenolic resins and as well in the synthesis of ordered mesoporous polymers with its unique characteristics is expected in the near future. Finally, this will also enlarge the potential applications of these materials towards other application fields like adsorption, separation, electrodes, etc.

# Chapter 7

## Nederlandse samenvatting

### 7.1 Mesoporeuze fenolharsen, een geavanceerde klasse van mesoporeuze materialen

Mesoporeuze materialen worden gekenmerkt door hoge specifieke oppervlakken, een groot porievolume en een nauwe poriegroottedistributie (mesoporie: 2-50 nm). Omwille van deze uitzonderlijke eigenschappen vormen zij uiterst geschikte kandidaten als dragermateriaal in heterogene katalyse.[1] Mesoporeuze fenolharsen, een geavanceerde klasse binnen de mesoporeuze materialen, combineren deze hoog poreuze eigenschappen met de karakteristieken van het overeenkomstige organische polymeer.[2]

### 7.2 Mesoporeuze fenolharsen, een vereenvoudigde synthese

Deze mesoporeuze fenolharsen en koolstof werden tot voor kort gesynthetiseerd via een 'harde templaat' methode.[3] Dit vraagt echter het gebruik van agressieve en milieu-onvriendelijke reagentia zoals waterstoffluoride. Bovendien is deze procedure door meerdere synthesestappen vrij arbeidsintensief. In 2005 rapporteerde de onderzoeksgroep van Zhao et. al. een vernieuwde syntheseprocedure van het mesoporeus fenol-formaldehyde hars via een eenvoudiger synthesepad, de zogenoemde 'zachte templaat' methode.[2] Hierbij wordt het zachte templaat vertegenwoordigd door een surfactant dat onder de juiste reactiecondities aggregeert tot micelstructuren. Deze micelfase fungeert als een vloeibaar templaat waarrond de monomeren fenol en formaldehyde polymeriseren. Na het gecontroleerd verwijderen van het templaat verkrijgt men een geordend mesoporeus fenolhars met een open poriestructuur. Bovendien kan via rechtstreekse carbonisatie het polymeer verder omgezet worden tot een mesoporeuze

koolstofstructuur. De procedure voor de synthese van mesoporeuze fenolharsen via de 'zachte templaat' methode is schematisch weergegeven in Figuur 7.1.
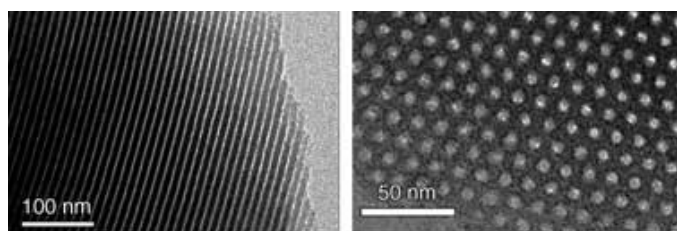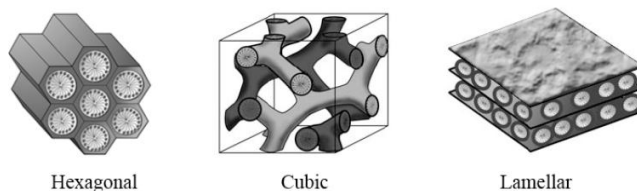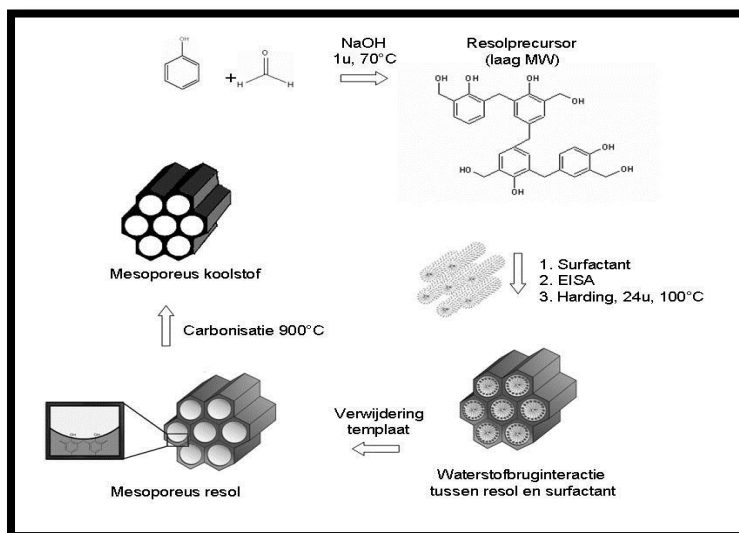


**Figuur 7.1 – BOVEN: Vereenvoudigde weergave van de synthese van mesoporeuze fenolharsen in aanwezigheid van een triblok copolymeer als zacht templaat. MIDDEN: Representatieve weergave van verschillende morfologieën van mesoporeuze materialen. ONDER: TEM-afbeeldingen van mesoporeus fenolhars. [2]**

### 7.3 Mesoporeuze fenolharsen, veelbelovende en hoogwaardige stabiele materialen

Met de publicatie van de onderzoeksgroep van Zhao et. al. ontstond een groeiende interesse in deze nieuwe materialen. Door controle van en inzicht in de verschillende reactieparameters konden bovendien verschillende varianten gesynthetiseerd worden. Bijvoorbeeld werden mesoporeuze membranen, poeders of monoliet-structuren verkregen (zie Figuur 7.2). Bovendien werden ook verschillende poriegroottes gaande van microporeus (< 2 nm) tot poriën van 7 nm verkregen. Voor een meer uitgebreid overzicht over de verschillende mogelijkheden en toepassingen wordt verwezen naar hoofdstuk 1. Verder werd aangetoond dat deze materialen een uitzonderlijk hoge mechanische en hydrothermale stabiliteit bezitten in vergelijking met hun silica tegenhangers en dat deze materialen zich bijzonder goed lenen voor de functionele groepsverankering en/of voor het incorporeren van actieve katalytische species.[4] Omwille van deze bijzondere eigenschappen bezitten deze materialen potentieel als dragermateriaal voor heterogene katalyse. In het tweede deel van dit onderzoekswerk werden deze materialen aangewend voor de incorporatie van verschillende functionele katalytische species en getest op hun katalytische performantie.
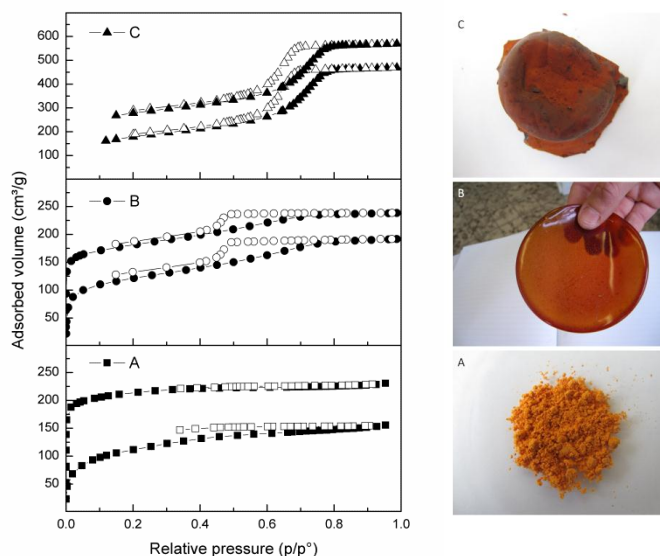


**Figure 7.2 – LINKS: Stikstofsorptie isothermen van mesoporeuze fenolische harsen en koolstof. RECHTS: macroscopische vorm van ongecalcineerde mesoporeuze fenolharsen. De materialen worden gesynthetiseerd volgens A: hydrothermale synthese, B: evaporation induced self-assembly methode, C: twee-fasensysteem.**

**7.4 Mesoporeuze fenolharsen als drager voor sulfonzure katalysatoren**

Zuur gekatalyseerde reacties kennen een belangrijk aandeel in talrijke industriële processen, zoals bijvoorbeeld bij krakingsprocessen van hogere koolwaterstoffen, maar ook in de productie van fijnchemicaliën of de synthese van farmaceutische producten.[5] Een belangrijke klasse van zure katalysatoren vormen de Brönstedtzure katalysatoren met een sulfonzure groep ($-SO_3H$) als actieve component. De vandaag vaak aangewende vloeibare sulfonzure katalysatoren (*p*-tolueensulfonzuur, zwavelzuur, chloorsulfonzuur, …) brengen echter opnieuw de klassieke nadelen van homogene katalysatoren met zich mee (corrosie, moeilijke scheiding, beperkte regeneratie, …). Omwille van deze redenen, bieden gesulfoneerde harsen als heterogene katalysator een veelbelovende oplossing. Het probleem van de commercieel beschikbare harsen  – vaak polystyreen/divinylbenzeen gebaseerd – is echter nog de beperkte stabiliteit in termen van uitloging waardoor de levensduurte van de katalysatorsystemen sterk beperkt is. [6]

In dit onderzoekswerk werd de mogelijkheid tot sulfonatie van mesoporeuze fenolharsen en hun potentieel als zure katalysator onderzocht. Hierbij werden mesoporeuze fenolische harsen gesynthetiseerd en post-synthetisch gesulfoneerd via vier verschillende manieren. Dit leverde zowel aromatische als alifatische sulfonzure groepen op, zoals afgebeeld in Figuur 7.3. Hierbij werden verschillende sulfonzure katalysatoren bekomen met een aciditeitsbelading tussen 0.5 en 2 mmol $H^+$/g.

Vervolgens werden de zure katalysatoren onderworpen aan relatief strenge uitlogingstesten in waterig midden. Hieruit bleek echter dat deze directe sulfonatie (methode 1) thermodynamisch sterk benadeligd is en de sulfonzure groep makkelijk afsplitst in zuur waterig midden. Ook de katalysatoren verkregen via sulfonzure silanering (methode 3 en 4) vertoonden een aanzienlijk verlies van zure protonen bij opeenvolgende uitlogingstesten. De tweede methode, via de alkylsulfonatie op de aromatische ring, bleek het meest stabiel te zijn in zuur waterig midden; slechts een kleine fractie van de zure protonen ging verloren bij consecutieve uitlogingstesten. Daarnaast werden deze katalysatoren gebruikt bij een Fisheresterificatie van azijnzuur en propanol als testreactie en werd hun regenereerbaarheid in een tweede katalytische cyclus gescreend. Hieruit bleek dat de stabiele alkylsulfonzure katalysator weliswaar een relatief lage conversie en turn over number vertoonde, maar wel een stabiele katalytische performantie bezat in een tweede katalytische run.
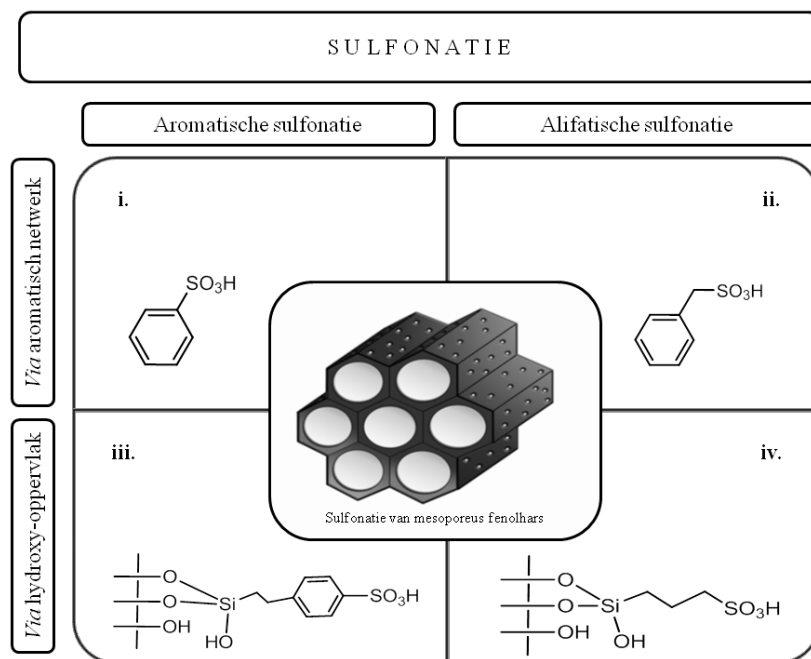
**Figuur 7.3 – Overzicht van de verankering van verschillende sulfonzure groepen op een mesoporeus fenolhars.**

## 7.5 Gesulfoneerde mesoporeuze fenolharsen als drager voor chirale diamine organokatalysatoren

Chirale diamine organokatalysatoren zijn zeer gekende en effectieve katalysatoren voor stereospecifieke katalytische reacties.[7] De laatste jaren is men intensief op zoek naar stabiele manieren om deze katalysatoren te verankeren op een dragermateriaal. Door te kiezen voor een covalente verankeringmethode, observeert men echter vaak een gereduceerde activiteit en selectiviteit in vergelijking met hun homogene analogen. Dit wordt toegeschreven aan de chemische modificatie van de katalysator, nodig voor de covalente verankering van de katalysator. Een alternatieve manier die de laatste jaren opgang maakt, is de verankering van een homogene katalysator via een niet-covalente weg.[8] Hier gebeurt de immobilizatie via een elektrostatische interactie tussen de katalysator en het dragermateriaal. Deze benadering vraagt geen modificatie van de katalysator, waardoor de katalytische eigenschappen gelijk blijven of in sommige gevallen zelfs verbeteren.

In dit tweede deel, wordt een chirale diamine katalysator, m. n. een derivaat van het aminozuur *L*-Phenylalanine, niet-covalent gebonden via een zuur-base interactie op het

gesulfoneerde fenolisch hars. Deze elektrostatische interactie wordt weergegeven in Figuur 7.4.[9] In dit onderzoek werd de invloed van de aard van de sulfonzure groep (alifatisch vs. aromatisch) op de katalytische activiteit van de verankerde katalysator geëvalueerd. Hieruit bleek dat de gesulfoneerde materialen een aanvaardbare activiteit en een middelmatige enantioselectiviteit vertoonden in vergelijking met andere gesulfoneerde mesoporeuze materialen.
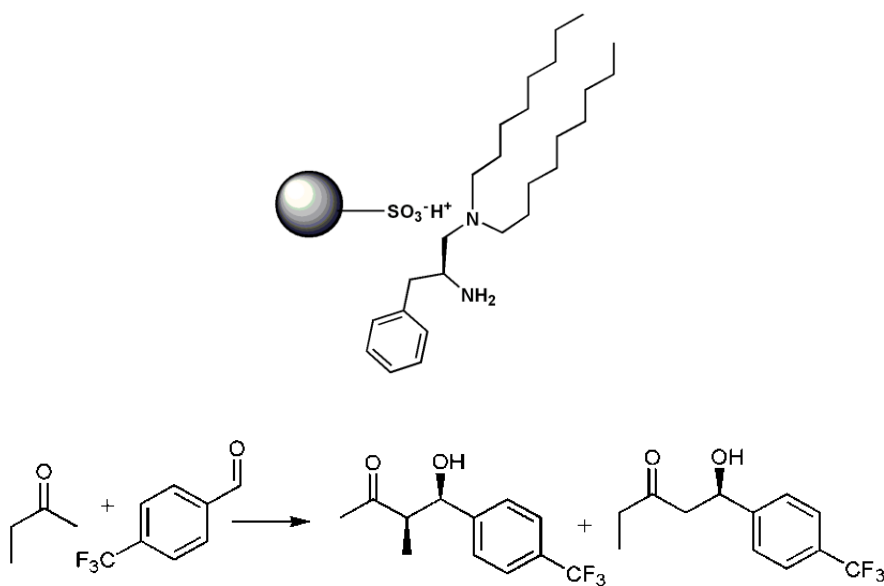


**Figuur 7.4 – Niet-covalente immobilizatie van een *L*-phenylalanine gebaseerd derivaat op een gesulfoneerd fenolhars via een zuur-base interactie als chirale katalysator voor de aldol reactie van butanon en 4-(trifluoromethyl)benzaldehyde.**

**7.6 Mesoporeuze fenolharsen als drager voor vanadium en titanium oxide**

Vanadium en titanium oxide zijn veelgebruikte katalysatoren in tal van industriële oxidatieprocessen zoals de oxidatie van koolwaterstoffen, epoxidatiereacties van olefinen, enzovoort.[10, 11] Voor deze metaaloxide katalysatoren wordt er vaak gebruik gemaakt van silica als dragermateriaal. Hoewel dit anorganisch oxidemateriaal zijn nut reeds heeft bewezen, vormt de verlenging van de duurzaamheid van deze katalysatorsystemen heden de grootste uitdaging. De beperkte hergebruikbaarheid wordt voornamelijk

toegeschreven aan de geringe stabiliteit van de siloxaanbruggen in het silicanetwerk en de hoge uitlogingsgraad van de actieve metaaloxide species tijdens de katalyse.[12]

In dit onderzoekswerk werd de mogelijkheid onderzocht om het huidige silica te vervangen door mesoporeuze fenolharsen als dragermateriaal voor vanadium en titanium oxide. Deze nieuwe katalytische systemen werden op meerdere manieren gesynthetiseerd waarbij verschillende reactieparameters werden gevarieerd. Hierdoor werd een uitgebreid gamma aan vanadium en titanium oxide katalysatoren verkregen. Deze nieuwe materialen werden vervolgens grondig gekarakteriseerd. Hieruit bleek dat zowel de geometrie, de oxidatietoestand als de belading van de fenolhars-gebaseerde katalysatoren voldeden aan de verwachtingen voor een potentiele actieve katalysator. Er werd echter opgemerkt dat de karakterisatie van de metaaloxide species, welke voornamelijk gebaseerd is op spectroscopische analyses, sterk bemoeilijkt werd door de donkere kleur en de amorfe natuur van de mesoporeuze fenolpolymeren.

Vervolgens werden de katalysatoren uitvoerig getest in drie geselecteerde testreacties en vergeleken met de silicakatalysatoren als referentie. Hieruit bleek echter dat de nieuw ontwikkelde katalytische materialen – in tegenstelling tot de silicamaterialen – slechts minimale tot geen katalytische activiteit vertoonden in de drie testreacties. Tal van inspanningen ten spijt, kon de katalytische activiteit evenwel niet verbeterd worden. Bijkomende filtratie- en uitlogingsexperimenten gaven een mogelijke verklaring voor de waargenomen inactiviteit en ondersteunden de hypothese van de 'kritische drager-zuurstof-metaalbinding'. Hierbij vormt het breken van de drager-zuurstof-metaalbinding een cruciale stap in de reactiecyclus. Een (te) sterke interactie van de metaaloxide species met de fenolische drager zou de mogelijkheid tot het vormen van het actieve peroxocomplex, zoals voorgesteld door stap 2 in Figuur 7.5, verhinderen. Om deze reden blijken mesoporeuze fenolharsen niet de ideale kandidaten ter vervanging van silica als dragermateriaal. Toch heeft dit onderzoek bijgedragen tot zeer waardevol inzicht in de katalytische activiteit van gedragen metaaloxiden. Zij ondersteunen het recente debat in de literatuur over de 'kritische drager-zuurstof-metaal binding' voor katalytische oxidatiereacties. [10, 13]
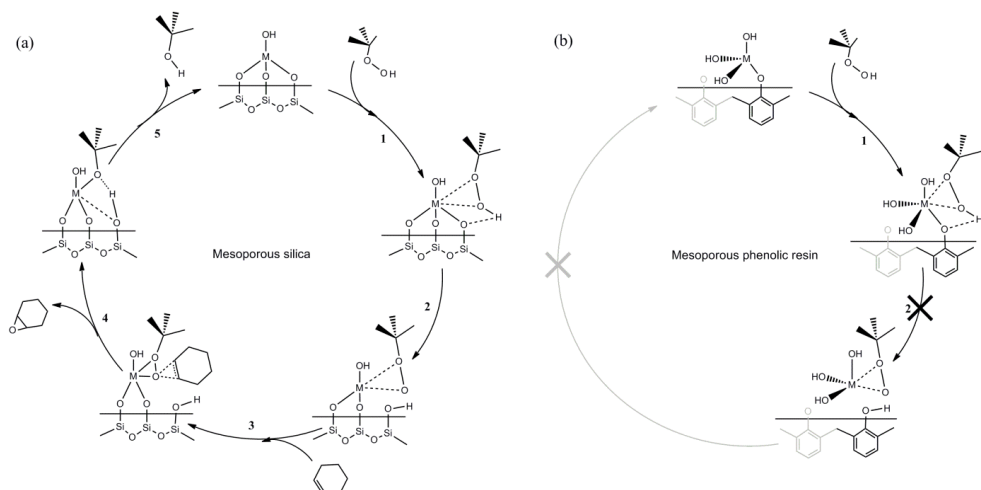
**Figure 7.5 – Reactiemechanisme van de cyclohexeen oxidatie met silica en fenolhars als dragermateriaal, met de cruciale breking van de drager-zuurstof-metaalbinding in stap 2 en de regeneratie van de katalysator in stap 5 (M = V of Ti).**

**7.7 Mesoporeuze fenolharsen als drager voor een Mangaan-salen complex**

Epoxiden zijn veelzijdige bouwstenen in de organische chemie. Hun inherente polariteit en de spanning in de drieledige ring maakt dat ze gemakkelijk stereospecifieke ringopeningreacties kunnen ondergaan met nucleofielen om zo 1,2-difunctionele producten te vormen.[14] In het bijzonder zijn optisch zuivere epoxiden met twee vicinale stereogene centra interessant als intermediair bij de bereiding van verschillende biologisch en farmaceutisch actieve componenten. Synthese van epoxiden gebeurt vandaag voornamelijk via oxidatie van olefinen, waarbij de chirale epoxidatie van ongefunctionaliseerde alkenen in het bijzonder echter niet voor de hand liggend is. Het ontbreken van substituenten vereist namelijk een chirale katalysator die de chiraliteit induceert. De laatste twintig jaar is het gebruik van chirale transitiemetaalcomplexen als epoxidatiekatalysator zijn sterk toegenomen.

Een zeer gekende klasse van dergelijke transitiemetaalcomplexen zijn de zogenaamde mangaan-salencomplexen (zie Figuur 7.6). Eén van de nadelen van deze homogene complexen is echter de snelle deactivatie door vorming van inactieve dimere µ-oxo species.[15] De grootste uitdaging is dan ook deze actieve complexen te isoleren via verankering van deze katalysatorsystemen op een heterogene drager. Bovendien kan door de keuze van het verankeringspunt ook gericht ingespeeld worden op de benaderingswijze van het substraat naar het actieve complex. Momenteel wordt er vooral gebruik gemaakt van silicamaterialen als drager, maar ook klei, actieve kool of polystyreengebaseerde harsen zijn reeds gerapporteerd.[16] Echter blijkt de stabiliteit en

in het bijzonder de covalente binding tussen het dragermateriaal en het complex vaak de zwakke schakel in de regeneerbaarheid van deze katalysatorsystemen. Om deze reden is men nog steeds actief op zoek naar de ideale drager voor verankering van dergelijke katalysatoren.
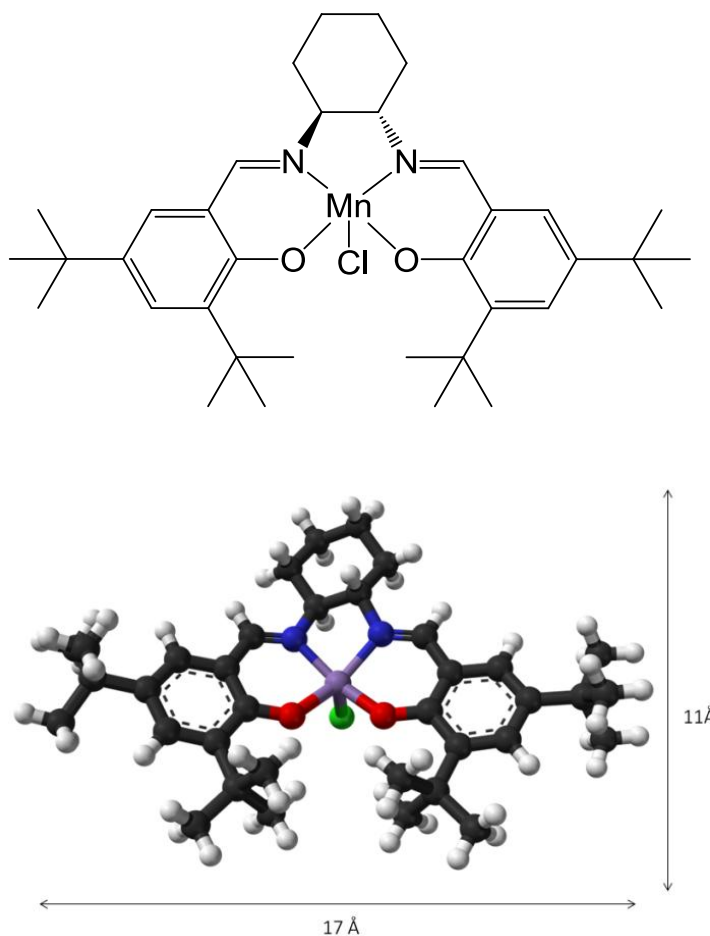


**Figuur 7.6 – Structuurformule (BOVEN) en bol- en staafmodel (ONDER) van de Jacobsen katalysator met weergave van de ruimtelijke afmetingen.**

In dit project werd de mogelijkheid onderzocht om mesoporeuze fenolharsen te introduceren als dragermateriaal voor dergelijke mangaancomplexen. De Jacobsenkatalysator werd verankerd via een rechtstreekse en eenvoudige verankeringstap via een drager-zuurstof-metaal binding, zoals afgebeeld in Figuur 7.7. De bevestiging van een succesvolle verankering via verschillende analysetechnieken vormde echter één van

de grootste probleempunten in het onderzoek. Deze katalysator werd tot slot gescreend voor zijn katalytische activiteit en enantioselectiviteit in de asymmetrische epoxidatiereactie van 1,2-dihydronaftaleen (Figuur 7.7). Hiertoe blijkt dat deze katalysator een hoge katalytische activiteit bezit. Tot slot werd de regenereerbaarheid in een tweede katalytische cyclus getest. Hierbij werd besloten dat deze nieuwe katalysatorsystemen veelbelovende katalytische stabiliteit vertoont.
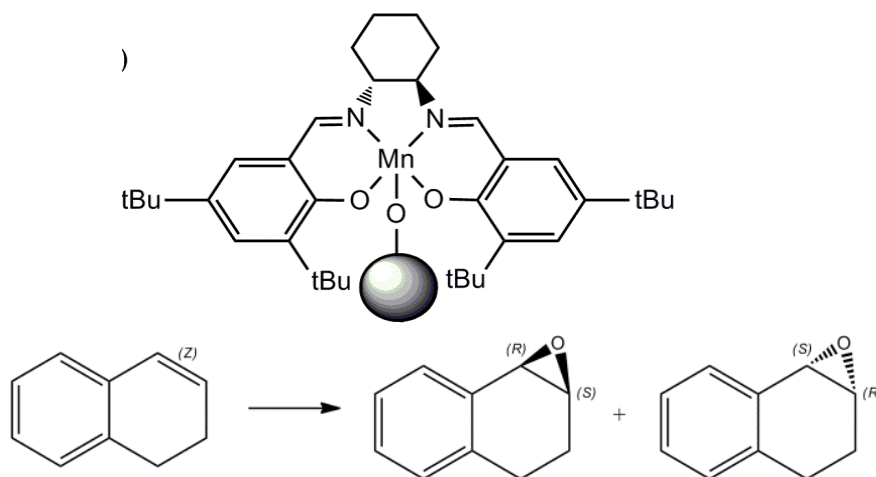


**Figuur 7.7 – BOVEN: Verankering van de Jacobsenkatalysator op het oppervlak van een mesoporeus fenolhars. ONDER: Enantioselectieve epoxidatie van diline (1,2-dihydronaftaleen).**

**7.8 Conclusie en toekomstperspectieven**

Mesoporeuze fenolharsen vormen een geavanceerde klasse van mesoporeuze materialen. Deze materialen kennen een sterk vernette en poreuze structuur, afkomstig van de fenolische component en formaldehyde, en de capaciteit tot vorming van een mesoporeus polymeer. In dit onderzoekswerk werd een overzicht gegeven van de recente ontwikkelingen in de synthese van deze nieuwe materialen. Met name de huidige vooruitgang binnen de functionalisatie van en de heterogene element-impregnatie in mesoporeuze fenolharsen werd belicht. Verder werd er ook inzicht verschaft in de stabiliteit van deze poreuze polymeren en de potentiële toepassingen als dragermateriaal in heterogene katalyse, als adsorbens in adsorptie en als elektrode in elektrochemie werden grondig besproken. Vervolgens werden drie zeer specifieke functionalisaties uitgevoerd. Door de specifieke natuur van deze mesoporeuze materialen vormde de

karakterisatie van deze nieuwe katalysatorsystemen een grote uitdaging. Tot slot werden deze materialen getest in een specifieke katalytische reactie. In het bijzonder de verankering van een Mangaan salen type katalysator vertoonde veelbelovende resultaten. Tot slot, het onderzoek naar mesoporeuze polymeren is zeer recent. De ontwikkeling van mesoporeuze harsen staat nog steeds in zijn kinderschoenen en situeert zich op academisch niveau. Bijgevolg resten er nog vele vragen onbeantwoord. Het zal nu de taak zijn om inzicht te verkrijgen in deze boeiende materie. Voornamelijk op het gebied van gefunctionaliseerde polymeerprecursoren wordt er grote vooruitgang verwacht (bv. melamineharsen en andere stikstofhoudende polymeren.[17]) Een eventuele introductie van deze materialen in de industriële wereld heeft bijgevolg nog een lange weg af te leggen...

## 7.9 Referenties

[1] P. Van Der Voort, C. Vercaemst, D. Schaubroeck, F. Verpoort, *Phys Chem Chem Phys*, **2008**, 10, 347-360.

[2] Y. Meng, D. Gu, F.Q. Zhang, Y.F. Shi, H.F. Yang, Z. Li, C.Z. Yu, B. Tu, D.Y. Zhao, *Angew Chem Int Edit*, **2005**, 44, 7053-7059.

[3] R. Ryoo, S.H. Joo, S. Jun, *J Phys Chem B*, **1999**, 103, 7743-7746.

[4] I. Muylaert, M. Borgers, E. Bruneel, J. Schaubroeck, F. Verpoort, P. Van Der Voort, *Chem Commun*, **2008**, 4475-4477.

[5] J.H. Clark, S. Elings, K. Wilson, *Cr Acad Sci Ii C*, **2000**, 3, 399-404.

[6] R. Xing, N. Liu, Y.M. Liu, H.W. Wu, Y.W. Jiang, L. Chen, M.Y. He, P. Wu, *Adv Funct Mater*, **2007**, 17, 2455-2461.

[7] Y.Q. Wang, J. Song, R. Hong, H.M. Li, L. Deng, *J Am Chem Soc*, **2006**, 128, 8156-8157.

[8] S.Z. Luo, J.Y. Li, L. Zhang, H. Xu, J.P. Cheng, *Chem-Eur J*, **2008**, 14, 1273-1281.

[9] A.L.W. Demuynck, J. Vanderleyden, B.F. Sels, *Adv Synth Catal*, **2010**, 352, 2421-2426.

[10] I. Muylaert, P. Van Der Voort, *Phys Chem Chem Phys*, **2009**, 11, 2826-2832.

[11] K. Leus, I. Muylaert, M. Vandichel, G.B. Marin, M. Waroquier, V. Van Speybroeck, P. Van Der Voort, *Chem Commun*, **2010**, 46, 5085-5087.

[12] Y. Deng, C. Lettmann, W.F. Maier, *Appl Catal a-Gen*, **2001**, 214, 31-45.

[13] B.M. Weckhuysen, D.E. Keller, *Catal Today*, **2003**, 78, 25-46.

[14] S. Shylesh, M.J. Jia, W.R. Thiel, *Eur J Inorg Chem*, **2010**, 4395-4410.

[15] A.R. Silva, C. Freire, B. de Castro, *Carbon*, **2004**, 42, 3027-3030.

[16] P. Das, A.R. Silva, A.P. Carvalho, J. Pires, C. Freire, *Catal Lett*, **2009**, 129, 367-375.

[17] K. Kailasam, Y.S. Jun, P. Katekomol, J.D. Epping, W.H. Hong, A. Thomas, *Chem Mater*, **2010**, 22, 428-434.